Craniofacial Bone Density is Regulated by Thyroid Hormone in Zebrafish

Catherine M. May

A Master's submitted to the Faculty of

the department of Biology in partial fulfillment

of the requirements for the degree of

Master of Science

Boston College
Morrissey College of Arts and Sciences
Graduate School

December 2019

Craniofacial Bone Density is regulated by Thyroid Hormone in Zebrafish

Catherine M. May

Advisor: Sarah McMenamin, Ph.D.

Thyroid hormone (TH) facilitates developmental transitions, particularly by modulating cell proliferation and differentiation. Its role in regulating skeletal growth is well documented[1,2,3,4]. Previous work from our lab and others have demonstrated that hypo- and hyperthyroid fish display changes in bone shape, ossification and the timing of ossification[5]. Zebrafish (*Danio rerio*) develop bone quickly, grow indefinitely throughout their lives, are highly amenable for imaging, and are a valuable model for skeletal biology research. Using *Danio rerio*, we sought to study the long-term effects of TH on bone density by rearing and comparing normal euthyroid (Eu) with a transgenically thyroid-ablated hypothyroid (TH-) and mutant hyperthyroid (TH+) fish.

We found that TH strongly affects bone density and volume. We further hypothesize that TH is critical for the timing and fidelity of skeletogenesis. In hormone-dysregulated fish, we found that massive bone and cartilage exostoses grow on the dentary. Thyroid hormone's effects are highly bone-specific: in TH- fish, we see reduced density in many craniofacial bones, but also increased volume and mineralization in other regions of the dentary. These data suggest that TH plays a critical role in coordinating bone mineralization with growth.

TABLE OF CONTENTS

LIST OF TABLES

LIST OF FIGURES

ACKNOWLEDGEMENTS

I'd like to acknowledge Dr. Matthew Harris for providing us with Amira software and a computer, on which all of our data was generated and analyzed. I'd like to thank L. Patricia Hernandez for providing us with a Density Phantom, which was crucial for obtaining absolute density measurements and for quantifying and comparing bone density. I would also like to thank Dr. Jeff DaCosta, Dr. Yinan Hu, Stacy Nguyen, Dr. Alex Browman and the Boston College Statistics Department for their help with R Studio statistical scripting, tests and analyses.

BACKGROUND

The study of skeletal morphogenesis has been a topic of intense interest for over a hundred years. Developmental phenomenon such as skeletal cell condensation, mechanically-induced ossification and ontogenetic timing are historically rich areas of intellectual exploration[9]. More recently, an interest in ontogeny and gene regulatory networks (GRN) has been an area of growing interest to theoretical biologists[10]. While much attention has been given to the role of gene regulatory networks (GRN) in ontogeny, the regulatory effects of hormones on controlling ontogeny remains an area of under-investigation, particularly in the field of evo-devo[11,12].

During development, hormones serve to coordinate environmental signals (like nutritional availability) to organismal phenotype. They also allow for phenotypic plasticity in response to changing ecological factors[11]. Hormones also play a crucial role in determining the timing of developmental transitions and coordinates metamorphosis to favorable ecological conditions[13,14]. Evolutionary modifications to endocrine regulation can lead to neoteny or paedomorphism, for example, in Mexican axoltls[13].

Using mutant and transgenic fish with low, normal and high levels of thyroid hormone, we disrupted normal ontogeny to test whether skeletal characters associated with distinct life history stages are regulated by thyroid hormone (TH). We controlled levels of TH in developing fish from 4 dpf to 1.5 years of age, including the time period when metamorphosis occurs. By altering TH levels, we observe substantial phenotypic variation.

We found that TH strongly influences skeletal development, in terms of volume, density, shape and mineralization rates of craniofacial bones. Furthermore, we found that TH- fish

demonstrate altered timing of life history stages. TH+ fish also demonstrate accelerated and precocious bone growth that resulted in hyper-mineralized bones and skeletal abnormalities. TH- fish experience developmental delay, decreased rates of growth and osteological abnormalities. TH is required for proper skeletal growth during metamorphosis, and when altered during critical developmental time windows, can have severe phenotypic consequences for the organism.

Thyroid Hormone in Skeletogenesis

Over a hundred years ago, researchers hypothesized that tissues in the body experience some sort of chemical communication that regulates organ growth[15]. Anatomists had long known about the presence of glands and hypothesized about their function. Researchers reasoned that secreted factors could non-locally affect the anatomy and physiology of developing organisms. Cunningham published "*Hormones and Heredity*" in 1921 and referred to the influence of hormones on heredity as "chemical Lamarckism"[18]. In 1926, Harington first synthesized thyroxine, which stimulated interest in the field of hormone biology[15]. Shortly thereafter, Nobel Prizes were awarded to several hormone biologists for characterizing estrogen, testosterone and progesterone[15]. Hormones have been recognized as necessary for proper bone growth since the 1930's[16,17,19,20].

Recent work from our lab demonstrated that TH-dysregulation leads to patterns of skeletal defects including changes in shape, ossification and the timing of skeletogenesis[5]. Thyroid Hormone (TH) is instrumental during developmental transitions, particularly by facilitating skeletal changes during metamorphosis. Its role in stimulating new skeletal growth is well documented[1,2,3,4]. Hypothyroidism (TH-), or a lack of TH, results in growth retardation,

truncated bone length, disorganized tissue, delayed endochondral ossification, and under-mineralization of bone[16,21,22,23,24].

TH affects the regulation of many genes and acts to regulate chromatin in a temporospatial manner by recruiting enzymes to methylate or acetylate chromatin[22,25]. But how hormones actuate differential gene regulation is less well understood. A central feature of skeletogenesis is the condensation of mesenchymal tissues to form the bone matrix[27]. How cells adhere, condense, and initiate differentiation and execute species-specific body plans is an important topic in the evolution of skeletogenesis[27,28,29]. The rate at which cells undergo epithelial to mesenchymal transitions to form osteo-inductive mesenchyme depends on BMP levels[30]. Merrill et al., demonstrated through chick-quail chimeras that BMP in mesenchyme can lead to divergent developmental timing and subsequently species-specific skeletal morphology. Indeed, the signaling crosstalk between BMP and TH pathways have

Conceptual foundations have been laid by Fisher and Franz-Odendaal, for how skeletal gene regulatory networks (GRN) in bone condensations have evolved through co-option of more ancient gene regulatory networks[26]. Ontogenetic programs for bone and cartilage are distinctly different processes, with their own evolutionary history; thus, we reason that thyroid hormone has evolved specific relationships with GRN. Altering this relationship has consequences for both osteogenesis and chondrogenesis. We propose that hormonal profiles are also species-specific and have evolved the role of temporally coordinating skeletal growth.

Zebrafish Model

Zebrafish are an excellent model organism for orthopedic research and for probing fundamental mechanisms in skeletal biology. Zebrafish demonstrate rapid skeletal growth beginning at 2-3 days post-fertilization (dpf), full skeletal maturity at 3-6 months, high

conservation of developmental pathways, bone homology between mammals and fish, voluminous egg production and strong skeletal regenerative potential[34,35,36,37,38]. Zebrafish contain acellular and cellular bone and exhibit life-long skeletal growth through intramembranous, perichondral and endochondral ossification[8,35].

While numerous studies have used goitrogenic agents, like methimazole, thiourea, and propylthiouracil, these drugs have off-target effects[18,39,40,41]. Using a transgenic system, we only had to administer one drug treatment at 4 dpf, to ablate the thyroid follicles, eliminating the need for daily drug treatments. Experimental design of endocrine studies has also been complicated by the use of mammalian models, which transmit maternal TH to the fetus via the placenta. Zebrafish provide the advantage of being oviparous, allowing for precise control of TH during development. Mammal models may have less severe skeletal defects than fish perhaps due to access to exogenous sources of TH, such as in utero or through maternal TH transmitted to offspring during nursing. We maintained a strict TH-free diet for our fish, which allowed us to observe phenotypic outcomes unbuffered by trace TH levels.

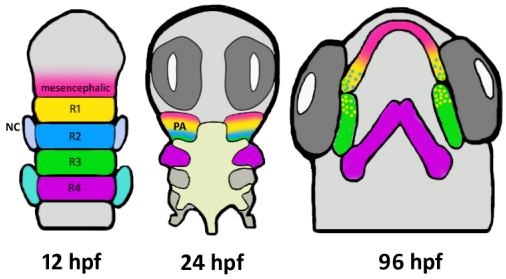

Figure 1. Zebrafish skeletal development. Rhombomeres (left). Pharyngeal arches (middle). Presumptive jaw (right). Color coding demonstrates NCC migration and skeletal contribution.

The zebrafish craniofacial skeleton largely forms from condensations of neural crest derived cells[38] (NCC) which migrate from embryonic pharyngeal arches into the facial mesenchyme around 3 days post-fertilization (dpf) (Fig. 1). Neural crest mesenchyme determines craniofacial patterning and timing of osteogenesis, primarily through Cyclin D and Runx2[42]. NCCs give rise to cartilage and bone-producing progenitors[43,44]. Bipotential progenitors expressing Runx2, Sp7 and Sox9 localize to the growing edge of the mandible and require

IHH[45,46,47], which leads to increased osteoblast and chondrocyte activity[46,47] through Sox9[48,49,50,51], a transcription factor that interacts with thyroid hormone[51]. Chondrocytes begin to form cartilage as early as 2 dpf[52]. Dermal Bones, including the opercles and parasphenoid begin to mineralize as early as 3 dpf[53,54]. Around the time of thyroid ablation (4 pdf), NCC migration is complete and the template for craniofacial bones is largely set[55], with the exception of the dentary/palatoquadrate joint, the retroarticular bone (projecting off the dentary towards the joint) and the mandibular symphysis, which will continue major phases of development until ~14 dpf[56].

Our study

Previous work in our lab has demonstrated that TH- fish display a variety of bone and cartilage defects, including changes in bone shape, ossification and delays in the timing of ossification[5]. However, we also observed the growth of massive lesions on the tip of the dentary and at the jaw joints. We therefore reasoned that mineralization was also affected by altered TH profiles. We initially hypothesized that the massive lesions on the jaw would be hyper-mineralized. We therefore conducted a case control study to determine the effects of thyroid hormone on adult bone density. We reared conditionally-ablatable TH- fish that produces and allows for the selective removal of TH-producing follicles. Using transgenically ablated TH- fish, we have discovered a rare phenotype consisting of bone and cartilage lesions that form at the midline of the lower jaw (at the mandibular symphysis) and at jaw joints.

1.0 CHAPTER 1

1.1 Bone Mineral Quantifications

1.1.1 Introduction

Bone mineral quantifications have been conducted using computed tomography since the 1970's[57]. While TH signaling has been known to strongly regulate the development of skeletal tissues[58], bone mineral studies have primarily focused on pathology. Few studies in zebrafish investigate skeletal growth beyond early development, leaving gaps in our understanding of osteogenesis and osteo-pathology in juveniles and adults. We have published prior studies that focus on skeletogenesis in zebrafish and demonstrated that TH- fish display a variety of bone and cartilage defects, including changes in bone shape, ossification and delays in the timing of ossification[5]. A previous study also found that Increased TH levels accelerate the ossification of both the ceratohyal and opercle is a dosage dependent manner[39]. Having too much or too little thyroid hormone can be highly disruptive to osteogenesis. We sought to characterize bone mineralization in fish reared under different thyroid hormone profiles using micro-CT data to quantify tissue mineral density in adult fish ranging from 14-28 mm SL.

1.1.2 Methods

Transgenic System

We utilized a Tol2 genetic manipulation kit to generate a conditionally ablatable transgenic line, Tg(tg:nVenus-2a-nfnB). This allowed us to administer drug treatment and selectively ablate hormone-producing thyroid follicle cells at 4 dpf[59]. A nitroreductase cassette allowed for the selective ablation of thyroid follicles with the addition of metronidazole (MTZ). We treated fish with 10 mM MTZ overnight to generate TH- fish, while control Eu fish were given a 1% DMSO control. At 5 dpf, we confirmed the Venus-expressing thyroid follicles had been ablated. TH- fish were then reared on a TH-free diet consisting of rotifers, artemia and Spirulina flakes. It should be noted that our TH- fish are merely hypothyroid and not completely thyroid hormone-free. Cultured chondrocytes have also been observed to express thyroglobulin (Tg) in vitro, suggesting a cell-specific way to locally modulate TH levels, even in absence of thyroid hormone-producing follicles[60]. However, ELISA experiments conducted by McMenamin et al., reveal almost undetectable levels of TH in adult TH- fish[59]. It is possible; however, that clusters of chondrocytes may produce and secrete Tg in developing cartilage template.

Opallus, a mutant for hyperthyroidism (TH+), contains a mutation that causes constitutive activation of the Thyroid Stimulating Hormone Receptor, resulting in hyperthyroidism[59]. Using transgenically thyroid-ablated TH- fish and *opallus* we conducted quantitative densiometry experiments using 3 treatment groups with different TH profiles (Eu, TH-, TH). Fish were collected between 1-16 months, when head sizes reached between 4-6 mm. Basic metrics were recorded including body size, head size, age and TH condition. Fish were euthanized and placed in 4% PFA in PBS overnight. Fish heads were micro-CT scanned using a Bruker SkyScan 1275 in a custom low-density foam. All scans were performed with 45 kV and 200 uA of current, a scanning resolution of 10.5 um, 360-degree scanning, random movement, 4-frame averaging, flat-field correction and a rotation step of 0.2°. Density quantification data

were then generated for the segmented bones using Amira's Material Statistics function (Amira 6.5, Thermo Fisher Scientific FEI. Hillsboro, Oregon, USA).

Selection of Bones

We selected key craniofacial bones of differing mineralization modes (endochondral, dermal, mechanical) and embryological origins (mesoderm, NCC). Most of the bones we investigated appear during the first peak of osteogenesis (dentary, opercle, quadrate, ceratohyal)[41]. We chose bones that were previously demonstrated to be strongly affected by TH profile[5]. We generated preliminary data and ran a power analysis to determine our sample size. Our final study included 111 total fish, with a sample size of 37 fish per TH condition. We selected fish for head lengths in the range of 4-6 mm (body sizes between 14 mm – 27 mm SL). Within approximately 1 month (or 12mm body length), major skeletal defects were detectable between TH-/TH+ and Eu fish. Although we size-matched heads to allow for comparison between Eu, TH- and TH+ fish, it should be noted the age at which the head sizes were reached differed greatly between TH treatment groups. Age for fish ranged from 4 – 21 months, with the average age for Eu, TH- and TH+ fish as 10, 11.8 and 7 months, respectively.

Sample Collection

We attempted to collect samples that are optimally size matched for both body size and head size between all 3 treatment groups. However, due to differences in developmental growth rates, age was subsequently unequal between groups. There are inherent differences in the developmental timing of mineralization between Eu, TH- and TH+ fish. For instance, in our whole head analyses, we found that TH- fish had slower mineralization rates, about 45% slower than Eu. Alternatively, TH+ had over 200% faster growth rates than Eu. While inherent

differences in developmental timing complicated our attempts to standardize our analysis, our best fit linear models were highly predictive and robust.

Scanning Settings

Preliminary scans we conducted indicated variations in density between scans taken on different days. Even small differences in moisture content within the tube affected density values. Though we used the same scan settings for every scan, we found inter-scan variation to be as much as 23 grey values between replicate scans of the same fish. Thus, we decided to acquire absolute density measurements using a hydroxyapatite (HA) phantom (D4.5, QRM Möhrendorf, Germany), which would allow us to compare density across our 21 scans. Using the phantom values from scan reconstructions, we created a calibration curve using measurements from 5 rods of varying density (roughly 0, 50, 200, 800 and 1,200 mg HA/cm^3) to obtain absolute density quantifications. For each scan, we included the HA phantom in the 15 ml tube, surrounded by a foam mold equal to the thickness surrounding our specimens.

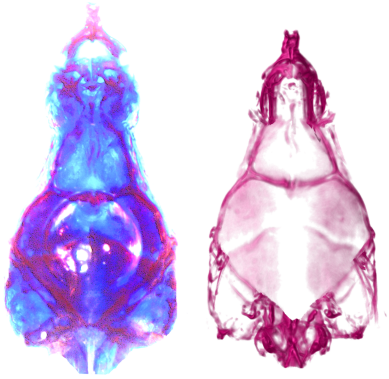

Figure 2. Alizarin specimen references. Skeletal Staining (left) with Alizarin Red (bone) and Alcian Blue (cartilage). Micro-CT specimen thresholded from 40-255 grey values. (right).

Raw projection images were reconstructed using NRecon (Bruker, Kontich, Belgium) software with the following specifications: dynamic range of 0.004 - 0.1909, 41% beam hardening, ring-artifact reduction, flat field correction and misalignment compensation. Reconstructed images were cropped to 900 x 900 pixels and imported as bmp stacks into Amira. Each scan was thresholded in Amira from 40-255 grey values to exclude background and non-skeletal tissue from the analyses. Skeletal preps were stained with Alcian Blue and Alizarin Red

to confirm that our 3D reconstruction thresholding of bones visibly matched bone present in the skeletal preps (Fig. 2). Individual bones were then segmented in Amira using the 3D selection tool to segment the model into the following Material layers: dentary, dermatocranium, otolith, opercle, kinethmoid, hyoid, jaw joint, mandibular symphysis and the lesion (Fig. 3). The jaw joint included portions of the dentary, retroarticular and palatoquadrate bones that are adjacent to the joint itself. Spot measurements were taken in ImageJ to test how much precision was required between segmented borders to obtain reproducible results.

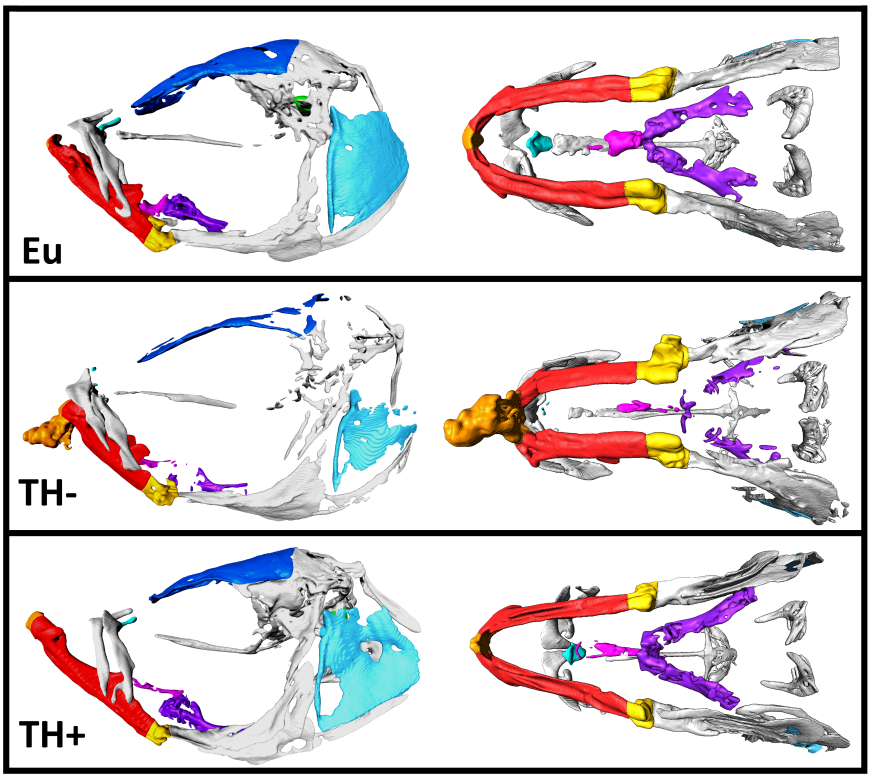

Figure 3. Amira 3D segmentations. Lateral view (left). Ventral view (right). Dermatocranium (blue), mandibular symphysis/lesion (orange), dentary shaft (red), jaw joint (yellow), kinethmoid (teal), otolith (green), opercles (light blue), basihyal (pink) and ceratohyal (purple).

Post-scan Processing

Once the bones were segmented, quantitative data was generated using the Material statistics function in Amira for the following factors: count, volume, mean, max and cumulative sum. Volume is count*$(10.5)^3$, as 10.5 um per pixel was our scanning resolution. Cumulative

sum, or the sum of all grey values, is an approximation of bone mass. The mean, or average density, is the cumulative sum divided by count. We also collected density measurements for the whole head.

For each scan, a calibration curve was generated by importing the phantom image into ImageJ and using a circular lasso to select and measure each rod's average grey value. Values for all 5 rods were recorded, along with the known phantom values. We plotted phantom values against observed values (reported by the company) and obtained a linear equation and R^2 value. The R^2 value for the fits were between 0.9998 - 0.9999, showing a very good linear fit. The equation was then re-arranged (ie. x=(y-16.8)/(0.1)) and uncalibrated density measurements were substituted into the equations (as y) to determine calibrated HA (x). Additional quantifications were conducted using two alternative methods (Bruker software and ImageJ using maximum spot measurements) to cross-validate our methods and confirm reproducibility.

Statistical Analysis

We next conducted statistical analyses. Using a Global Test of Linear Model Assumptions, we determined that some of our data demonstrated unequal variance, non-normality, and skewness issues, posing potential problems for violating basic assumptions of ANOVA analyses. Consulting with the Statistics Department at Boston College, we decided to use Tukey's Ladders of Power test to determine the optimal transformation value (lambda) for each bone to achieve normality. Each optimal lambda value was multiplied by the density value to transform the data. The Shapiro-Wilk Normality Test was then used to determine if the post-transformation values were normally distributed after Tukey transformation. After transformation, all of our data was normally distributed with the exception of the dermatocranium and otolith density data. Skewness was detected in our otolith dataset, which

posed potential problems for rank-based tests; however, each group exhibited left tail skews. Therefore, we performed the Kruskal-Wallis One Way ANOVA by Ranks, instead of a One-Way ANOVA test for both the dermatocranium and otoliths. Post-analysis we adjusted our p-values using the Benjamini and Hochberg method (supplemental Table 1).

To determine the power of our study to detect the effects of thyroid hormone on bone density, we conducted a sensitivity analysis, which indicated that for 3 conditions (TH-, TH+ and Eu), with a sample size of 37 fish per condition, a significance level of 0.05 and a power of 0.8, we determined that we can detect moderate effect sizes of 0.299 or higher (Cohen's F). Most of the effects of TH on bone density we detected were much higher than 0.5. In fact, TH condition was almost as good a predictor of bone density as head size, which is a very strong correlate of bone density alone. Many of the bones we surveyed demonstrated a large effect size for TH on bone density. We therefore concluded that the magnitude of TH condition on bone density was very large for the dentary, dermatocranium, opercle, kinethmoid, hyoid, joint and whole head density.

Otolith Quantification

In order to quantify the morphological defects in otolith mineralization, we implemented a scoring system to determine the degree of defectivity in three categories: shape, position and quantity. The quantity category assigned 1 point for each missing and/or extra otolith per fish. The position category included ectopic ossifications and an ossified otolith pocket; and for each defect 1 point was assigned. The shape category included misshapen, fused, globular and undersized otoliths and for each defect 0.5 points were given. We also counted otolith pairs to determine differences in quantity and scored them as: normal (both otoliths per pair is present), slightly defective (one otolith missing), moderately defective (if a

whole pair was missing), highly defective (3 or more otoliths missing, or extra otoliths were present). We created a frequency table per each categorical variable and conducted a Chi-Squared Contingency test to determine if a contingency existed between TH group and otolith defect severity.

1.1.3 Whole Head Analysis

TH- fish have a larger head to body size ratio than Eu or Op, as well as developmental delays[61]. As expected, TH- fish took much longer to reach the average head size than Eu or TH+, due to general developmental delays associated with hypothyroidism. The distribution of body size in our sample is fairly equal among groups, with the mean body size as 21-22 mm SL. While we tried to collect a balanced dataset for both body size and head size, there are more TH- fish with bigger heads because TH- fish have proportionately larger heads than Eu. The average head size for all groups is between 4.8 - 5.1 mm. Age is distributed unevenly in the dataset because TH+ are precocious and TH- are developmentally delayed[41]; for example, a TH+ fish may take only 3 months to reach the size of a 6 month old Eu, while TH- could take 12 months. The average ages for Eu, TH- and TH+ are 7-11 months. It should be noted that our analyses matched specimens by head size, not age. If we age-matched specimens, TH- would be highly under-mineralized when compared to Eu. However, we decided to compare bone densities between groups of roughly equivalent head sizes. Our prior anatomical assessment looked at younger adults, but by size matching our specimens, we were able to observe “catch-up growth” in the developmental delayed TH-[5]. We found overall differences in whole head density between TH groups (Fig. 4). TH- bones were significantly less dense, while TH+ bones were significantly more dense.

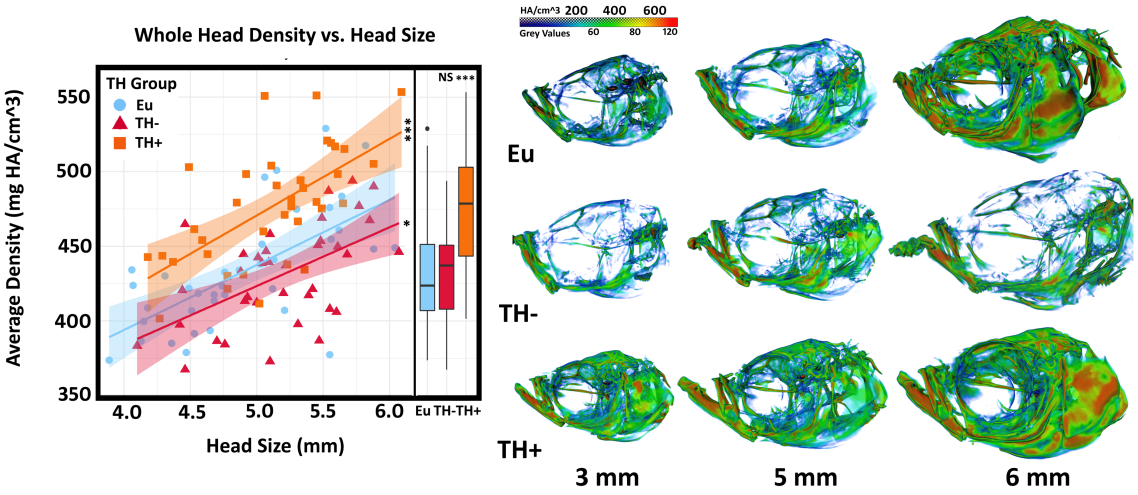

Figure 4. Whole Head Density (left). Average bone density in mg HA/cm^3. Amira models with Bone Density Heat Map (right). Color map legend shows Calibrated HA values.

1.1.4 Dermatocranium Analysis

The dermatocranium is composed of paired frontals, parietals, pterotics, and supratemporals. For the purposes of our study, we only segmented out the frontal and parietal bones. The frontal and parietal bones are acellular compact bone[8]. The frontal bones originate from mesoderm and NCC sources and the parietal bones are mesoderm-derived. Distinct regions of growth occur at the sutures between the frontal and parietal bones[62]. We conducted density quantifications to determine if TH-dysregulated fish bones were less dense than Eu. Indeed, we found that TH- bones have much less dense dermatocraniums than Eu, while TH+ are significantly more dense (Fig. 5).

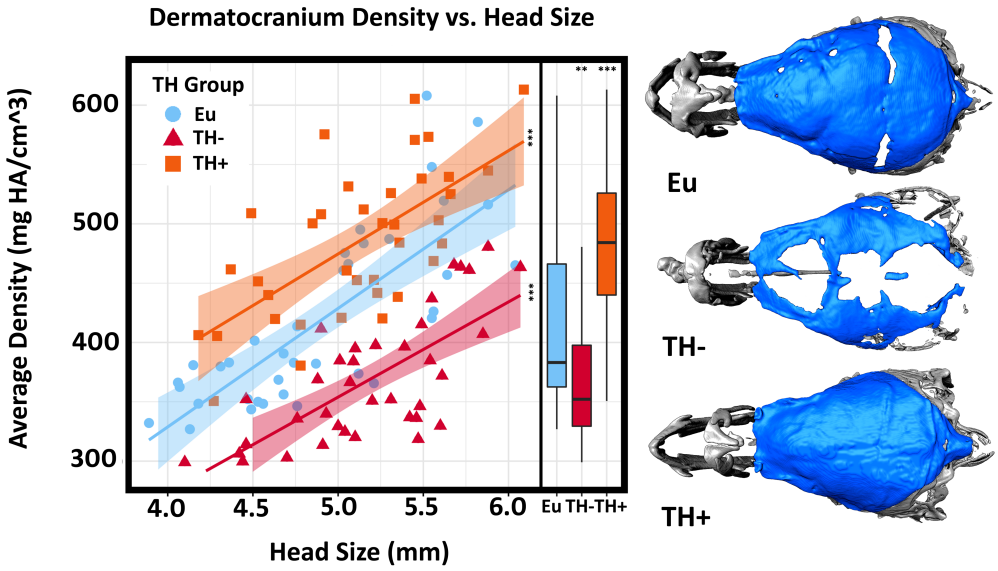

Figure 5. Dermatocranium Density (left). Average bone density in mg HA/cm^3. Dorsal view of 5 mm heads (right). Dermatocranium (dark blue).

We found that TH- fish dermatocraniums are considerably developmentally delayed and that the skull remains under-mineralized well into late adulthood. Sutures of the skull normally remain open during development, during which the skull is still growing, and only fuse later in adulthood[63]. In paedomorphic organisms, the dermatocranium demonstrates a juvenile-like character and fails to fully ossify[5,64]. We previously reported that the frontal and parietals never fully ossify or fuse in TH- fish[5]. However, in our scans, we did observe TH- fish that fully ossified their dermatocranium, but only at very large sizes (above 26 mm SL). While mineralization of the skull is severly delayed in TH- fish, it is precocious in TH+. Although Schilling et al., report that skull ossification is complete by approximately 60 dpf, or 17 mm, we found that our fish took much longer on average to reach full ossification[65].

We also observed major differences in bone volume for the dermatocranium between TH groups (Fig. 6). TH- fish had significantly less dermatocranium volume than Eu or TH- fish.

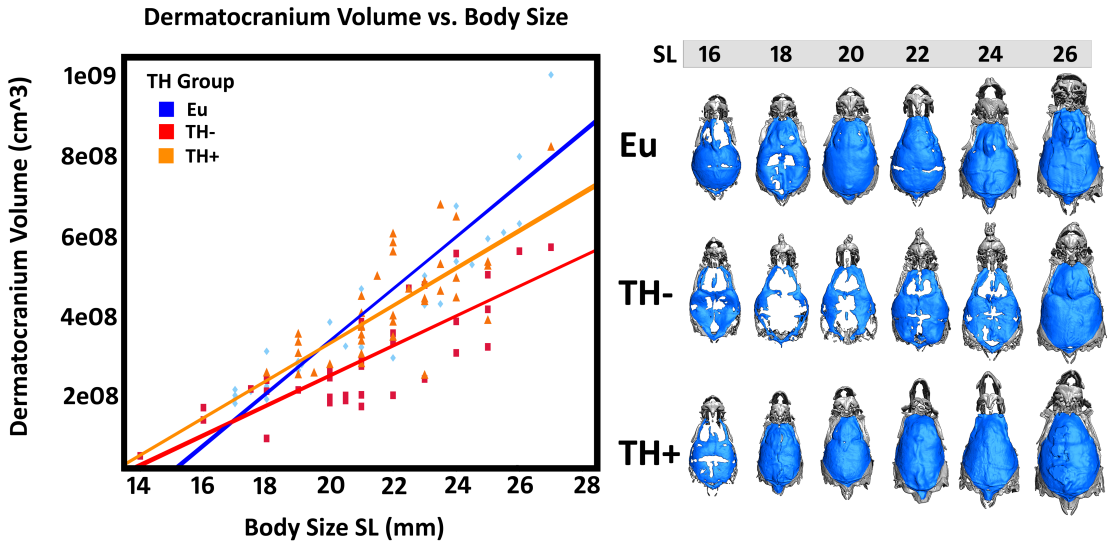

Figure 6. Dermatocranium Volume during growth (left). Dermatocranium mineralization (right). Of body sizes 16-26 mm SL (head sizes range from 3.7-6.3 mm).

1.1.5 Opercle Analysis

Opercles are bones that support the gill cover in fish[53]. They are cellular, compact bones derived from both dermal and NCC sources. Opercles are the first bones to mineralized, at around 3 dpf, before we ablate our TH- fish[53]. Yet, the opercles are moderately affected by TH profile, with defects in patterning reported in TH-dysregulated fish[5]. Opercle bone density is lower in TH- (Fig. 7). In TH-, the lateral edge of the opercles remain under-mineralized and in both TH- and TH+ fish, with holes present in the opercle well into adulthood.

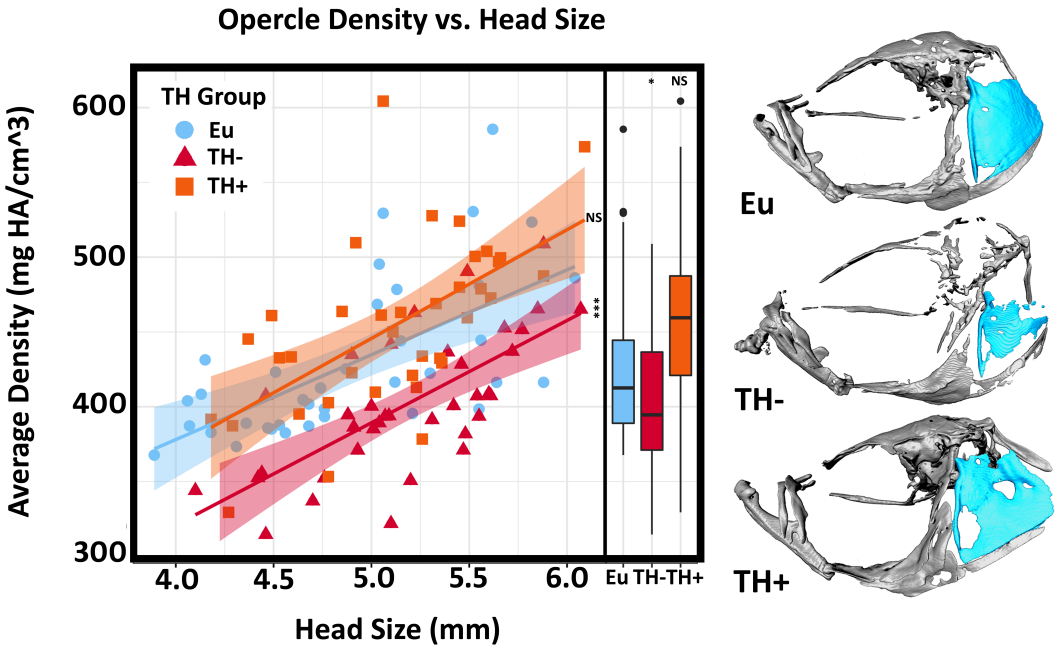

Figure 7. Opercle Density (left). Average bone density in mg HA/cm^3. Lateral view of 5 mm heads (right). Dermatocranium (light blue).

1.1.6 Kinethmoid Analysis

Kinethmoid is cellular, compact bone derived from mesoderm, which aids in jaw protrusion during feeding[66]. The kinethmoid mineralizes based on mechanical loading from premaxillary protrusion during feeding[8,66]. As expected, we found that TH- fish have highly under-mineralized kinethmoids (Fig. 8). It has previously been reported that TH+ fish develop smaller, under-mineralized kinethmoids[41]; however, we found that TH+ fish have denser kinethmoids than Eu.

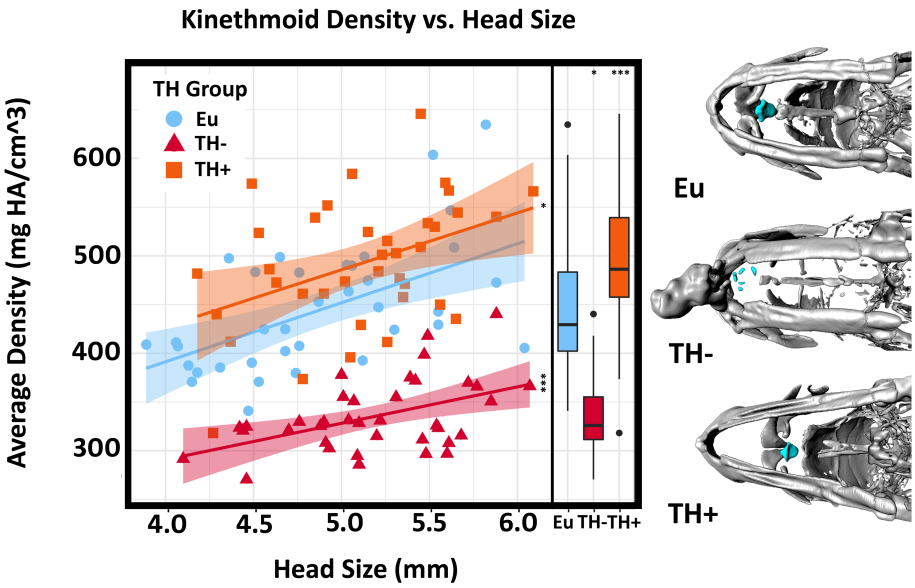

Figure 8. Kinethmoid Density (left). Average bone density in mg HA/cm^3. Ventral view of 5 mm heads (right). Kinethmoid (teal).

1.1.7 Hyoid Analysis

Hyoid depression is used by fish for predation and is critical for proper feeding mechanics[67]. The normal larval to adult transition involves skeletal, behavioral and kinematic changes that promote changes in feeding style[67]. TH- fish were found to retain larval-like feeding behaviors in terms of mouth gape width and premaxillary protrusion[67]. We analyzed two components of the Hyoid complex: the basihyal and the ceratohyal. The basihyal is a tubular bone that ossifies endochondrally and the ceratohyal is cellular bone. Prior studies have reported an increase in ceratohyal ossification in TH+ fish[39] and we indeed found that the ceratohyal and basihyal bones are significantly more dense in TH+ than Eu (Fig. 9).

Based on functional data by Hernandez et al., we predicted that feeding kinematics would lead to an inverse relationship between density in the kinethmoid and density in the hyoid[66]. Because TH- fish have under-mineralized kinethmoids, we hypothesized that feeding

compensation may increase hyoid density. However, we found that the kinethmoid and hyoid are both significantly less dense in TH- than Eu (Fig. 9). Likewise, we found that TH+ have both denser kinethmoids and denser hyoids than Eu.

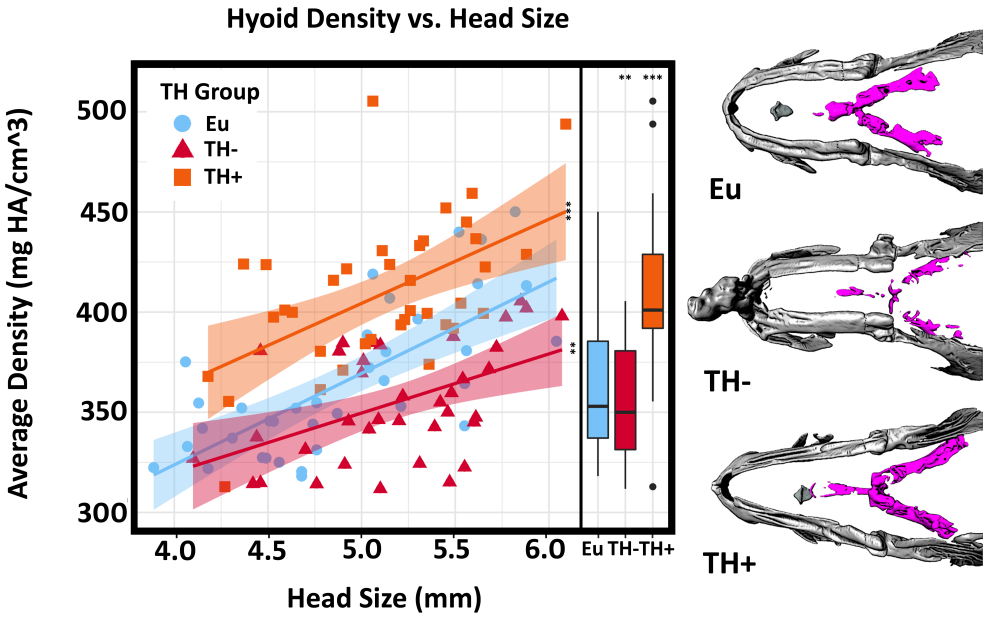

Figure 9. Hyoid Density (left). Average bone density in mg HA/cm^3. Ventral view of 5 mm heads. Hyoid (purple).

1.1.8 Otolith Analysis

Otoliths form through mineralization of organic matrix in the otic capsule and are crucial for both hearing and sensory functions[68,69]. A normal adult zebrafish contains 3 pairs of otoliths: lapillus, sagitta and astericus (Fig. 10). The sagitta forms first, followed by the lapillus, then the astericus [69]. TH has been observed to affect otolith crystallization in trout by altering the biochemistry of the developing otic capsule[68]. We hypothesize that fish with altered TH would experience defects in otolith mineralization.

Although the otolith density did not differ significantly between TH groups, we observed numerous defects in otolith mineralization. TH group was significantly associated with otolith shape defects, positional defects and quantity defects.

Experiments by Shiao et al., found that TH inhibitors retarded growth by as much as 40% during metamorphosis in tarpon fish[40]. Previous studies have observed altered growth rates in the sagitta and lapillus otoliths after treatment of a TH inhibitor in metamorphic flounder[70]. Astericus mineralization is not complete until after metamorphosis[70].

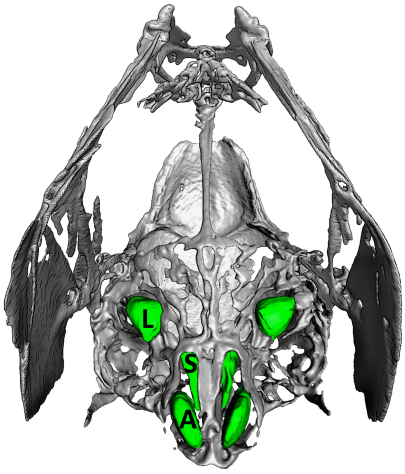

Figure 10. Otolith anatomical map. Ventral view of 5 mm Eu skull. Otoliths (green). L (lapillus), S (sagitta), A (astericus).

Interestingly enough, we found that astericus quantity was less variable in Eu and TH+ than the other otoliths. However, TH- fish still showed significant deviations in astericus quantity, which suggests that TH plays an important role in regulating otolith mineralization beyond metamorphosis.

Otolith Defects

Previous studies on Sparc, a bone protein that binds to collagen, demonstrated severe otolith defects when knocked down, including undersized, extra, ectopic, missing, fused otoliths[115]. To test whether TH group affected otolith morphology, we tabulated defects into a frequency table and ran a Chi-Squared Contingency Analysis. TH- fish demonstrated a contingency between missing/extra otoliths and hormonal profile. We found some TH- fish had many missing otoliths, but oddly enough some TH- had up to 4 extra otoliths (Fig. 11C).

Furthermore, we observed that both TH- and TH+ had a greater number of irregularly shaped, fused, globular, asymmetrical, missing or undersized otoliths (Fig. 11D).

Shape defects were significantly contingent with TH group. Both TH- and TH+ fish demonstrated abnormal otolith numbers (both missing and additional otoliths).

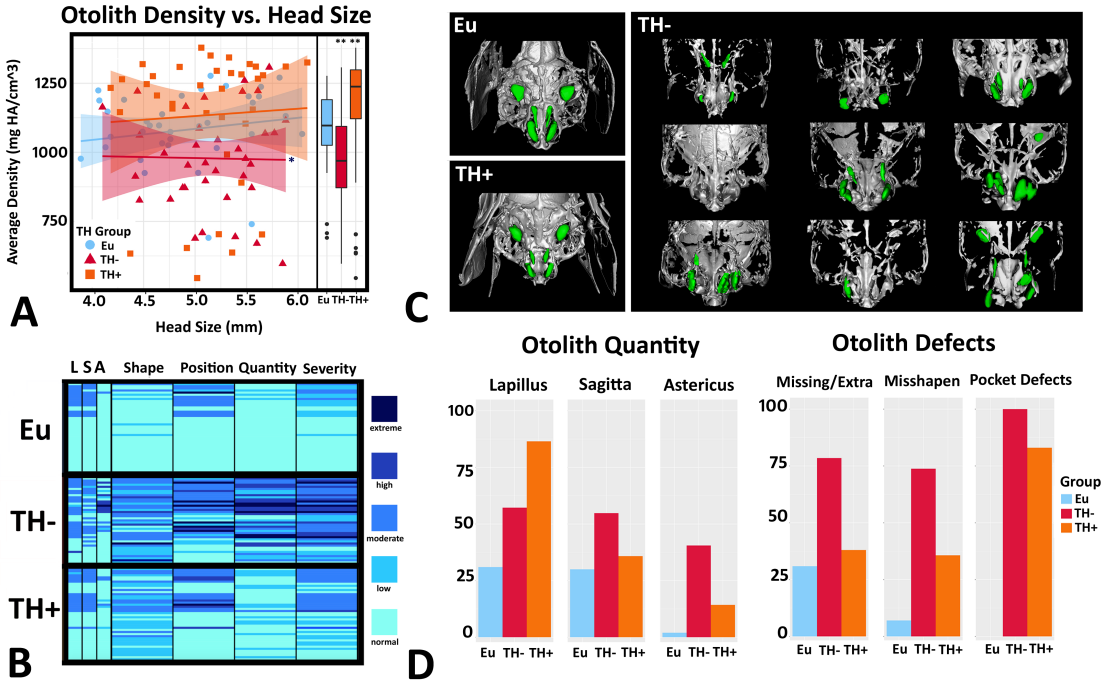

Figure 11. A) Otolith Average Density. Average bone density in mg HA/cm^3. **B)** Heat Map of otolith defects. Each row is a specimen. Scores range from normal (teal) to extremely defective (dark blue). **C)** Ventral view of 5 mm heads. Otoliths (green). Eu (top left). TH+ (bottom left). TH- (right box). **D)** Otolith Quantity and Otolith Defects (percent defective).

Both TH- and TH+ bones also had significantly more ectopic ossifications and ossified pockets (Fig. 11D). TH appears to be a requirement for normal otolith mineralization.

1.1.9 Whole Dentary Analysis

The dentary appears as early as 2 dpf in fish as a template called Meckel's cartilage[56]. Dermal tissue around the dentary begins to ossify around this cartilage template around 3.5

dpf[56]. The dentary is a dermal, NCC-derived bone and is highly dependent on TH, with major changes in shape and ossification occurring under different TH profiles[5]. We noticed the growth of massive bony lesions occurring at two different regions on the dentary and decided to analyze them as separate regions, to obtain intra-bone and whole dentary density measurements. The whole dentary segmentation included the mandibular symphysis, mandibulary symphysis lesion, main dentary body and joint regions (dentary, retroarticular and palatoquadrate). We found that whole dentary density did not differ significantly between TH- and Eu (Fig. 12). However, TH+ had much denser jaws than Eu.

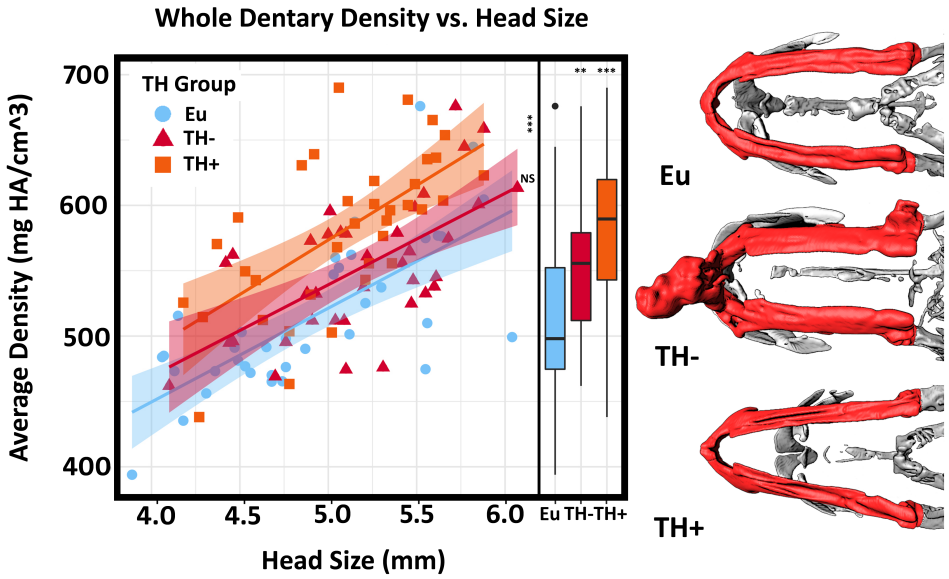

Figure 12. Total Dentary Density (Left). Average bone density in mg HA/cm^3. Ventral view of 5 mm heads (right). Whole Dentary segmentation (red).

The dentary has been defined as a functionally integrated system by some[71]. While the dentary may be its own distinct developmental module, we identified regions of high variance within the dentary; in particular, in the symphysis and jaw joints of our TH- fish. Other studies have stated that craniofacial modularity can be considerably shifted by even minor genetic pertubations[72]. By breaking the normal regulation of TH on skeletal cells, we observed specific

regions of the jaw disproportionately affected by TH. We propose that TH-dysregulation may be a disruptor of modularity. Our results seem to indicate the presence of distinct regions that are differentially dependent on TH to produce robust morphological outcomes.

1.2.10 Intra-dentary Analysis

In order to conduct a comparison of density in the mandibular symphysis lesion, we segmented out the normal mandibular symphysis on Eu and TH+ fish and compared the values to the mandibular symphysis and lesion in TH- fish (MS/Lesion). We originally hypothesized that TH- lesions were hyper-mineralized and expected the average density of the MS/Lesion and Joints to have much higher mean densities in TH- and TH+ bones. Despite TH- fish having much larger MS/Lesion bone mass and volume, the overall density of the mandibular symphysis and lesion bone density did not significantly differ between Eu and TH- (Fig. 13). Although 83% of TH- fish form bone lesions, the bone is essentially of the same density as the dentary bone, from which is protrudes from. Futhermore, the dentary was the only bone in our study to not show reduced ossification in TH- fish. In fact, the dentary shaft was even more dense in TH- than Eu (Fig. 13). While mandibular symphysis morphology is similar

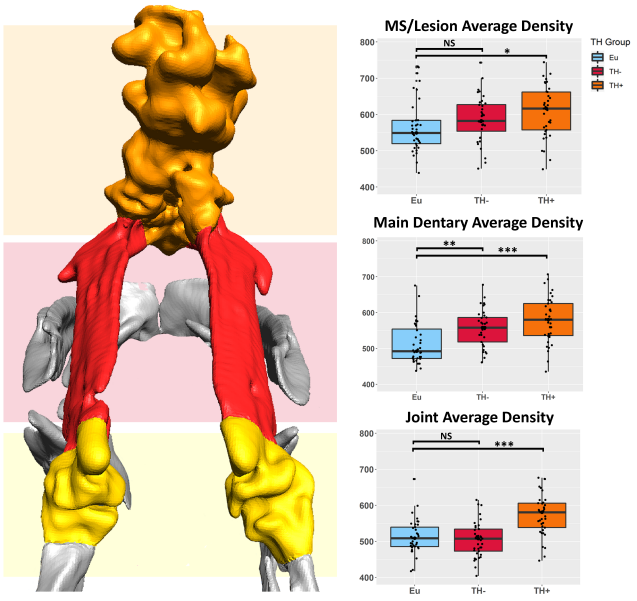

Figure 13. Dorsal view of 5 mm TH- head (left). Mandibulary symphysis and Lesion (orange). Dentary Shaft (red). Joint (yellow). Average density plots (right). Average bone density in mg HA/cm^3.

between Eu and TH+, TH+ bones have a much denser symphysis. The MS/Lesion area appears robust; it is the only bone region we analyzed that is not dramatically altered with changing TH levels. We also hypothesized that we would see a greater amount of density variation in our TH- dysregulated fish, but to our surprise we found TH- actually had much less variance than Eu. The dentary shaft and the joints both show large effect sizes for TH action on bone mineralization, while the MS/Lesion density showed the lowest response to TH profile.

The dentary shaft demonstrates paradoxical differences in density between Eu and TH-/TH+ bones. Both TH- and TH+ had statistically denser dentarys than Eu. Paradoxically, having too little or too much TH in zebrafish leads to a denser dentary shaft in adult zebrafish. We further investigated this finding by using spot measures for maximum density in ImageJ. The maximum density for the dentary is also considerably higher in TH- fish (Fig. 14).

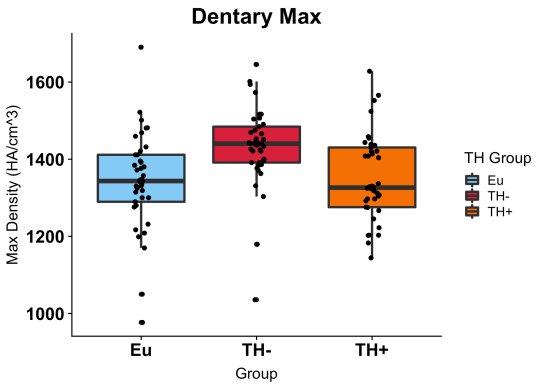

Figure 14. Maximum Dentary Shaft Density. Average bone density in mg HA/cm^3.

Although TH- grows massive bony lesions at the jaw joint (dentary, retroarticular, palatoquadrate junction), the joint density does not differ significantly between TH- and Eu. Despite the joints being much larger in TH- and containing more bone mass than Eu or TH+, joint density scales proportionately as the joints grow larger. However, TH+ joint density is significantly greater than Eu, despite having joints of comparable size.

1.2.11 Mineralization Discussion

Overall, we see a trend in under-mineralization of craniofacial bones in TH- fish (with the exception of the dentary). At sizes under 14 mm SL, differences in density are very dramatic due to developmental delays in TH- and precocious development in TH+. However, given enough time to reach equivalent head sizes, many TH- bones remain comparably under-mineralized. As expected, the dermatocranium is dramatically less dense in TH-. The opercles and hyoid are also moderately less dense in TH- fish. The kinethmoid appeared to be particularly sensitive to a lack of TH and is highly under-mineralized, as well as being much smaller in volume. We were surprised to find extreme defects in otolith mineralization including missing, extra, fused and ectopic otoliths. In TH+ fish, all the bones we analyzed were denser than Eu, with the exception of the opercle. TH+ fish also had significant defects in otolith morphology (otolith quantity, shape, ectopic ossifications and pocket defects). Even though TH+ fish had somewhat normal mandibular symphysis and joint morphology, they were significantly more dense than Eu.

Neoteny, in terms of bone development, can be defined as a slowed rate of mineralization in mutant bones compared to wild type. In almost all the bones we investigated, we see reduced rates of mineralization in TH- fish. When comparing the slopes of the linear models, the TH- dermatocranium, kinethmoid and opercle bones develop 160-400% slower than TH+. The dentary, hyoid and whole head mineralize 200-300% faster in TH+ than TH- fish. In our TH- fish, we see larval-like mineralization rates, as well as altered adult skeletal morphology. Mineralization is not only delayed, but abnormal. In our TH+ fish, we see the opposite trend; accelerated rates of mineralization that result in precocious skull development and hyper-mineralization.

TH- and TH+ skeletal phenotypes demonstrate a wide range of defects in ossification, indicating the importance of TH on bone growth, size and mineralization. We initially predicted that the massive bony lesions growing off of TH- jaws at the mandibular symphysis and jaw

joints would be hyper-mineralized; however, we found no significant differences in bone density despite the massive increases in bone mass and volume. However, we observed a paradoxical effect of increased density in both TH- and TH+ for the dentary shaft.

Given recent attention to problems in biological statistical analysis, we conducted a power analysis and calculated effect sizes for all bones in addition to obtaining p-values[111]. We considered not only significant p-values, but also the magnitude of the effect of TH on bone mineralization. Our most highly affected bones were the kinethmoid and dermatocranium.

We found that TH strongly drove differences in mineralization between treatment groups, although the direction of the effect depends upon the bone. TH showed extreme effects on driving dermatocranium and kinethmoid density, with TH condition having higher effect sizes than head size (head size is highly predictive of density values). For all of the bones except the dentary, TH- fish had less density than Eu. The dermatocranium and kinethmoid exhibited the largest effect sizes, demonstrating TH has a strong effect on mineralization.

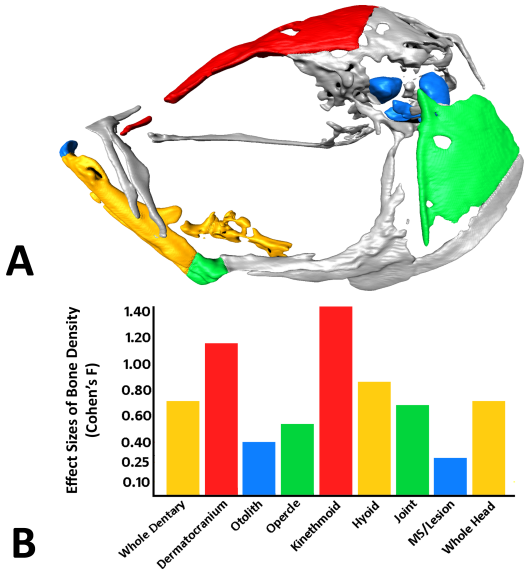

Figure 15. A) Skull color-coded by Density Effect Sizes. Red, most severely affected. Orange, highly affected. Green, moderately affected. Blue, lowly affected. **B)** Bar plot of Bone Effect Sizes (Cohen's F). Detection limit is 0.299.

TH has a strong impact on the rate of mineralization and is almost as strong a predictor of density as head size is. Given a head size and TH group, we can predict with good accuracy how dense the bones are. Our best fit linear models include TH group, with both head size and age as predictors of bone density. Our models can account for roughly 50% - 60% of observed differences in bone density. Many factors potentially affect

growth rates and mineralization, including nutrition, rearing tank density, light, temperature and social hierarchy. Anecdotally, it has been observed that larval tank density plays a large role in growth rates; thus, we kept our tank densities between 20-30 fish per tank to minimize non-hormonal factors from altering mineralization rates. While our models have strong predictive power, presumably, the other 50% of variation in bone density can be attributed to other factors like nutrition, tank density during larval rearing and social hierarchy (in which bigger fish can monopolize resources). However, TH is a strong determinant of the rate and extent of craniofacial mineralization in life history.

Our mineral density quantification study demonstrates a strong relationship between TH and bone density. The effect sizes for density were quite high indicating that TH acts very strongly to influence craniofacial bone mineralization. We conducted model testing and selected highly significant linear models to better understand how bone density is a function of TH group and head size (density ~ TH group + head size). Our linear models have very high R^2 values. In particular, the dermatocranium and kinethmoid density models explain 70% of the variance observed. Variance in the dentary, opercle and hyoid models can be explained around 55% by knowing TH profile and head size. While other factors play into bone density, our models are strongly predictive of bone density from knowing just TH profile and/or head size. We wanted to know how strongly TH group is compared to head size. The effect sizes for TH action on bone density are comparable and sometimes larger than that of head size. We, therefore, conclude that TH exerts a high magnitude of effect on bone mineralization in zebrafish heads.

2.0 SKELETAL PHENOTYPE

2.1 Hypothyroid Skeletal Phenotype

2.1.1 Introduction

TH signaling has been reported to affect cell population dynamics in presumptive cartilage by modulating the switch between proliferation and hypertrophy[19,27]. While hypothyroidism causes developmental delays and can lead to overall smaller adult skeletons, we hypothesize that it also causes delays in the natural progression of stem cell differentiation to prospective cell fate lineages. Hu et al., describe persistent cell proliferation in neuromast cells of TH- fish well beyond the appropriate developmental time window[61]. McMenamin et al., also describe hyper-proliferation of melanophores and xanthophores in TH- fish[59]. This indicates that TH might, likewise, act to regulate cell proliferation in the skeleton. TH-dysregulation may cause hyper-proliferation and prevent cell maturation and differentiation.

Thyroid hormone (TH) is becoming increasingly recognized as a crucial regulator of cell fate in a number of tissues, including bones and cartilage[19,23,32,73]. TH is a critical factor regulating stem cell fate decisions in skin, muscle, eye, brain and intestinal tissues[4,23,74]. It can affect the regulation of many genes through driving chromatin-level changes in a tightly controlled temporal manner[22,25]. How precisely thyroid hormone regulates stem cell fate is unknown, but studies have shown its role in stimulating BMP and HH expression[73,75].

2.1.2 Methods

To better delineate between different skeletal tissue types, we utilized a clearing and staining protocol consisting of 0.024% of Alcian Blue in 60% acetic acid and 0.25% Alizarin Red overnight. To clear the specimen, we also used 1% trypsin, 1% KOH and glycerol. Specimens were then mounted in OCT and cryo-sectioned at 20-40 um width before being mounted onto slides. For fluorescent imaging of skeletal pathways, we used two fluorescent reporter lines to detect BMP and SHH signaling in post-embryonic fish: Tg(sp7:EGFP)[76] and Tg(BRE:eGFP(mw29))[77]. Images were taken on an Olympus Inverted Microscope using identical microscopy settings.

2.1.3 Skeletal Phenotype

Previous work in our lab has demonstrated that TH- fish display a variety of bone and cartilage defects, including changes in bone shape, ossification and delays in the timing of ossification[5]. However, we also noticed pathological growths on the jaw at the mandibular symphysis (Fig. 16, orange) and the jaw joint (Fig. 16, yellow) in adult fish. Massive exostoses grew from a bony stalk on the dentary into cauliflower-like projections that extended rostrally and ventrally. These bony lesions contain disorganized regions of bone, cartilage, and groups of melanophores. The bone lesions appear to progressively increase in size after the onset of the larval-to-juvenile metamorphic transition (10-12mm or 1.5 months) and continue growing throughout the life of the fish.

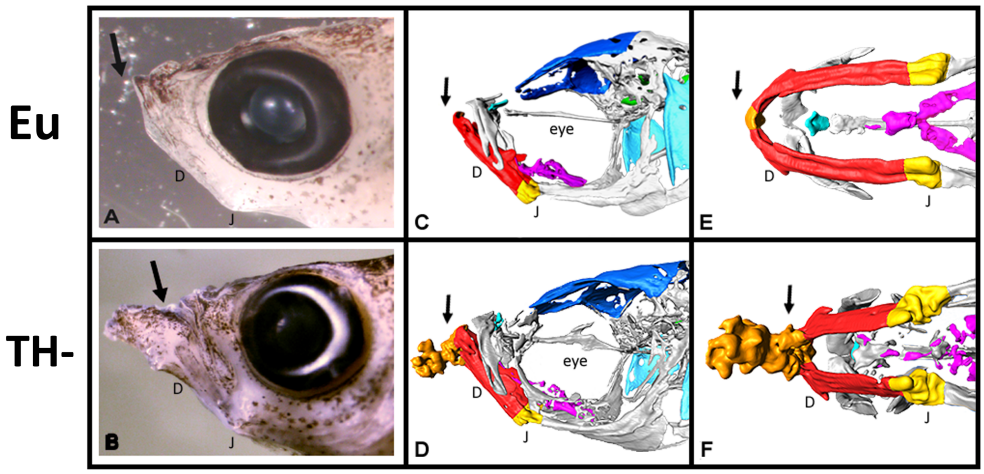

Figure 16. Hypothyroid Phenotype. Adult Eu and TH- fish (left) Micro-CT of adult zebrafish heads (right). Lateral view (C,D) Ventral view (E-F). D, dentary. J, jaw joint. Lesion, arrows.

We looked at osteoblast activity using a sp7:EFGP reporter line. We noticed high sp7 expression in the tip of the bony exostoses, indicating active osteogenesis in older adult fish (Fig. 17). As expected, osteoblast activity is high in the exostoses of adult TH- fish. In terms of characterizing the pathology of the exostoses, sp7 activity indicates that the bone lesion is caused, at least in part, by osteoblastic activity. Additional experiments would determine if other factors, like hyper-proliferation, are also involved.

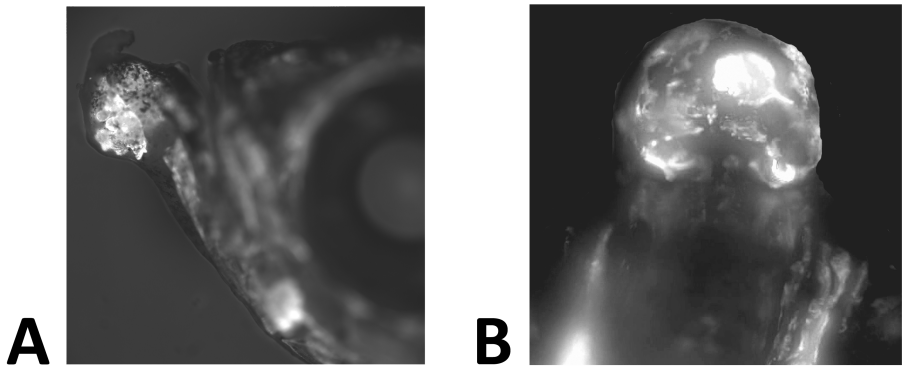

Figure 17. Osteoblast fluorescent reporters in adult TH- fish (white). **A)** Lateral view of the lesion. **B)** Ventral view of the lesion.

While we have yet to conduct more mechanistic experiments that target specific pathways, we hypothesize that TH-dysregulation affects cell proliferation and leads to the growth of massive bone lesions. TH receptors have been shown to promote SHH and IHH signaling[78] and mediate bone development by acting on stem cells through BMP4[73]. In Euthyroid fish, bound thyroid receptors inhibit SHH during developmentally appropriate time periods (Fig. 18). We hypothesize that in the absence of TH, persistent SHH signaling may affect downstream HH and BMP signaling.

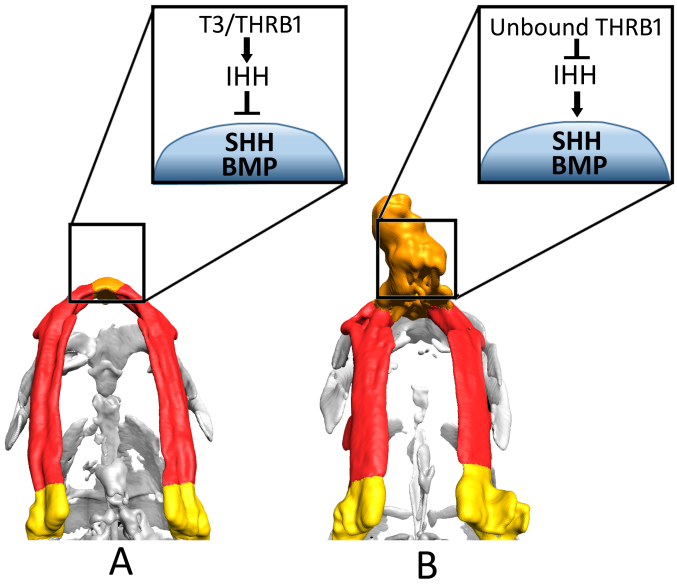

Figure 18. Concept Diagram of Proposed Mechanism. Ventral Jaw cartoons. **A)** Eu. **B)** TH-. Inset, proposed TH pathway.

Stem cells play a normal role in development, but their persistence beyond appropriate developmental time windows can lead to cancerous lesions[79]. Neural crest stem cells (NCSCs) can self-renew and give rise to multipotent MSCs, bone, cartilage, fat and melanocytes[80]. Cell lineage tracing experiments with GFP-labeled NCSC markers has revealed that a subset of post-migratory NCSC can persist in other adult tissues[74,81,82]. We hypothesize that TH- fish fail to exit a larval growth program, that stem cells remain hyper-proliferative beyond metamorphosis and that massive lesions result from cell differentiation defects. We, therefore, reason that TH may directly change expression of stem cell populations and permit continual self-renewal at the expense of differentiation.

2.1.4 Fluorescent Reporters

BMP and SHH have been identified as critical factors for NCSC self-renewal[79], as they play a crucial role in TH-mediated metamorphosis[83]. Pre-pubertal mice experience increasing TH levels, which bind to TH receptors and subsequently increase IHH, while inhibiting SHH[78]. SHH/GLI expressing cells have been shown to contribute to ectopic bone ossification in a BMP-dependent manner[84,85]. In mammals, bone suture mesenchyme and joints contain a stem cell niche that remains competent into adulthood and which aids in repair[85,86,87,88,89,90,91]. Little is known about the signaling pathways that regulate stem cells in the zebrafish dentary; however, in cranial bones, the suture mesenchyme (located between bones) have unique signaling micro-environments with SHH, BMP2/4, and FGF8 that maintain stem cells[92,93,94]. We hypothesize that a lack of TH leads to a temporospatially expanded stem cell niche, by acting on BMP and SHH pathways.

BMP

BMP regulates skeletal cell condensation, in which groups of cells begin to compact, adhere and form a distinct cartilage anlange[95]. Skeletal cell condensations continue to increase in size through cell proliferation and cadherin expression and cease growth when BMP signaling is inhibited[27]. The loss of BMP was also found to affect the transition between cell proliferation to differentiation[27]. We hypothesize that TH alters BMP regulation, leading to changes in cell differentiation and bone patterning.

We reason that persistent expression of BMP in the jaws of TH- fish may prevent cell differentiation and lead to the over-proliferation of skeletal cells. Indeed, we found evidence of

ectopic and prolonged BMP signaling in TH- fish, precisely at the location where massive bone lesions formed. At 6mm, an ectopic BMP signal is present in the presumptive dentary/palatoquadrate joint (Fig.19, left panel) At 20+ mm, TH- fish maintain strong BMP expression, with a sharp boundary delineating a BMP negative tip (Fig. 19, middle panel). Lesion formation is co-local with ectopic signaling centers, which may implicate TH-mediated stem cell regulation in lesion formation.

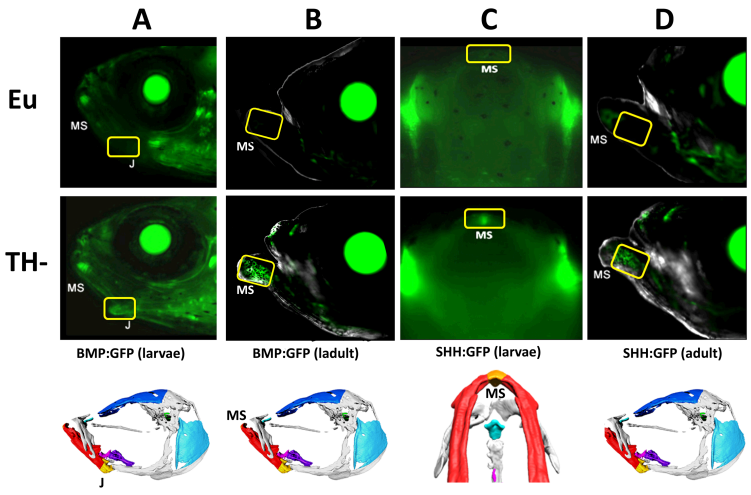

Figure 19. Fluorescent reporters (top). **A)** BMP:GFP in larvae. **B)** BMP: GFP in adult. **C)** SHH:GFP in larvae. **D)** SHH:GFP. MS, mandibular symphysis. J, joint. 3D model (bottom panel) for orientation.

SHH

Many tumors arise from inappropriate stem cell renewal[96]. One such pathway regulating stem cell proliferation is the SHH-Gli pathway, which is highly associated with osteosarcomas[97,98]. SHH is a developmentally expressed ligand important for patterning, cell proliferation and stem cell renewal[7]. SHH binds to the Patch transmembrane receptor to facilitate GLI transcription factor binding[97,99]. HH signaling can suppress BMP, which is critical for the differentiation of stem cells into mature bone-producing cells[100].

Preliminary data from transgenic fluorescent reporters showed ectopic SHH signaling in the rostral dentary, at regions where lesions form. Using fluorescent SHH reporter fish, we noticed the presence of ectopic signaling centers in 6 mm and adult TH- fish (Fig. 19C). At 20+ mm, SHH is strongly expressed in the TH- dentary (Fig. 19D). We hypothesize that ectopic

skeletal tissue in the mandibular symphysis of TH- fish may be caused by heterotopic expression of HH pathway effectors in cells residing at the mandibular symphysis.

While our preliminary data is merely correlational, our SHH and BMP fluorescent findings provide a clear future detection for testing mechanistic hypotheses. Of particular interest is the formation of ectopic bone in TH- fish. SHH has been shown to be important for maintaining undifferentiated chondrocytes, while IHH facilitates maturation and differentiation[78,84]. We propose that TH plays a causal role on these pathways and alters stem cell fat during skeletogenesis.

2.1.5 Histopathology

We hypothesize that TH is required to deplete populations of stem cells after metamorphosis and that without TH, stem cell populations persist into adulthood and give rise to bony lesions. TH- fish grow massive bone lesions that emanate from a bony stalk on the dentary and grow into cauliflower-like projections containing regions of bone, nested islands of cartilage and pigment spheres (Fig. 20). The bone lesions in TH- fish are often accompanied by a cartilage lining, cartilage-capped regions, ectopic tissue and groups of melanophores embedded within cartilage.

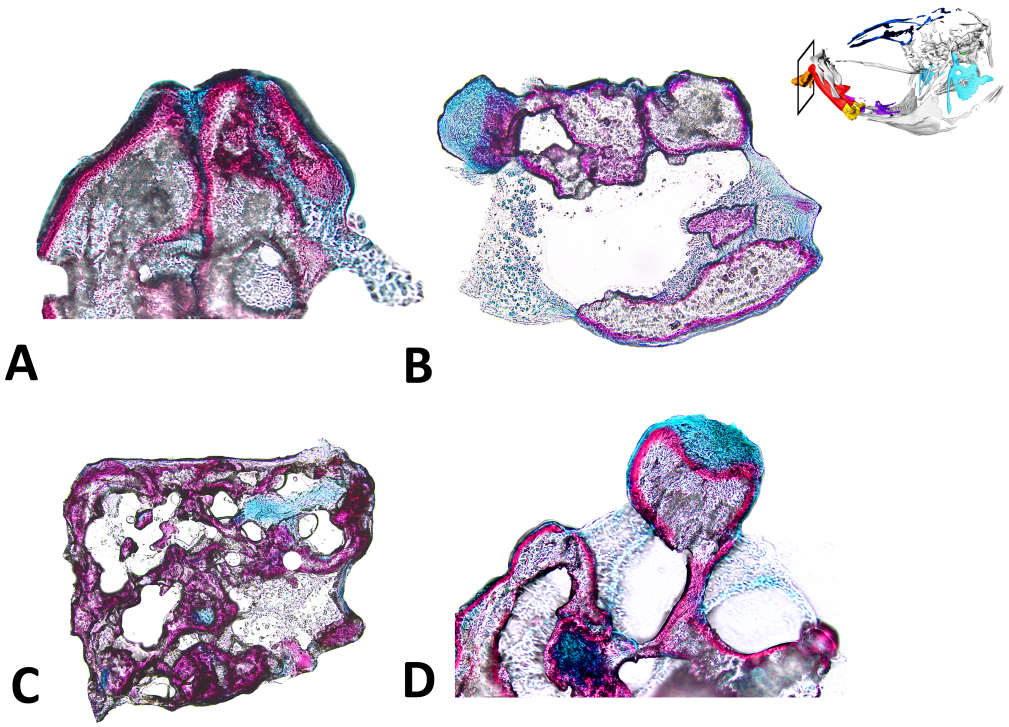

Figure 20. TH- Lesion Histology. 30 um Histological sections of a 21 mm TH- fish bon lesion at 20x magnification. Staining: Bone (Alizarin Red). Cartilage (Alcian blue). **A)** Mandibular symphysis (transverse). **B)** Cartilage capped region with the lesion (sagittal). **C,D)** Islands of cartilage inside of the lesion (sagittal).

The lesions in TH- fish potentially have three cells types nested within it: bone, cartilage and groups of pigment cells, all of which are all neural-crest derivatives[44]. The histology strongly suggests that the lesions are comprised of bone and cartilage. However, we also noted the presence of groups of pigments cells embedded inside of cartilage in TH- lesions (Fig. 22). While we did not confirm the cells are melanophores, if truly present, they may be an indicator of a cell differentiation defect, as seen in multi-tissue cancers.

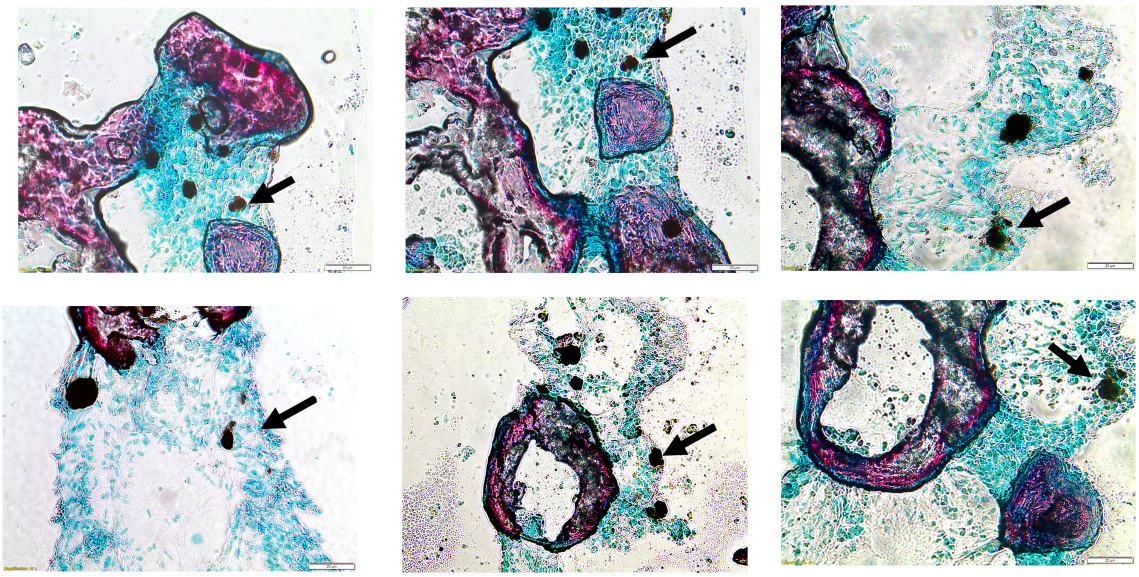

Figure 21. Pigmented Clusters of Melanophores embedded in cartilage. Histological frontal sections of a 21 mm TH- bone lesion at 20x magnification and 40 um sections. Staining: Bone (Alizarin Red). Cartilage (Alcian blue).

Our zebrafish joint segmentation includes the dentary, palatoquadrate and retroarticular bones and is considered a synovial-like joint similar to mammalian joints[101]. Articular chondrocytes line the bone and express Prg4, a crucial protein for lubrication, and in knockout mutants, fish experienced defects including cartilage erosion[101]. In TH- fish we observed abnormal joint histology, possibly indicative of a deterioration of articular cartilage (Fig. 22B).

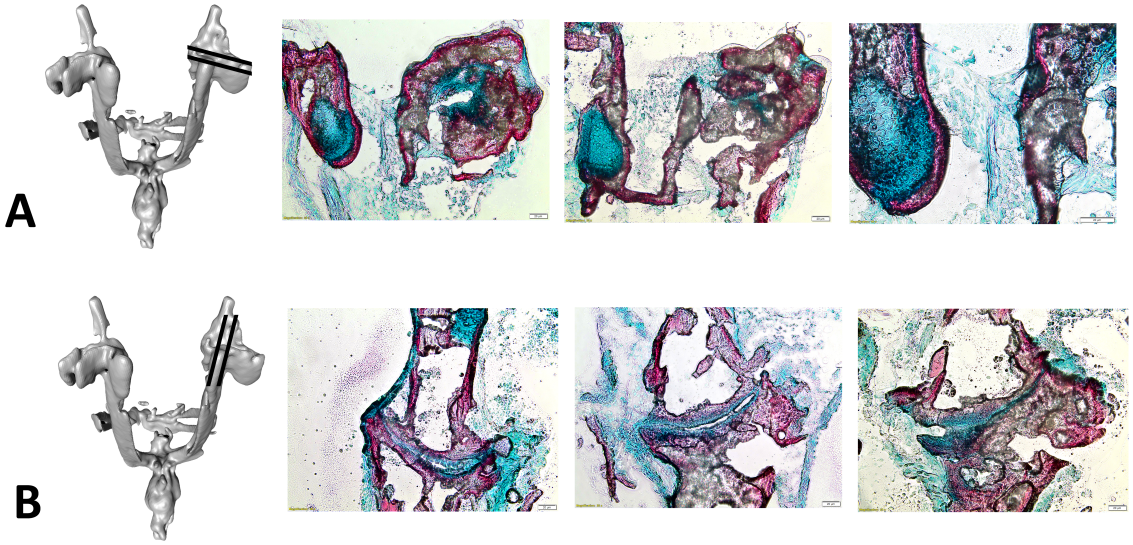

Figure 22. TH- Joint Histology of an adult TH- bone lesion at 20x magnification. 40 um sections **A)** Adult TH- joint lesion (transverse). **B)** Joint cavity (sagittal) Staining: Bone (Alizarin Red). Cartilage (Alcian blue).

2.1.6 Mandibular Symphysis Lesion

Mandibulary symphysis bone lesions are observed in TH- fish as early as 10-12 ml SL (Fig. 23). Most TH- fish grow massive lesions, comprising on average 25% of the entire dentary volume (maximum of 66%), which increases in size during head growth (Fig. 23).

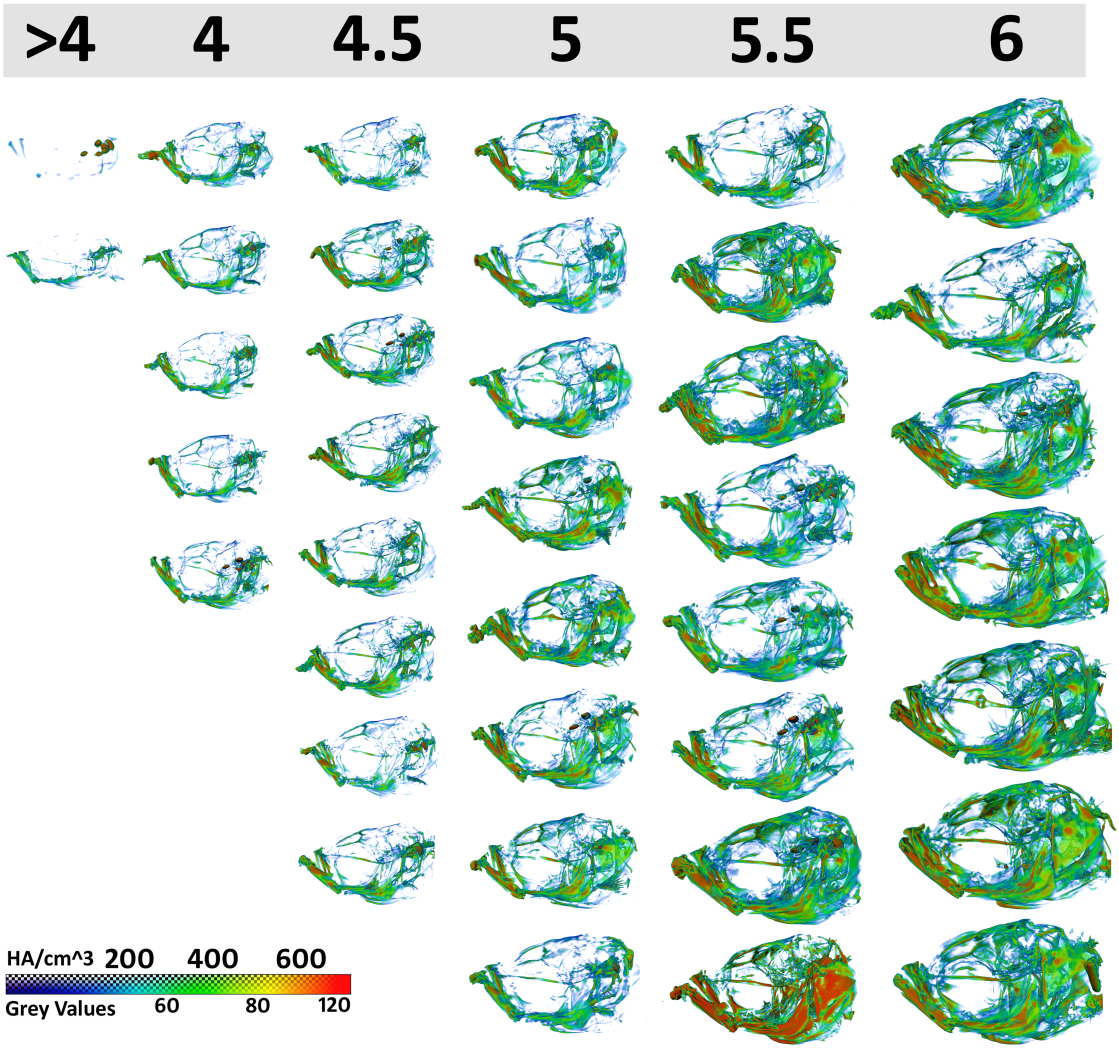

Figure 23. TH- Specimen Heatmap. Size series ranges from 2.5 - 6.5 mm (from left to right). Specimens not to scale.

2.1.7 Joint Lesions

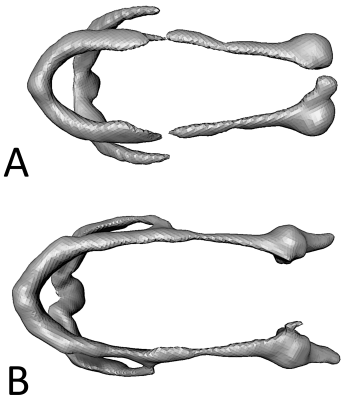

Figure 24. Developing TH- jaws (ventral view) **A)** 11 mm TH-. B) 12 mm TH-.

Joint development requires biomechanical stimuli for proper morphogenesis[52,102]. Brunt et al., demonstrated that regions of high mechanical stress in the jaw drive canonical Wnt signaling, particularly at the jaw joints at Meckel's cartilage[102]. In fact, a critical developmental time period for Wnt signaling and proliferation in joints is around 3-5 dpf, around the time of TH ablation. Wnt and mechanical stimuli can alter cell proliferation, migration, and condensation of presumptive joints[52]. We found that jaw joints on TH- fish grow massive lesions comprising on average 21% of the dentary volume (maximum 39%). Joint lesions are observed in TH- fish as early as 10-12 ml SL (Fig. 24).

Since TH- fish have previously been reported to have altered feeding kinematics[67], it is also possible that the mechanical loads on their jaws may differ from that of Eu; however, the morphological disparity between TH- and Eu should only become apparent beyond larval stages. We've seen dentary lesions occur as early as 10-12 dpf (Fig. 23), so it may be possible that TH may

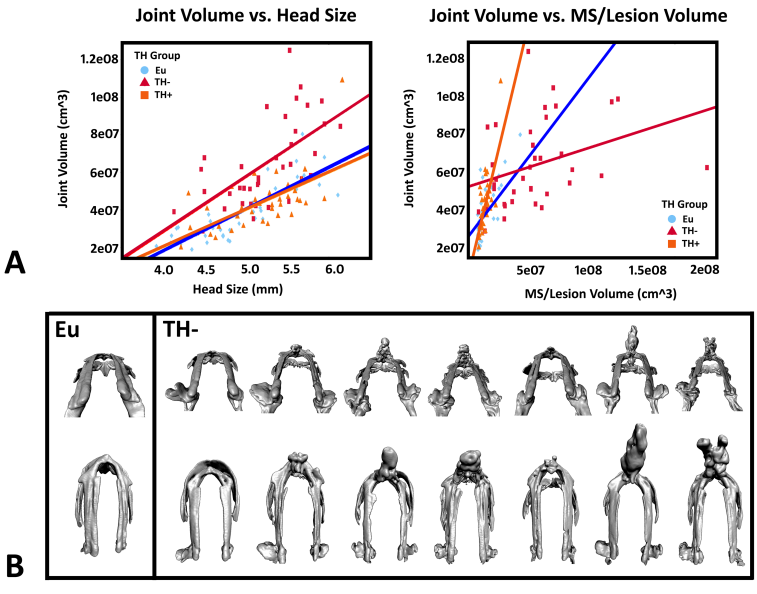

Figure 25. Joint Volume. A) Joint Volume vs Head Size (left). Joint Volume vs. MS/Lesion Volume (right). **B)** Ventral view of joints. Eu (left). TH- (right).

interact with Wnt signaling alone, or also indirectly through differential mechanotransduction. Other skeletal signaling pathways can also be affected by biomechanical stimuli including BMP and Ihh[52,103].

Fluctuating asymmetry has been observed in organisms subjected to developmental stressors and is defined as a "deterioration in developmental homeostasis" that leads to abnormal mophology[104]. We initially hypothesized that TH- Joints would have left-right asymmetry, but when we tested the width of left and right TH- joints, we found no significant differences using Welch's T-Test. Furthermore, we asked whether there was a difference between groups in asymmetry. We calculated the ratio between left and right joint width, then conducted a One-Way ANOVA on the asymmetry ratio. We found no significant differences between left and right asymmetry between TH treatment groups. TH- Jaw joints have defects, but their left/right asymmetry, notably, is not significantly disrupted.

Fish have a finite amount of calcium that is bioavailable. We asked how calcium deposition is allocated during growth and whether or not joint volume was negatively correlated to other changes in bone volume (Fig. 25A). For instance, does increased joint growth lead to decreased dermatocranium volume? We generated a correlation plot of Pearson correlation coefficients (a=0.05) and we did not find any correlation between larger joints and smaller bones in other regions. This may indicate that calcium accumulation is increased in TH- fish and not merely re-allocated.

2.1.8 Phenotypic Discussion

Our study provides insight into the role of TH as the "clock" that regulates the timing, size and shape of bones during development and mineralization. TH has previously been reported to act in a temporospatial manner on critical developmental pathways including

Wnt/Runx2, BMP, FGF, SHH and RA[6,31,32,33,34]. Preliminary histological and fluorescence data suggests that BMP and SHH levels are altered in TH-altered fish, at precisely the regions where we see ectopic bone and cartilage growth. We hypothesize that alterations in the hormonal-to-cell interface drives disorganized bone and cartilage growth at joints and bone sutures.

Adult stem cells have been identified in a wide variety of tissues, but often these cells are dormant[105]. We hypothesize that without proper TH signaling, stem cells maintain a larval growth program and fail to decelerate skeletogenic activity in adulthood. We hypothesize that TH- fish fail to properly deplete stem cell pools because it is TH-dependent. TH has been well established as an important factor regulating cell differentiation[6,16,22], thus we reason that TH- lesions result from differentiation defects.

TH might play a role in keeping skeletal stem cells in a proliferative state, preventing cell maturation and differentiation. We hypothesize that TH normally serves to deplete stem cell pools by inhibiting SHH. Aberrant Hedgehog signaling (HH) is highly associated with many tumor types and is a critical element for stem cell self-renewal[42]. TH- fish may experience delays in the natural progression of stem cells to their differentiation into prospective cell fate lineages. Histology suggests that the lesions contain up to 3 tissue types: bone, cartilage and pigment cells. While drastic differences in the size of the joints indicate alterations in cell proliferation, our histology points to potential cell differentiation defects as being the critical factor in the formation of bone lesions. In TH- fish, the formation of multi-tissue lesions begs the question of how TH might be regulating the switch between proliferation and differentiation.

Our histology and fluorescent reporter studies are preliminary; however, we have found some initial evidence that stem cell regulation may be altered in TH- fish. In particular, BMP and SHH signaling may show ectopic domains of expression that are co-local with precisely the regions we see bone lesions forming. Ectopic SHH expression at the mandibular symphysis is

present in TH- fish, but not Eu fish. Ectopic BMP expression is also present in TH- fish at the jaw joints.

This thesis would be remiss without mentioning alternative explanations for the bizarre and compelling osteochondroma-like phenotype in TH- fish. Three potentially confounding factors include transgene insertion, drug effects and ectopic expression. Since our non-treatment Tg(tg:nVenus-2a-nfnB) fish do not form skeletal pathologies, there is no indication that transgene insertion created off-target genetic effects. All of our transgenic fish were screened at 4 and 5 dpf for fluorescence in the thyroid gland (and its subsequent loss upon MTZ treatment); thus, it is unlikely that non-follicular cells are ablated during drug treatment. It is possible that during screening the sheer brightness of Venus expression in the thyroid follicles saturated contrast and prevented us from detecting diffuse cells (non-follicular) with low level GFP expression. It is also possible that drug treatment (DMSO and/or MTZ) itself may negatively impact development during a crucial time window for craniofacial skeletogenesis. Tg(tg:nVenus-2a-nfnB) fish that were treated with the DMSO control vehicle were generally sacrificed at younger ages than TH- fish, perhaps masking what is a late-emerging phenotype.

While zebrafish possess enormous potential as a model organism, its ill-defined genetic background, high genetic polymorphism and susceptibility to inbreeding depression should be acknowledged during experimental design as a factor that might confound results and reduce reproducibility[117,118,119]. For instance, craniofacial modularity was found to vary significantly between zebrafish lines (AB, Tuebingen)[72] and it is not clear if Tg(tg:nVenus-2a-nfnB) crossed into another background may produce different phenotypic results. Proper controls were implemented, but the possibility that unknown factors in the genetic background or leaky transgene expression may contribute to phenotypic phenomena cannot be discounted. Additional methods for independent validation are recommended for future experiments.

Future directions may include establishing a causal mechanism between TH regulation and cell fate in skeletogenesis. To this end, BMP and SHH are excellent candidates to further explore, as they may bridge the gap between hormonal regulation and gene regulation in skeletal stem cells. This area of research has the potential to offer mechanistic insight into the role of hormones in regulating the proliferation, differentiation and patterning of skeletal cell progenitors in development and disease.

3.0 THEORETICAL FRAMEWORK

Eco-Evo-Devo

Van Valen famously said that "evolution is the control of development by ecology"[106]. Hormones are an essential part of life history as they affect the timing of developmental stages, couple organismal growth to environmental signals, activate gene pathways and serve as an agent for developmental evolution[107,108]. Abouheif, Gilbert, Hall and others have championed the field of "eco-evo-devo," or the interface between an organism's environmental exposure, genetic regulation and developmental programming[18,109,110]. Ryuichi Matsuda laid the foundation for the role of endocrines in "pan-environmentalism," or the process of integrating environmental signals into the developing phenotype[18]. Hormones serve as the organism-environment interface and has been implicated in heterochronic changes to ontogeny, Matsuda termed "abnormal metamorphosis"[18].

We observed dramatic changes to the reaction norm of mineralization in fish with altered TH profiles. We hypothesize that our TH-dysregulated fish experience a loss of species-specific patterning, including proper growth and patterning of skeletal domains. The developmental trajectory, deviations in size and shape, and mineralization rates are highly altered in TH- and TH+ fish bones. A body work from our lab and others indicates that TH- fish experience some features of paedomorphosis by maintaining a larval growth program[59,61]. TH- fish contain bone regions that experience extended periods of growth, beyond normal developmental time windows. We hypothesize that without receiving the proper signals that terminate metamorphosis, TH- fish skeletal cells retain proliferative potential and continue to grow at accelerated rates. While we have yet to determine a causal relationship between TH

and skeletal stem cell dysregulation in our pathological bone, future directions should include mechanistic experimentation to establish a causal link between stem cell fate and TH profile.

Hormones in Development and Evolution

Hormones have evolved an integral role in controlling developmental trajectories in animals. Ancient hormone receptor pathways, like Retinoic Acid receptors (RARs), date back to the last common ancestor of bilaterians[113]. TH is not just utilized by vertebrates for development, but is also involved in invertebrate development, such as sea urchin larval metamorphosis[112]. Evidence from the chordate amphioxus suggests that components of the TH pathway have evolved multiple times independently[114]. We hypothesize that TH has canalized a critical role as an actuator of developmental programs in skeletogenesis.

We observed that all bones for TH- fish demonstrated under-mineralization with the exception of the early-ossifying dentary. The dentary shaft is more mineralized than Eu, while the joints and symphysis form massive bone lesions. Altering hormone regulation may cause disruptions in canalized programs for dentary development and lead to a loss of cell regulation, including proliferation and differentiation. One so-called missing link in Matsuda's pan-environmentalism hypothesis is an explanation of epigenetic-environment interactions that affect bone forming migratory cells, like NCCs[18]. TH may serve as this missing link by regulating the timing and rate of skeletal stem cells during developmental transitions. We conclude that TH is an important component of morphological development and evolution by acting to regulate developmental transitions and stabilize life history stages.

The timing and fidelity of skeletogenesis depends on proper TH regulation. Evolutionary alterations to TH regulation have been associated with paedomorphism and the retention of juvenile-like skeletal features. While we have yet to demonstrate what the causal mechanism of

TH action on bone mineralization is, our data indicates that TH may regulate SHH and BMP, key effectors of cell proliferation and skeletal tissue condensation. Research into Hormone regulatory networks have the potential to shed light on how morphology is shaped by development and evolution.

4.0 SUPPLEMENTAL

4.1 Supplemental Data

Comparison	Transformation Factor	Method	Analysis	Model	F statistic	Mean	Std	Adjusted R^2	Test P-val	TH- -Eu	TH+-Eu	BF Adj. p-val	FDR Adj. p-val
MS/Lesion Mass	-1*(mass)^-0.38	Boxplot	One Way ANOVA	density ~ TH group	49.67	1695100	2116507	NA	5.06E-16	<2e-16	1.56E-01	0.00E+00	0.00E+00
MS/Lesion Volume	-1*(volume)^-0.44	Boxplot	One Way ANOVA	density ~ TH group	54.37	25265124	30713646	NA	<2e-16	<2e-16	1.78E-01	0.00E+00	0.00E+00
Dermatocranium Density	-1*(density)^-0.558	Boxplot	KW One Way ANOVA by Ranks	density ~ TH group	40.773	424	79	NA	1.40E-09	2.81E-03	1.10E-04	2.24E-08	4.48E-09
Dermatocranium Volume	(volume)^0.191	Boxplot	One Way ANOVA	density ~ TH group	18.902	379559759	180458993	NA	7.86E-05	1.10E-02	1.17E-01	1.26E-03	9.67E-05
Otolith Density	(density)^2.907	Boxplot	KW One Way ANOVA by Ranks	density ~ TH group	18.902	1045.25	245.75	NA	7.86E-05	5.10E-03	7.30E-03	1.26E-03	9.67E-05
Opercle Density	-1*(density)^-0.802	Boxplot	One Way ANOVA	density ~ TH group	9.55	428.36	55.6	NA	1.52E-04	4.80E-02	1.20E-01	2.43E-03	1.74E-04
Kinethmoid Density	(density)^0.148	Boxplot	One Way ANOVA	density ~ TH group	85.19	424.38	87	NA	<2e-16	<2e-16	2.70E-03	0.00E+00	0.00E+00
Hyoid Density	-1*(density)^-0.946	Boxplot	One Way ANOVA	density ~ TH group	25.41	376.32	41.23	NA	9.02E-10	4.80E-01	7.00E-07	1.44E-08	3.61E-09
Joint Density	-1*(density)^-0.842	Boxplot	One Way ANOVA	density ~ TH group	18.06	530.01	59.37	NA	1.71E-07	7.50E-01	1.49E-05	2.74E-06	3.91E-07
Joint Mass	-1*(mass)^-0.07	Boxplot	One Way ANOVA	density ~ TH group	15.99	2950535	1308168	NA	8.26E-07	4.00E-07	5.02E-02	1.32E-05	1.47E-06
Joint Volume	-1*(volume)^-0.181	Boxplot	One Way ANOVA	density ~ TH group	22.9	48483452	21223747	NA	5.13E-09	<2e-16	1.50E-01	8.21E-08	1.37E-08
Whole Head Density	-1*(density)^-0.881	Boxplot	One Way ANOVA	density ~ TH group	17.16	446.74	42.5	NA	3.39E-07	9.80E-01	6.90E-06	5.42E-06	6.78E-07
Total Dent Dens vs. Head Size	(density)^0.069	Linear	One Way ANOVA	density ~ TH group + headsize	48.8	NA	NA	0.56	3.90E-10	7.00E-03	3.13E-07	3.90E-09	7.80E-10
Dentary Shaft Dens vs. Head Size	(density)^0.184	Linear	One Way ANOVA	density ~ TH group + headsize	48.09	NA	NA	0.56	8.66E-10	1.73E-09	1.20E-06	8.66E-09	1.44E-09
MS/Lesion Dens vs. Head Size	-1*(density)^-0.59	Linear	One Way ANOVA	density ~ TH group + headsize	12.97	NA	NA	0.246	1.34E-02	2.68E-02	5.20E-02	1.34E-01	1.34E-02
Joint Dens vs Head Size	-1*(density)^-0.842	Linear	One Way ANOVA	density ~ TH group + headsize	30.35	NA	NA	0.44	1.40E-09	2.80E-09	2.51E-05	1.40E-08	2.00E-09
Dermato Dens vs Head Size	-1*(density)^-0.558	Linear	One Way ANOVA	density ~ TH group + headsize	89.4	NA	NA	0.706	2.00E-16	4.13E-12	2.00E-05	2.00E-16	4.00E-16
Kinethmoid Dens vs Head Size	(density)^0.148	Linear	One Way ANOVA	density ~ TH group + headsize	84.72	NA	NA	0.69	2.00E-16	2.00E-16	0.00632	2.00E-16	4.00E-16
Otolith Dens vs Head Size	(density)^2.907	Linear	One Way ANOVA	density ~ TH group + headsize	5.98	NA	NA	0.119	3.30E-04	6.60E-04	9.00E-02	3.30E-03	3.60E-04
Opercle Dens vs Head Size	-1*(density)^-0.802	Linear	One Way ANOVA	density ~ TH group + headsize	36.88	NA	NA	0.49	6.35E-07	1.27E-06	3.20E-01	6.35E-06	7.93E-07
Hyoid Dens vs Head Size	-1*(density)^-0.946	Linear	One Way ANOVA	density ~ TH group + headsize	47.06	NA	NA	0.556	2.00E-16	1.54E-03	4.11E-07	1.00E-12	4.00E-16
Whole Head Dens vs Head Size	-1*(density)^-0.881	Linear	One Way ANOVA	density ~ TH group + headsize	39.2	NA	NA	0.51	3.05E-10	4.08E-02	6.04E-06	3.05E-09	7.62E-10

Table 1. Statistics Summary Table

Bone Density	All mean	All Std.	Eu mean	TH- mean	TH+ mean	Eu max	TH- max	TH+ max	LM R^2	LM Intercept	TH- LM Slope	TH+ LM Slope	TH- % slower	TH+ % faster
Whole Dentary	550.13	63.48	513.71	552.63	584.01	675.94	675.84	700.6	0.56	142.48	16.53	53.61	30.8	324.3
Dentary Shaft	547.82	64.84	509.33	555.84	578.28	675.46	677.56	706.61	0.56	127.99	23.33	51.75	45.1	221.8
MS/Lesion	589.65	75.6	565.51	594.94	608.51	732.64	872.13	744.18	0.25	233.78	9.26	28.03	33.0	302.7
Joint	530.02	59.37	512.41	504.84	572.79	673.02	614.94	676.5	0.44	252	-23.4	48.63	48.1	207.8
Dermato	424	79.01	418.11	369.31	484.59	608.04	480.56	613.11	0.71	-25.5	-75.77	46.46	163.1	61.3
Kinethmoid	424.38	87.04	445.43	335.3	492.42	634.72	440.28	645.79	0.69	184.038	-126.02	35.19	358.1	27.9
Otolith	1045.25	245.75	1080.52	951.54	1103.67	1276.86	1307.38	1378.4	0.12	1076	-129.25	22.94	563.4	17.7
Opercle	428.36	55.61	428.73	402.36	453.99	585.52	508.88	604.33	0.47	112.53	-45.6	10.995	414.7	24.1
Hyoid	376.33	41.23	364.56	255.26	409.16	450.11	405.49	505.31	0.56	168.507	-21.23	35.75	59.4	168.4
Whole Head	446.74	42.51	432.85	430.86	476.53	528.89	493.87	553.29	0.51	214.3	-15.27	33.817	45.2	221.5

Table 2. Bone Linear Model Table

4.2 Density Quantification Guide

Data Management

I recommend using cropped **.bmp** image stacks to reduce memory load Amira. Images can be scaled and/or cropped in ImageJ beforehand to reduce memory load (recommended 900 x 900). If you load 1,000s of high-resolution images into Amira, performance will greatly decrease as the memory load increases. This will cause lagging and can cause the program to crash while you are segmenting. You can make sweeping changes on entire image stacks using ImageJ.

ImageJ

Import BMP stack as an **Image Sequence** into ImageJ. Use the rectangular selection tool to choose the region of interest (ROI). Scroll through the image stack using the **slider** at the bottom. Ensure that every slice includes your ROI. Adjust borders of the selection tool as needed. When you're done, click on **Image,** then **Crop**. Every photo in your stack has now been changed. Save the whole stack as an **Image Sequence** to a new folder. Use appended file names to indicate that you have altered the dataset (ie dataset1_cropped_800x800).
Never write over original data!

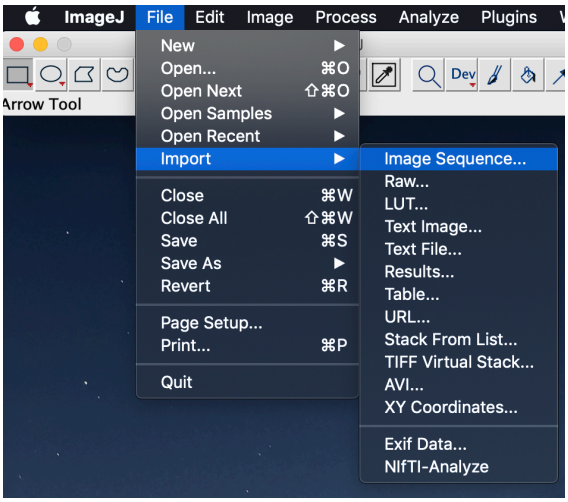

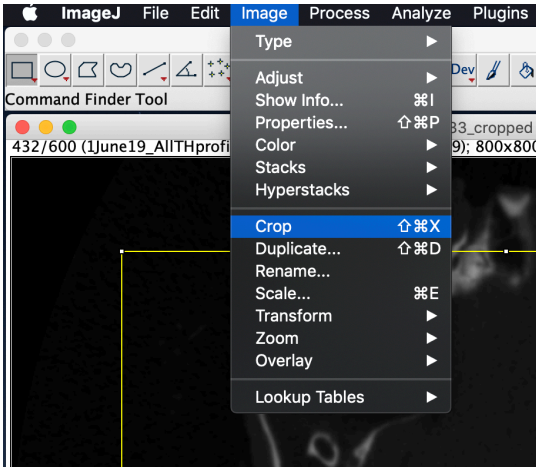

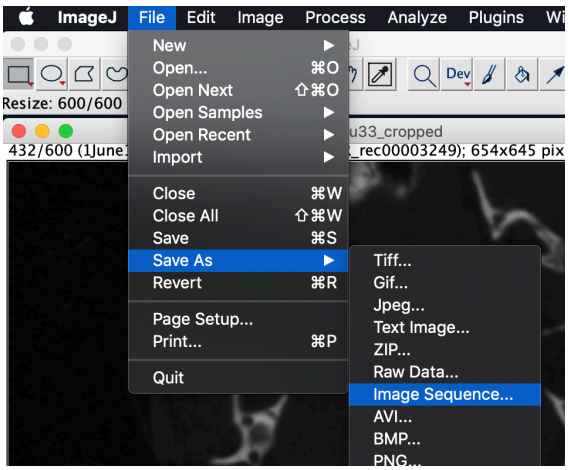

Setting up Amira

Load the cropped stack into Amira by selecting all the files, then dragging and dropping them into the main area of the Project tab. You can also click on File, then Open and load the dataset.

A note on windows: New users frequently encounter issues navigating Amira. The Project Window can be accidentally undocked and hidden in Amira. To re-dock the window, click and

drag the window to the left hand margin of Amira, abut half-way down. Release the window and it should dock on top of the Properties tab.
Amira will prompt you to enter a pixel size. Check the log file from the Bruker scan. I scanned at 10.5 um resolution, thus I entered in 10.5^3 as the voxel size. Setting these parameters only matters if you want to acquire length measurements or if you want to collect volume measurements.

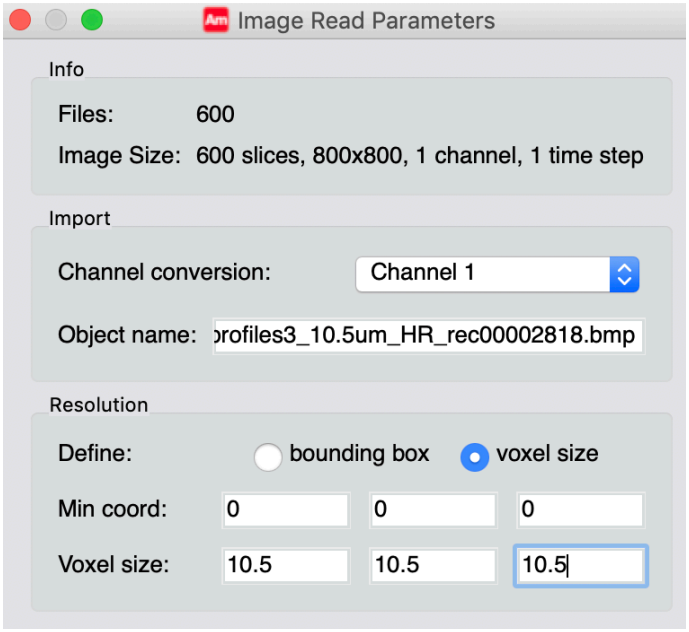

Once you have loaded the bmp files and will see a **green bar** that represents the Amira bmp stack. Click on the tiny **grey arrow** on the right-most side of the green bar.

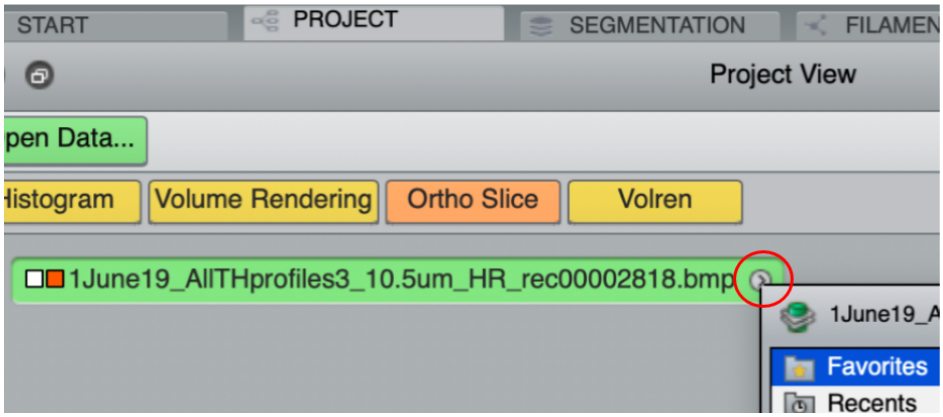

This will pop-up another box with options. Click on the icon of the tiny folder with yellow arrow to **Export As**.

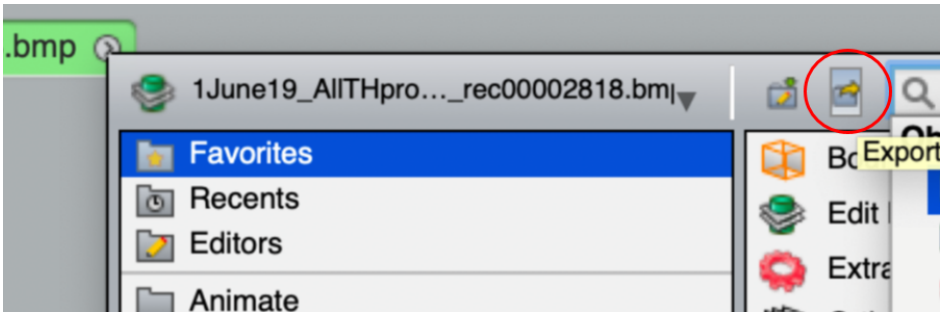

Select **Nifti** as file type. Amira handles this file format much better during segmentation. Save as **.nii** file. Delete the .bmp dataset. Drag and drop the Nifti file into the main window.

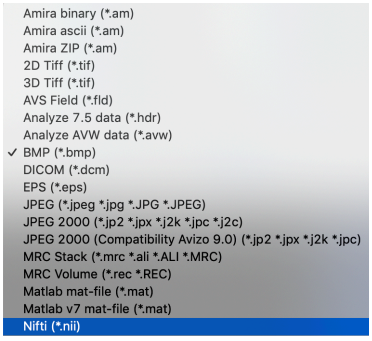

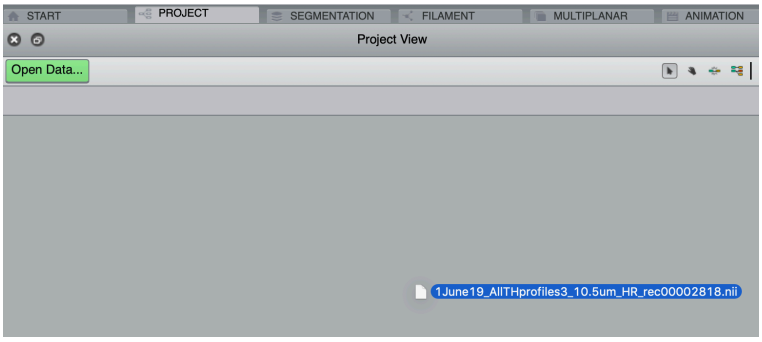

For segmentation, you will ultimately need 2 files: the **.nii** file and an **.am** file. By clicking on the Segmentation tab at the top, Amira will automatically generate an .am file. If you click back to the Project tab, you will now see an .am file.

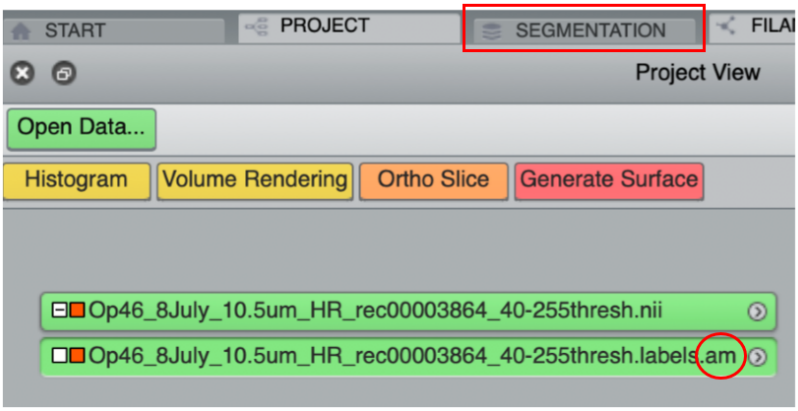

Save both files. If you need to stop segmentation and open it again on another day, drag both files into the Project window. Click on the .am file and select the .nii file in the **Image Data** section. Now the 2 files are connected and you can continue segmenting in Amira.

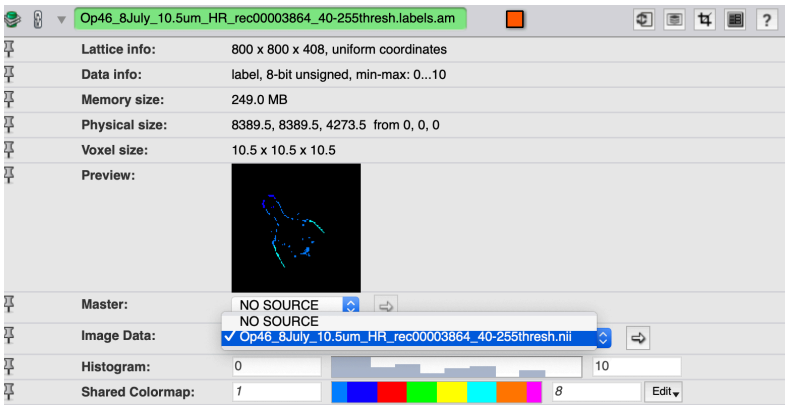

Now, click back onto the Segmentation Editor tab. The default setting is the orthographic/slice view of the data. If you want to segment in 3D, you will have to switch views.

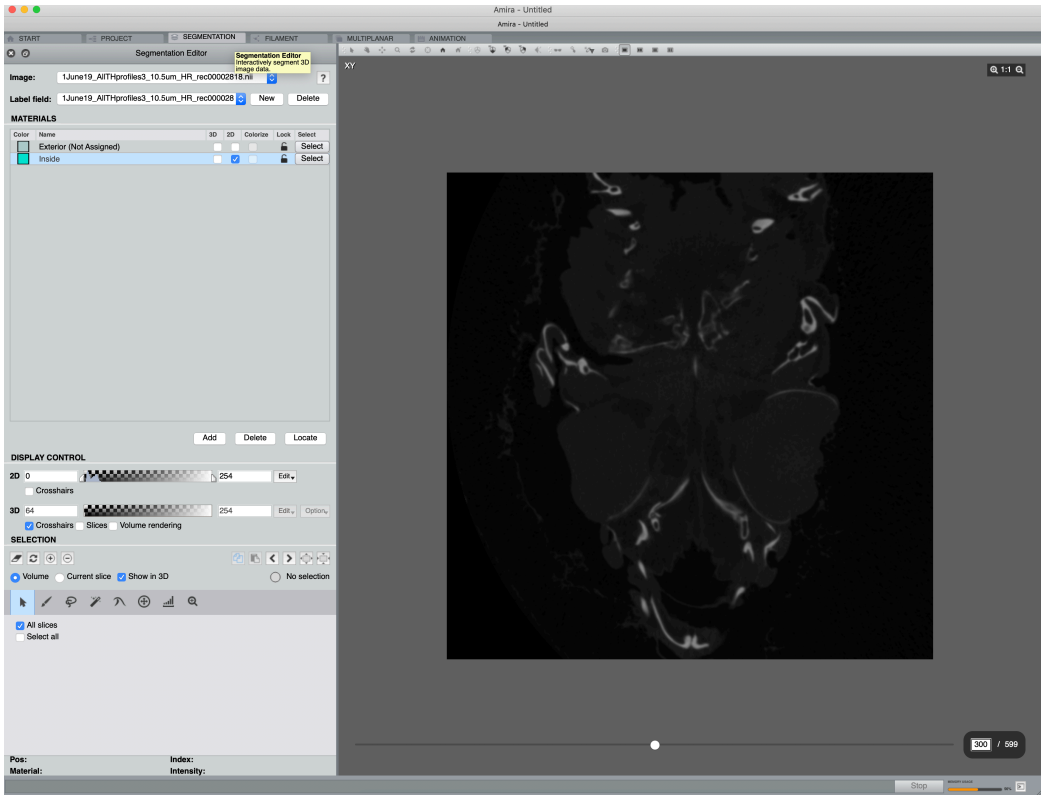

You can do this by clicking on the 4-panel icon at the top of the gray bar.

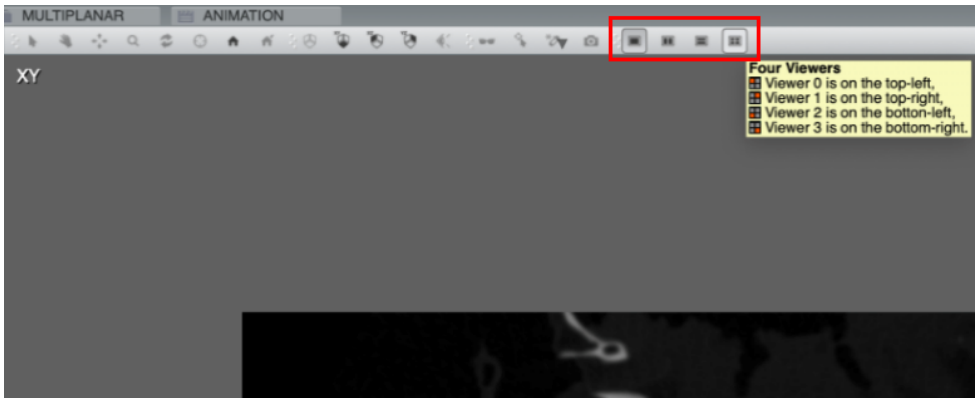

Now you have 3 orthographic views and a 3D panel that only displays 3D crosshairs.

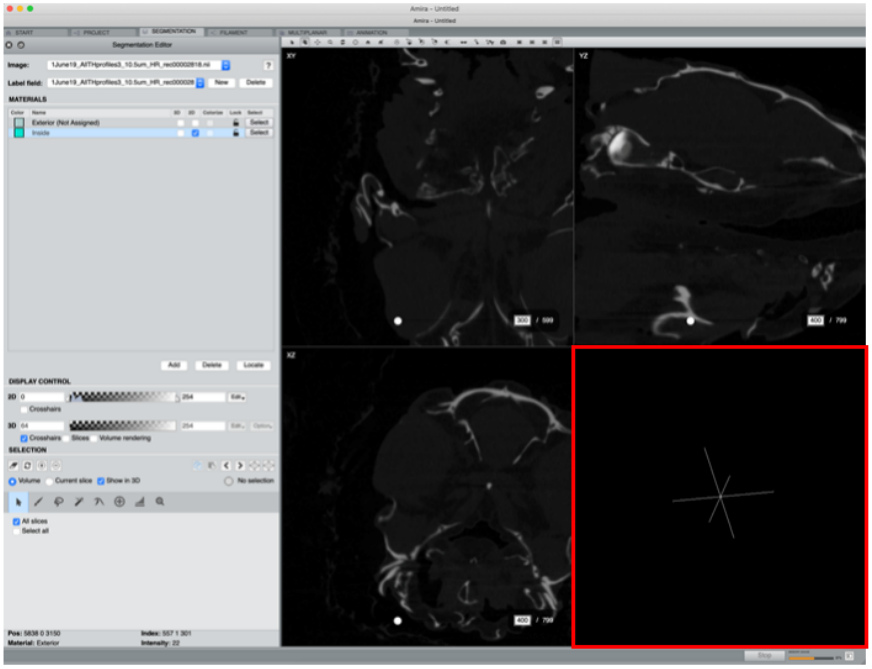

Click on the 3D crosshairs and rotate in 3D by clicking and dragging. Amira is now tuned into this 3D panel. Now click on the **Single Viewer** icon.

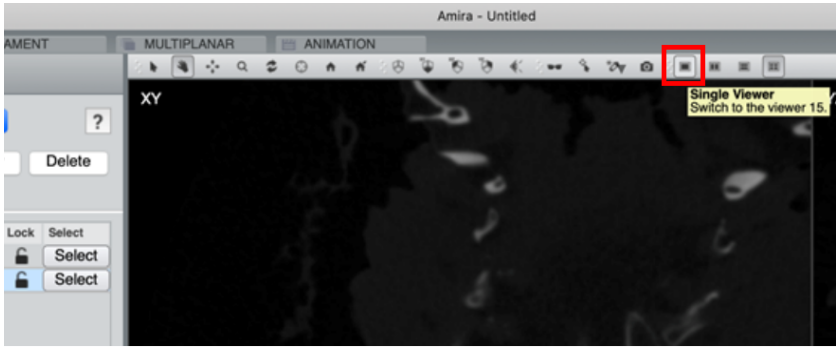

You are now in 3D view mode. The model is dark and opaque.

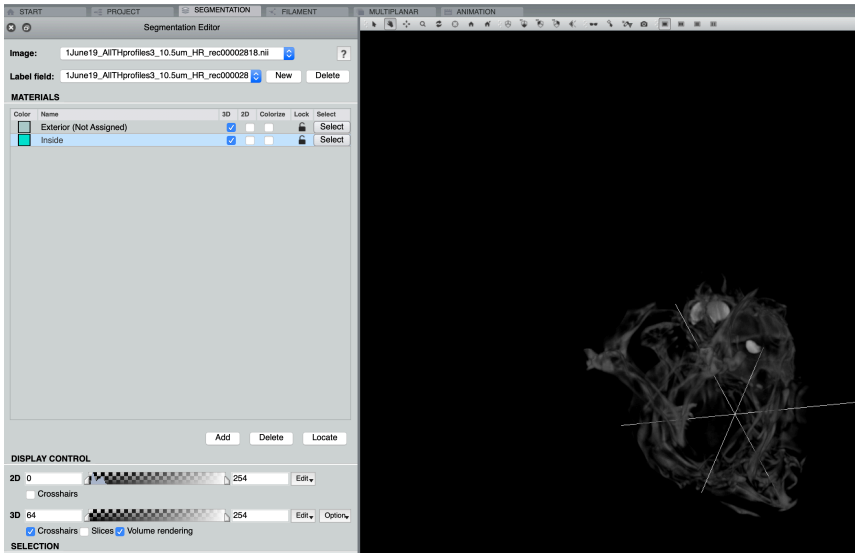

To increase brightness and contrast, adjust the **Display Control** Thresholding. This will not change the underlying data, but will make it much easier to delineate borders when segmenting. During the course of segmentation, you should check for hidden pixels by adjusting the range to 0-50. However, this will distort borders, so it is recommended you segment in a range more like 40-120.

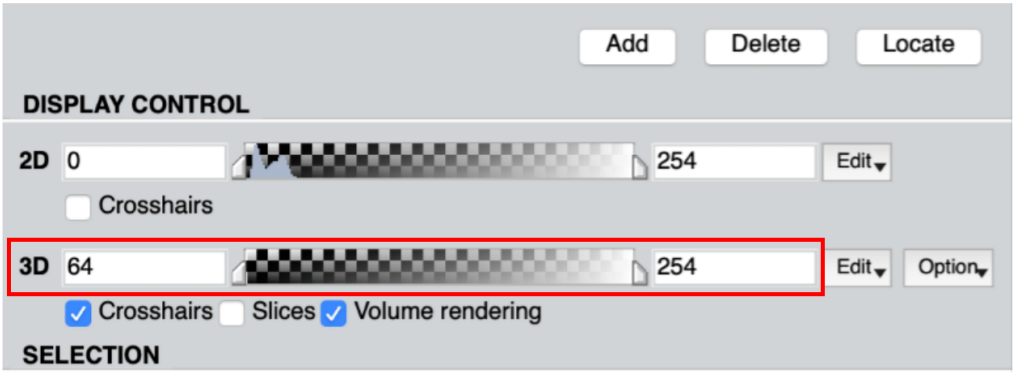

Click on the **Volume Rendering** button to see a greyscale image of the dataset. If you like, uncheck the crosshairs button.

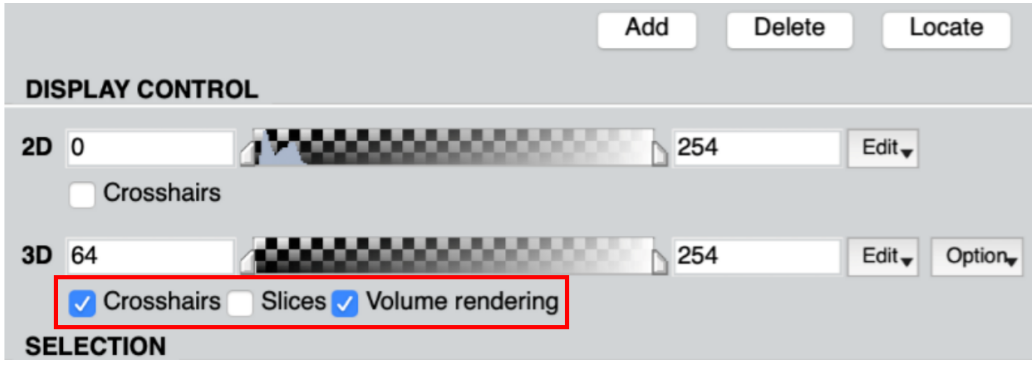

I prefer Specular view, so I select the **Option** button in the 3D display section, choosing **Specular**.

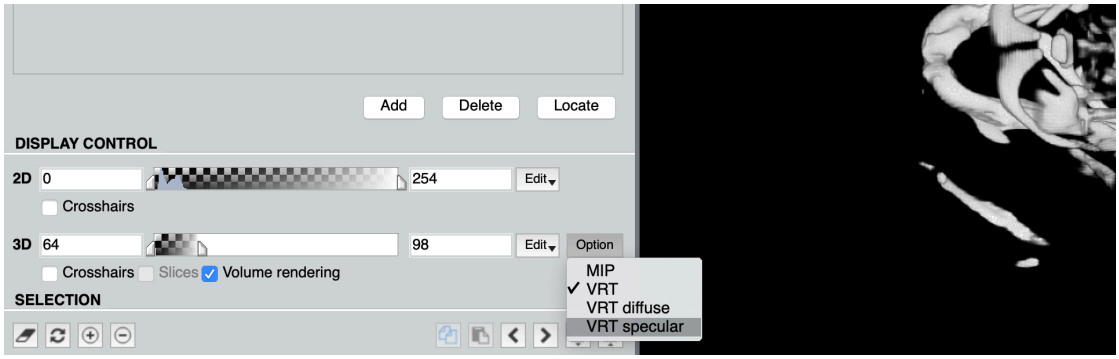

Now comes the most important part of segmenting. If you screw this up, you will end up seeing giant red lego blocks of your 3D model instead of your meticulously segmented bones. If you do this, there is no fixing the file and you have to start over. The critical step is **to select all of the pixels in the Exterior Layer, add them to the Interior Layer**, then **LOCK the Exterior Layer**.

The general concept of segmenting in Amira is that all the pixels of your scan must go somewhere. You can't really delete them. You can only move them to a new layer. If you delete a Material, all of the pixels will be added back to the Exterior Layer. Note that if you generate a surface, all materials will be displayed except for the Exterior Layer.

When you first start segmenting, all the pixels exist in the Exterior Layer (Amira calls Layers a **Material**). You must select them and add all the pixels to an **Inside** Layer. From there you can take from the Inside Layer and add pixels to other bone layers. To do this, you must use the Thresholding Tool to select from Exterior and add to Interior. Click on the Threshold Icon.

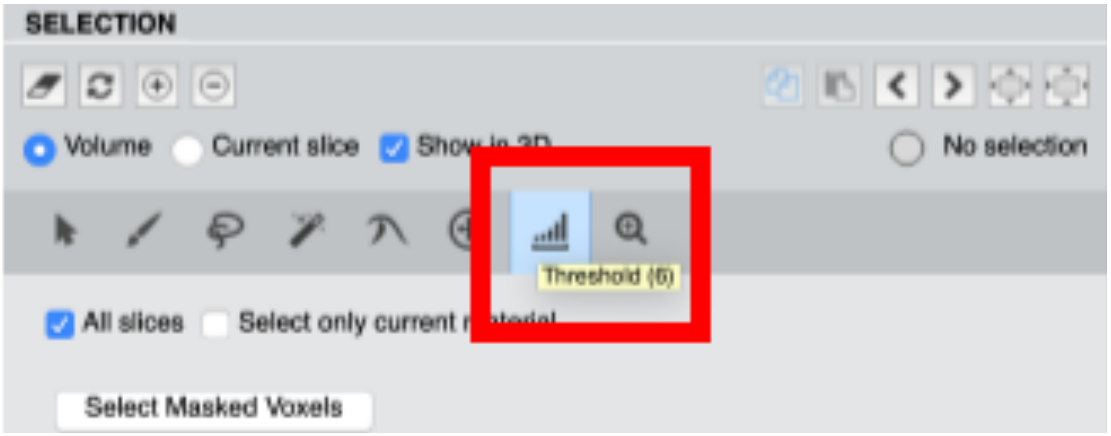

If you want to select all pixels, you can set the Masking Range from 0-255 pixels. To determine proper thresholding, it is recommended that you generate an Alizarin reference sample. From a skeletal prep, I confirmed that anything under 40 pixels is non-bone tissue and can be discluded from bone density quantifications.

Select Masking 39-255 and hit the **Select Masked Voxels Button**.

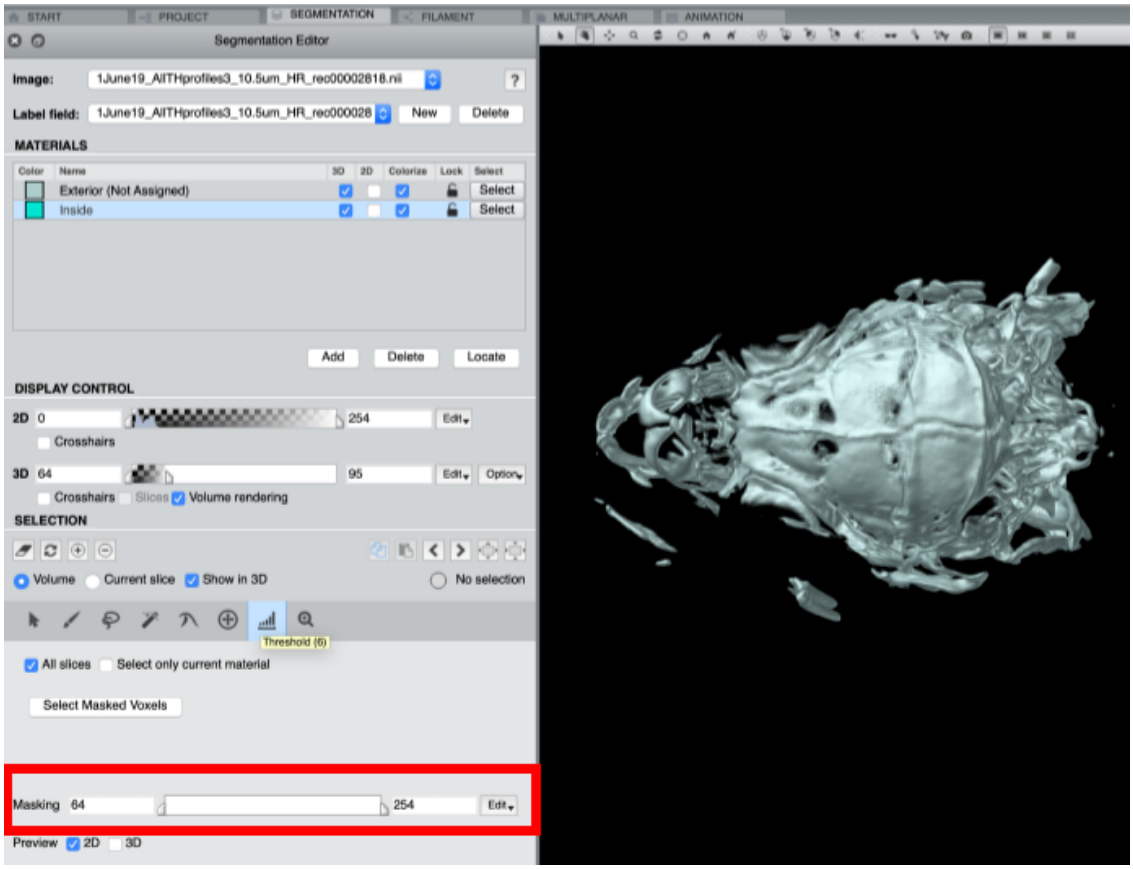

You want All Slices. Only check the Select only current material if you want to take away pixels from a specific bone layer, to add them back to another layer.

The selection will now show all the pixels highlighted in red. These pixels are only selected. You will have to add them to a layer to transfer them. You can do so by clicking on the **Inside Layer**. This will highlight the Layer in blue.

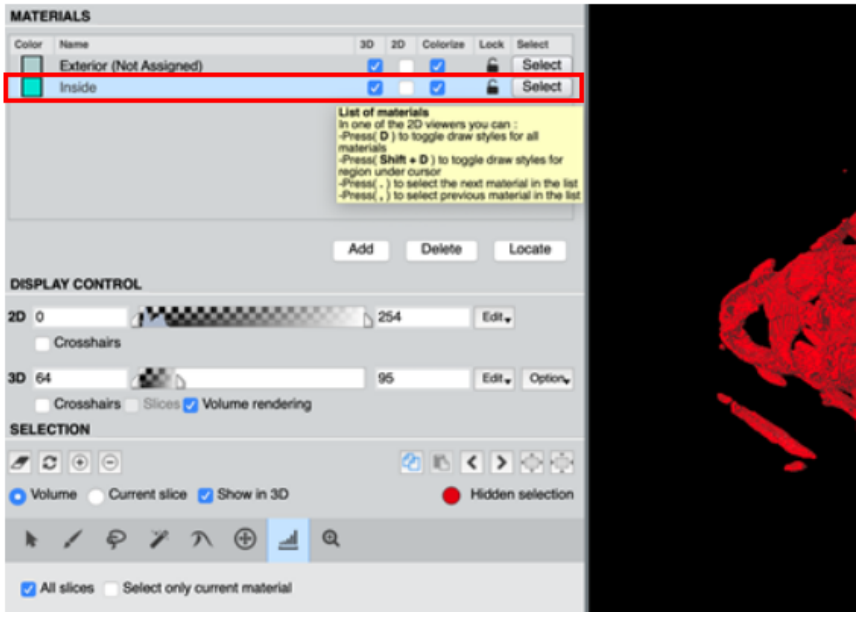

Now click on the **+** button in the Selection Toolbar Region.

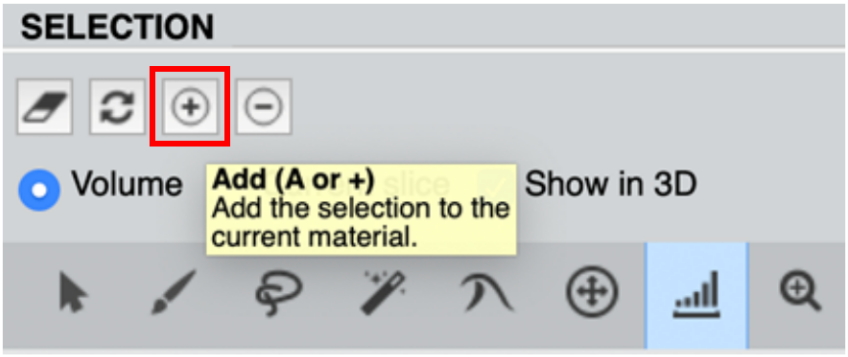

Now, all the pixels from Exterior have been added to Interior. Amira is not great at updating the layer's appearance after you've transferred pixels to new layers. For this reason, I continually click the **Colorize** button on and off to update the colorization. You will see the gray pixels become green. This confirms they have been added to the correct layer. If you want to change colors of Layers/Materials click on the green box to the left. You can then change colors.

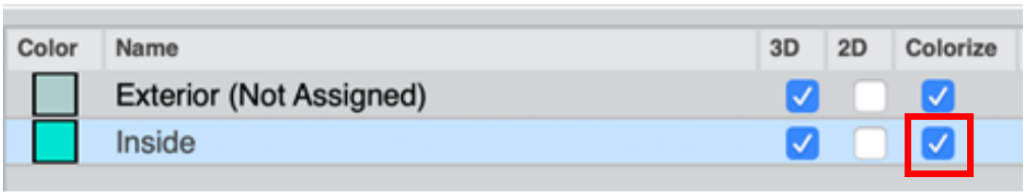

Now that all the pixels are in the **Inside** layer, you **MUST LOCK** the Exterior Layer. If you attempt to keep segmenting with the Exterior Layer unlocked, this will screw up your entire segmentation!!

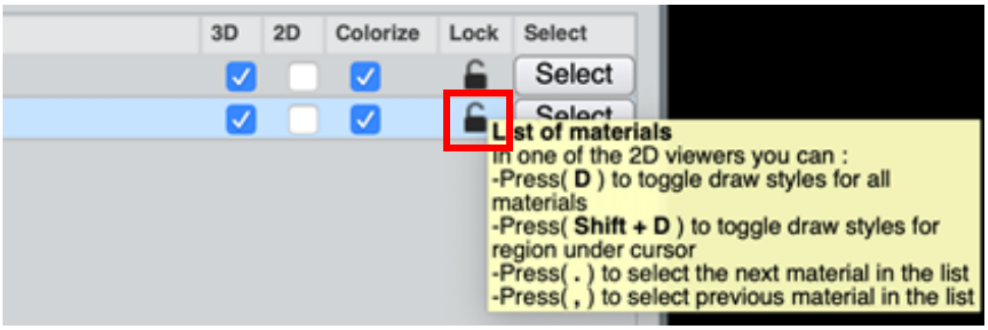

You can see below that the Exterior Layer has a lock symbol beside it.

I will also point out at this time that there is a big difference between true Thresholding and Display Control Thresholding. True thresholding will drop out all pixels below a certain range; this is done during reconstruction, or through ImageJ. You are losing real data when you threshold. This is useful when you want to disclude all non-bone pixels, but just make sure you are universally standardizing (and recording your methods) for thresholds so you can quantify density properly between specimens.

Display Thresholding doesn't change the underlying data, it only changes what you can see. For instance, when you load in a dataset, the skull looks a little translucent, which makes it hard to segment well-defined boundaries. In the picture below, the Display threshold is set from 64-231.

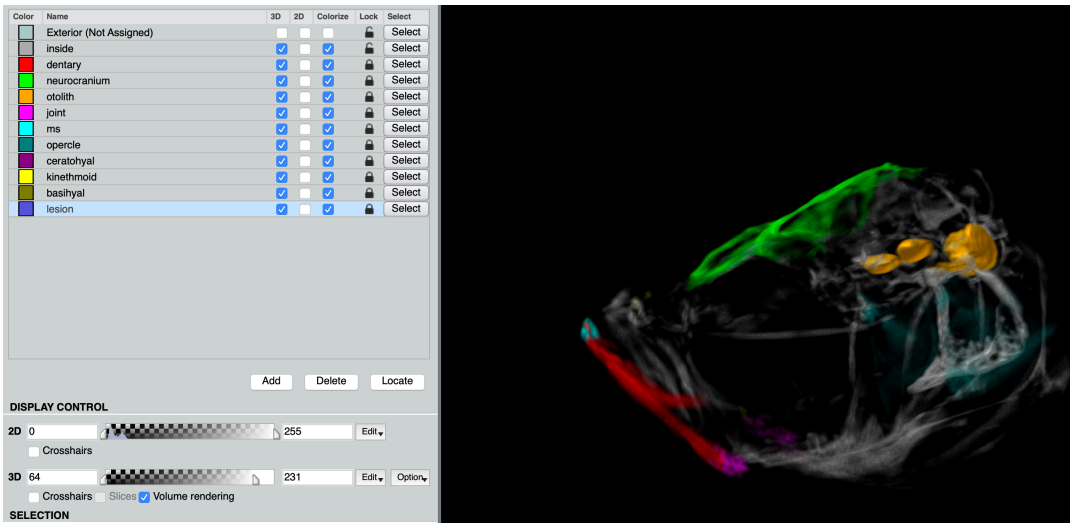

I changed the Display Thresholding so that the skull boundaries are much more visible. I segment with a high contrast display (ie 40-70). Then when I think I'm done, I'll check the bone segmentation by taking the range all the way down from 0-20 to check for very soft pixels that I might have missed. Before you finalize your quantifications, be sure to check that there are no hidden pixels between 0-20 that are in the wrong layer.

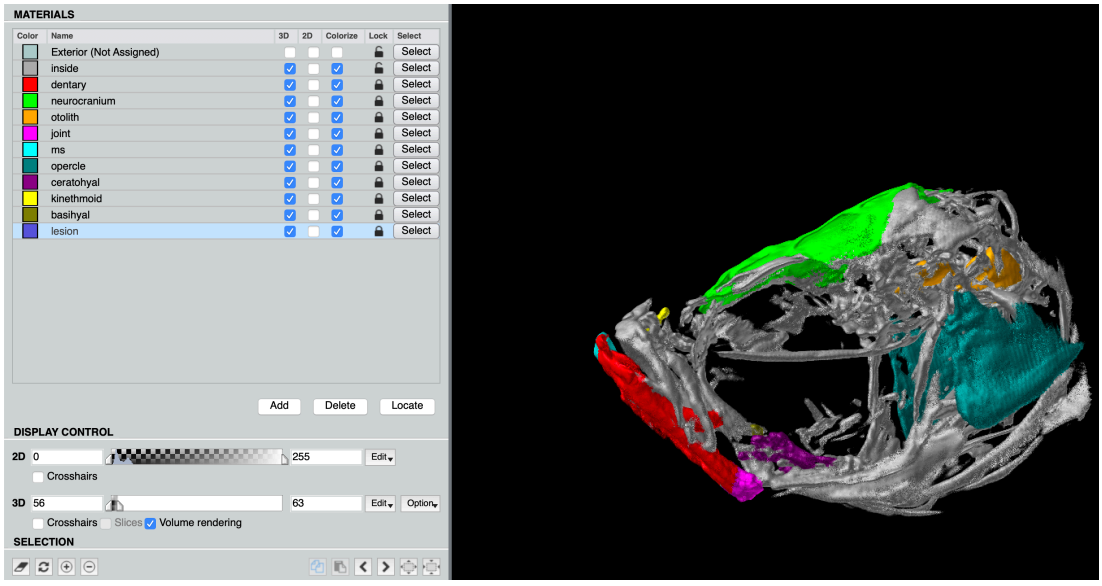

Another display feature includes showing 3D and colorization. For all the layers I'm working with, I check the 3D button and Colorize button.

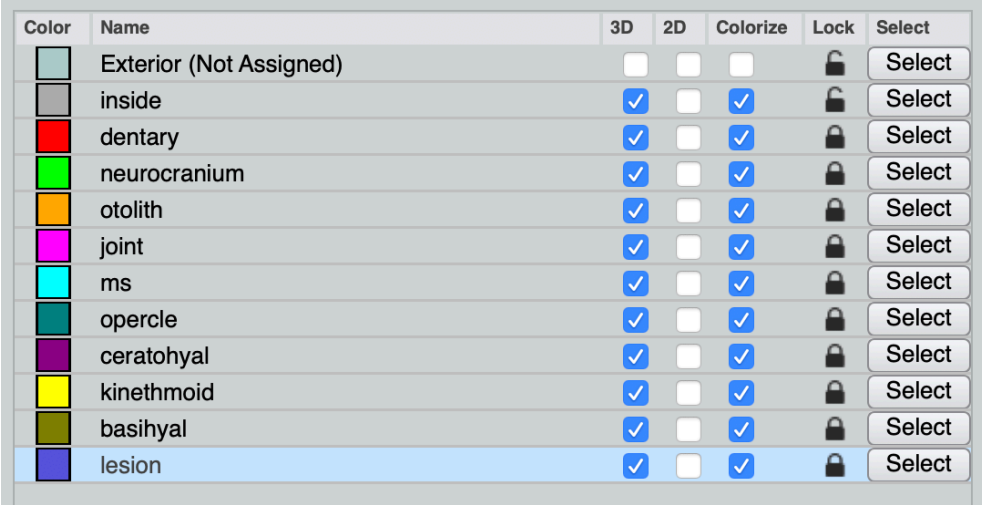

Now, to add a new Layer/Material, click the **Add** button. Double click on the New Material to name the bone. Note that if you want to automate analysis of the quantifications using R Studio, it is important to standardize the Layer names (case sensitive) and their order.

Note that both the Inside layer and the Bone layer are unlocked. This means that if you use the 3D Selection tool while you are segmenting, pixels from **BOTH** layers can be altered. If you are doing a multi-bone segmentation, this can **UNDO** all your work! Make sure that **ONLY** the layers you are working with are unlocked and **LOCK** all other layers!! The general concept of segmentation includes taking from one layer and adding to another layer. If two layers are unlocked, the default is that Amira will take pixels from one layer and add it to whatever layer is selected (highlighted in blue). Before you click the **Add** Button, make sure the selected layer is the one that you want to move pixels **to**.

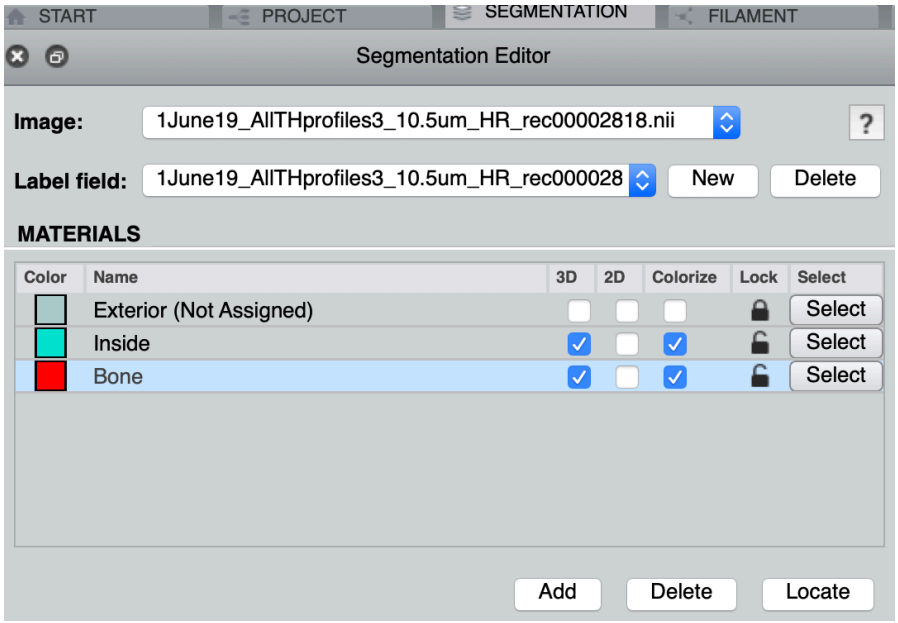

In the picture above, I will be taking from the **Inside** layer (which now holds all pixels) and adding them to the new Bone layer. You can do this by selecting the Freehand Lasso Tool and drawing a selection on the 3D model.

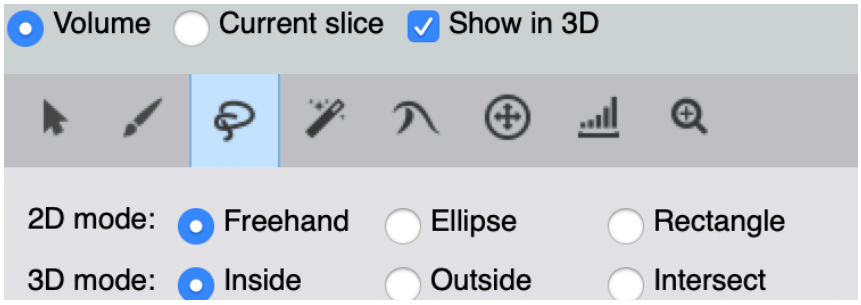

Below in red is the selection of the dentary shown in red.

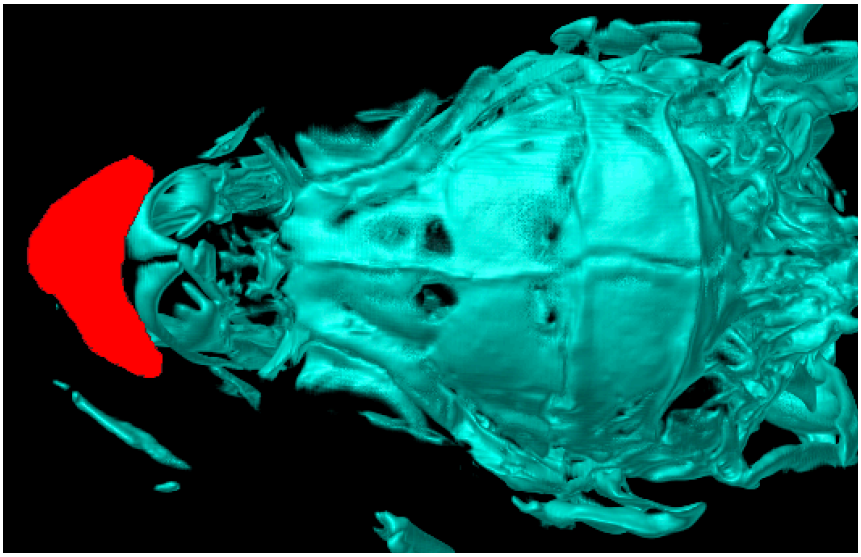

After clicking the **Add** button, then the **Colorize** checkmark on/off, I can see that region is now shaded in red. Pixels from the Inside (green) layer have now been added to the Bone (red) layer.

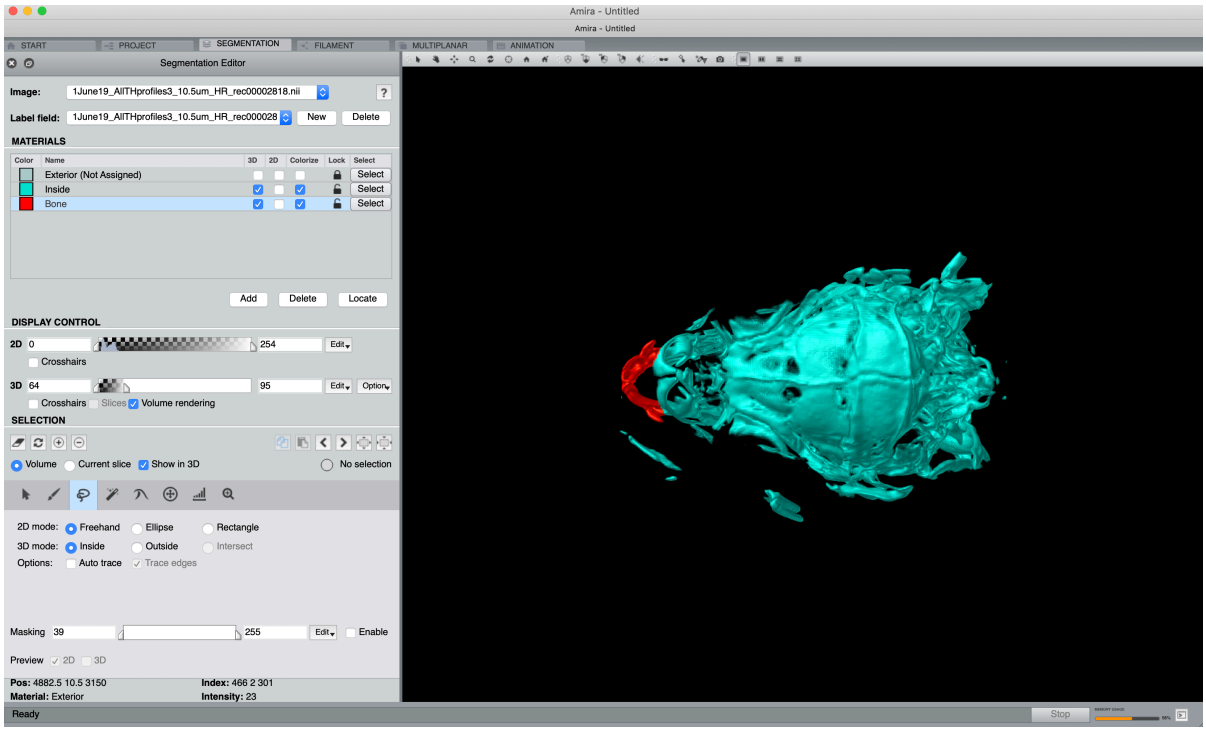

You will have to rotate the skull and continue selecting all the pixels to get the entire dentary. Take generous boundaries when segmenting, adding way more than you need to, because it will be easier to subtract it out later.

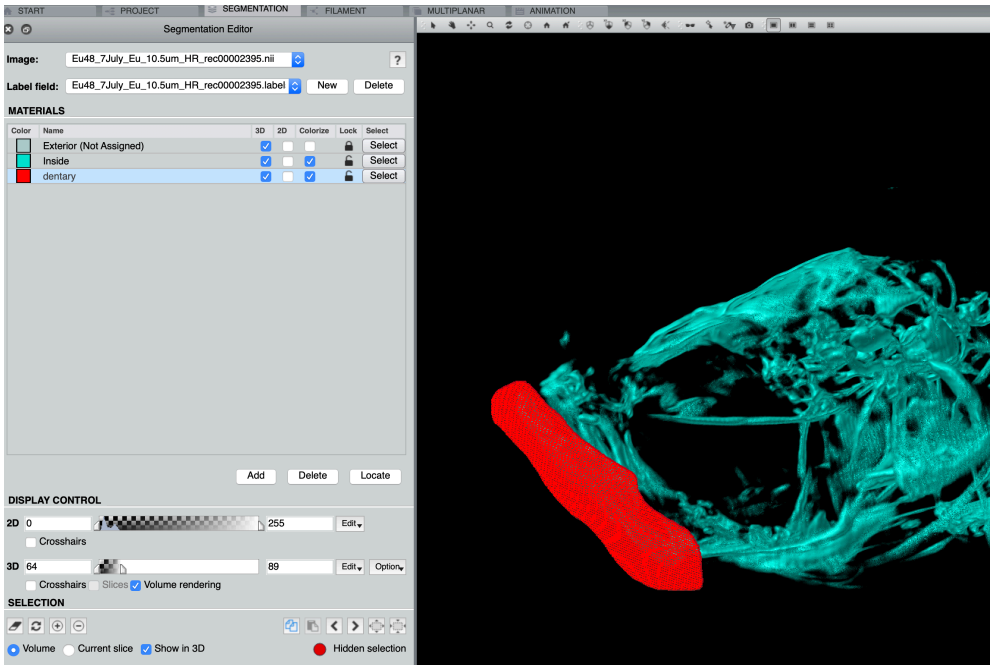

Rotate the skull in 3D to see what the selection looks like. I can tell that I also selected portions of the pre-maxillary, as well as the dentary. But since all of the dentary is selected, this is a good start. The most important aspect of getting good quantifications is learning spatial intelligence in

a 3D platform. This requires that you are constantly rotating, changing thresholding and layer visibility to make sure your bones have high quality segmentation.

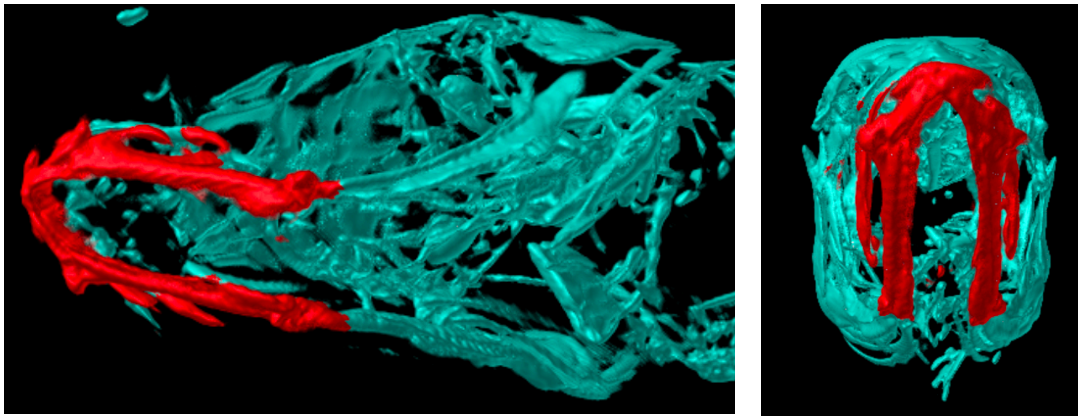

I know that I've over-selected for dentary pixels, so I will make the Inside layer invisible by checking off the 3D button on the layer. This leaves only the dentary layer visible. Now I can start removing the extra pixels from the dentary layer, adding them back to the Inside layer.

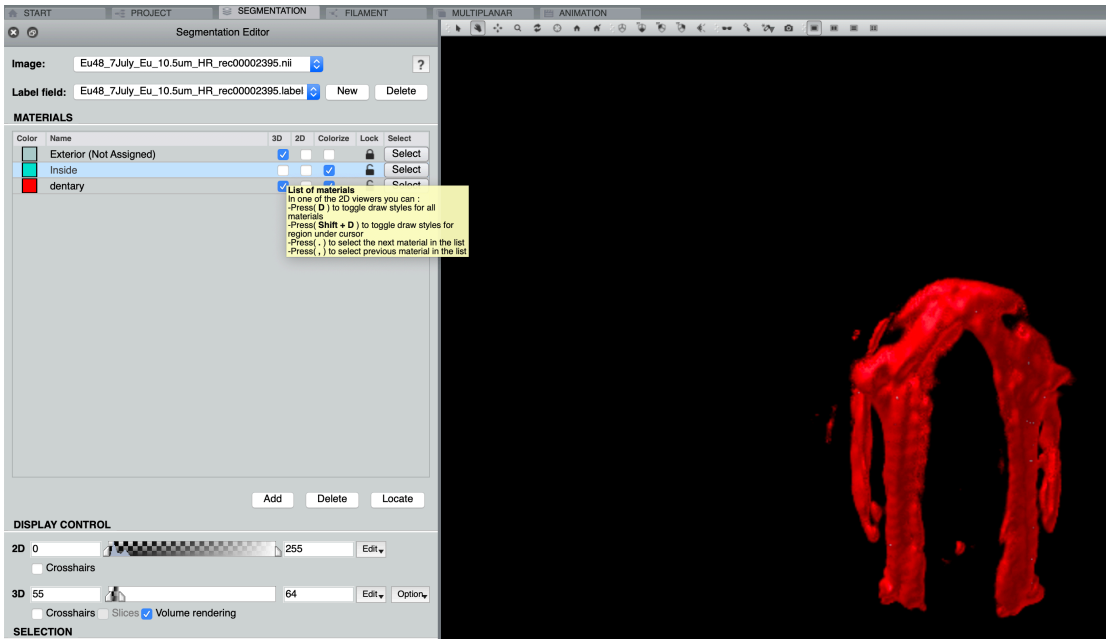

Use the lasso tool to select the extra pixels. Be cognizant of the layer you have selected, which layers are locked and make sure the layer you want to add to is unlocked.

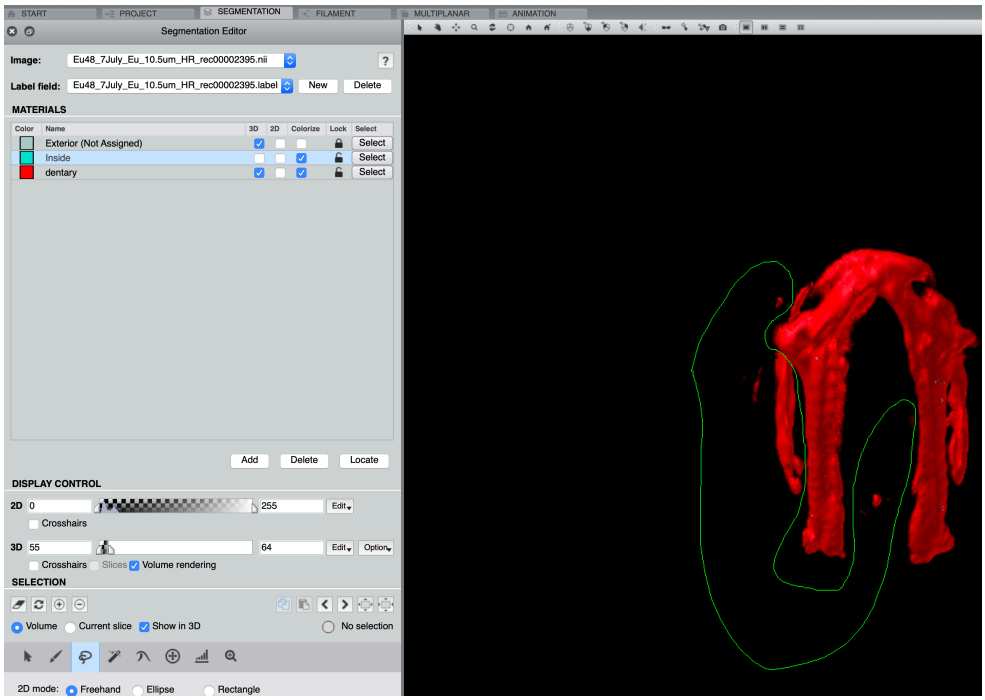

Click the 3D view button on/off to update the layer. You will now see that the extra pixels were subtracted from the dentary layer.

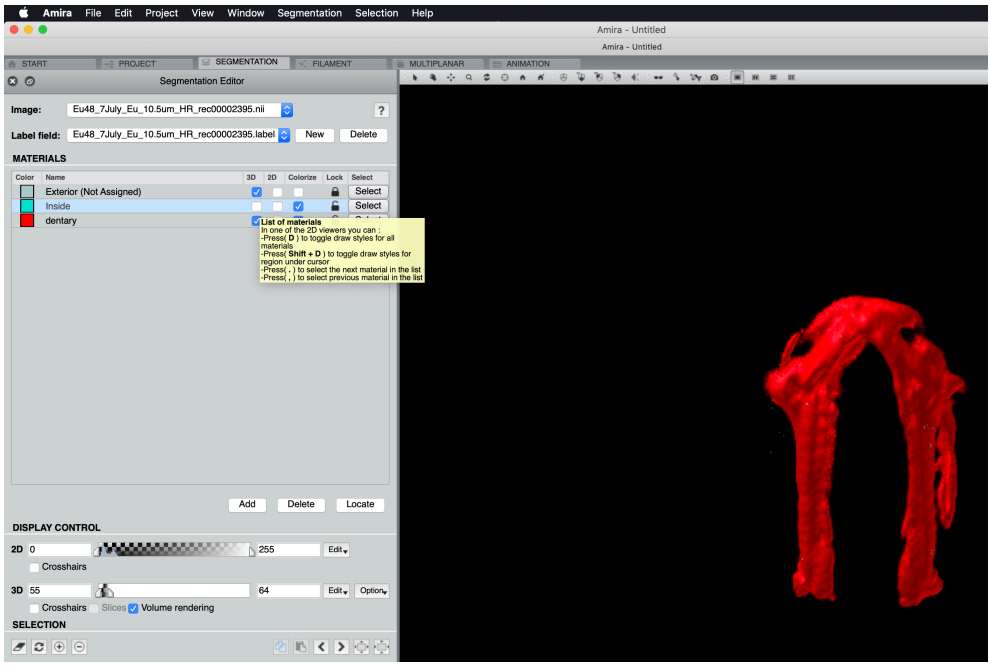

Keep doing this until the bone segmentation is accurate. You will need to rotate in 3D, zoom in and out, turn the Inside layer on/off to check for borders and inspect it from all angles to make sure you have a high-quality segmentation. Colorize the layers so you can better distinguish the boundaries between one bone and what it articulates to. Continually save the **.am** segmentation file!!

Once you are completely done with segmenting and you feel that its high quality, you are ready to generate a **Material Statistics** file that contains all the Layer/Material quantifications. To generate the Material Statistics file, click on the Project tab, leaving the Segmentation Editor. Click on the gray arrow on the right side of the .am green file bar. Click on **Measure and Analyze** and select **Material Statistics**.

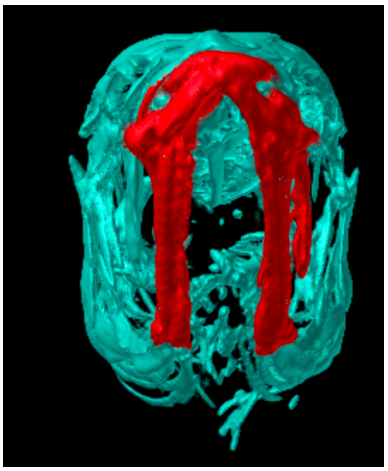

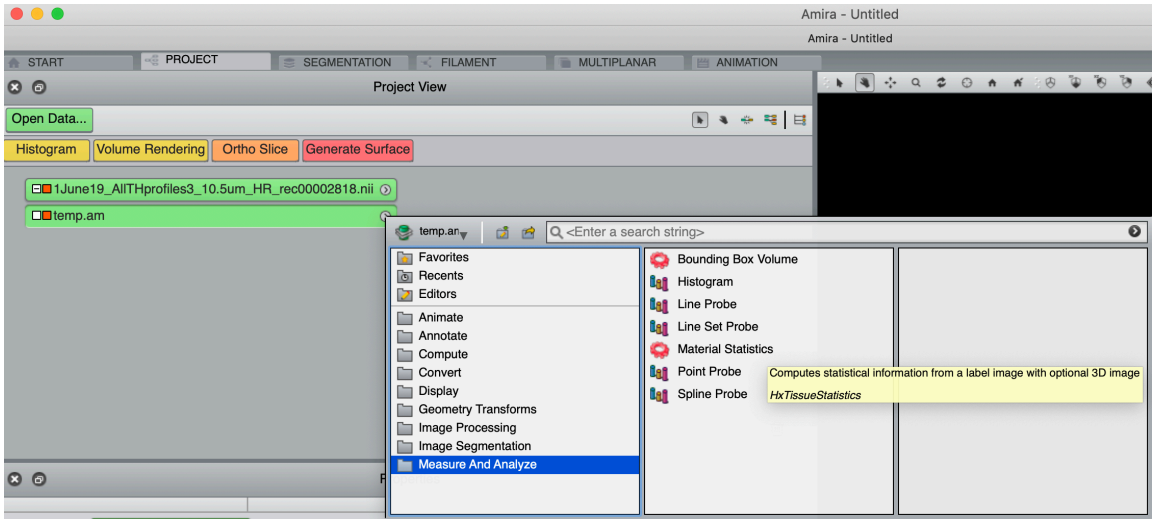

Amira will now generate a red Material Statistics Bar. In the Properties section, choose the **.nii** file as the **Field**. Choose the **.am** file as the **Vol**.

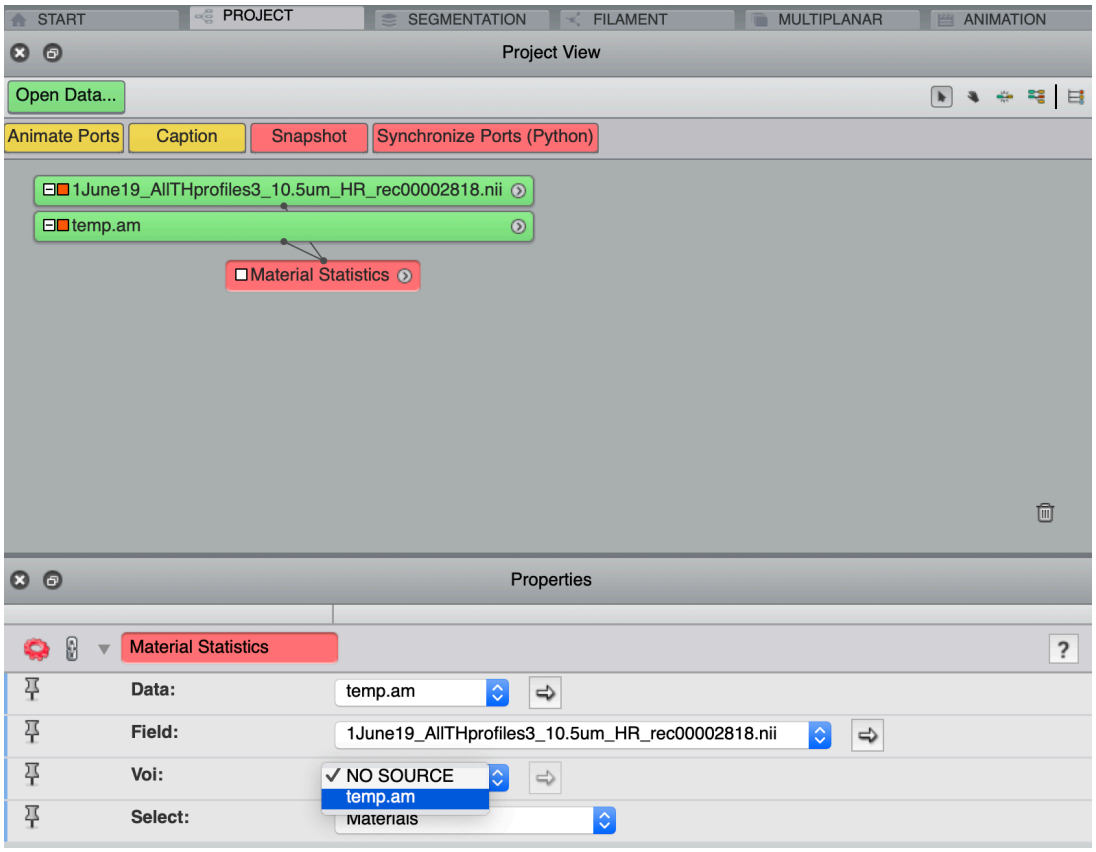

Select Materials and click Apply.

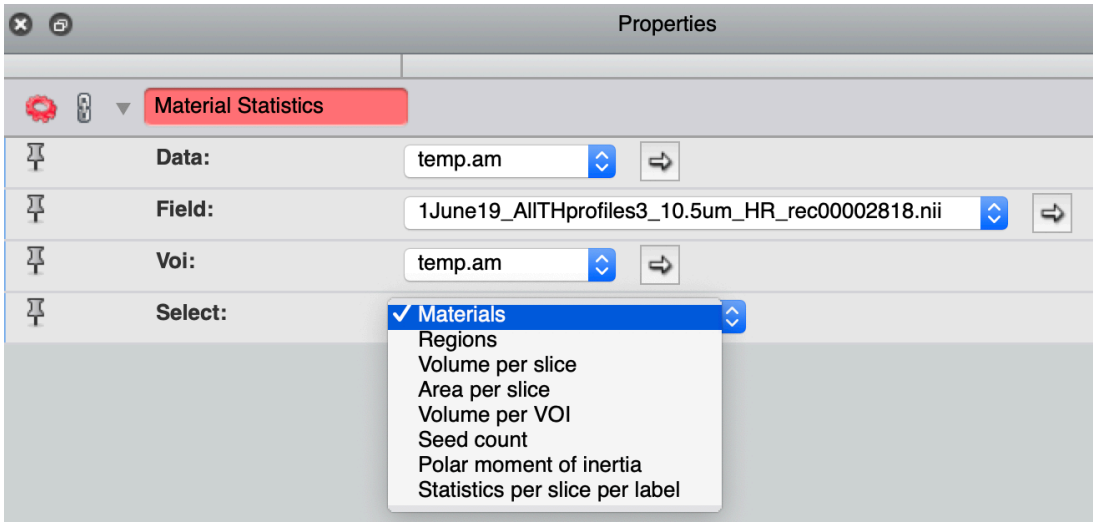

This will generate a green **file.MaterialStatistics** bar. Click on the grey arrow on the right of the bar. Then click on the folder with the arrow to **Export As**.

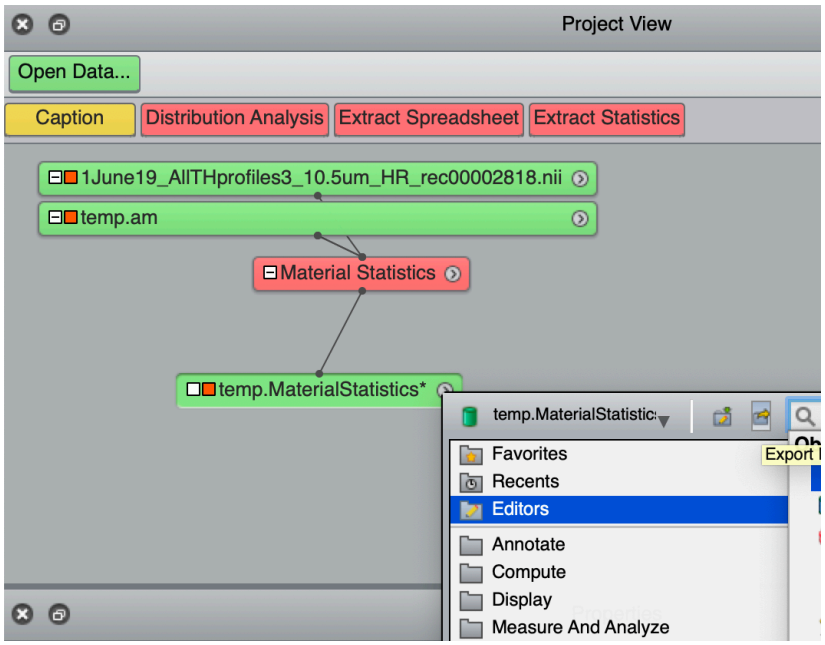

Save the file as a **.CSV** file!

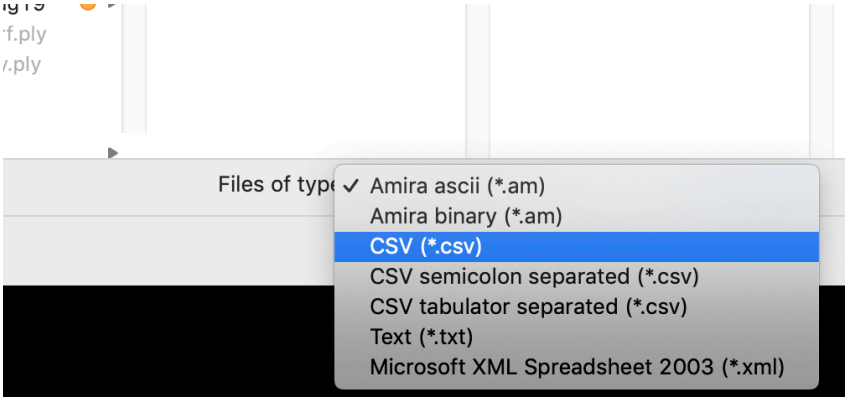

If you open up the .csv file you will see the following data:

	B	C	D	E	F	G	H	I	J	K	L	M	N
	Material	Label	Count	Volume	CenterX	CenterY	CenterZ	Mean	Deviation	Variance	Min	Max	CumulativeSum
1	Exterior	0	224233119	2.60E+11	4190.6914	4188.2036	1847.5784	8.2470589	6.8822751	47.365711	0	149	1.85E+09
2	Inside	1	1199312	1388353554	4637.9155	5223.2456	1822.8553	55.789757	15.965796	254.90665	40	169	66909324
3	dentary	2	71876	83205454.5	5846.1899	3120.6455	1363.9492	66.845398	22.611788	511.29294	40	161	4804580
4	neurocraniur	3	192043	222313777.9	5064.1021	4613.1465	2959.2563	52.589581	11.457886	131.28316	40	122	10099461
5	otoliths	4	56374	65259951.75	4176.356	6184.1221	2456.7271	125.06409	65.584366	4301.3091	40	248	7050363
6	opercles	5	94909	109869031.1	4327.9702	5656.8442	1604.8547	61.053955	15.91625	253.32701	40	129	5794570
7	kinethmoid	6	2412	2792191.5	5846.8936	3200.9678	2137.908	58.932423	13.566219	184.0423	40	103	142145
8	joints	7	27401	31720082.62	5371.8691	3721.4099	817.26984	69.306305	22.218372	493.65607	40	154	1899062
9	MS	8	3911	4527471.375	6241.0645	2664.6777	1889.6644	75.337509	27.02566	730.38629	40	146	294645
10	ceratohyal	9	38643	44734102.88	5153.3872	4237.7993	870.70172	56.371555	13.443295	180.7222	40	108	2178366

The important data is the **count**, **volume**, **mean**, **max** and **cumulative sum**. Count is like volume, but it has not been calibrated using the scan resolution voxel size. Amira generates the true volume by multiplying count by (10.5*10.5*10.5). If you did not set the voxel size when you imported the .bmp stack into Amira, these values are not correct. Mean is the average density, which Amira generates using Cumulative Sum divided by Count. Max value is the brightest pixel in the segmented bone. Cumulative Sum can be thought of as bone mass.

If you want to generate absolute density values for your quantifications and ensure comparable densities across multiple scans, you will need to use a phantom inside of each scan. Make sure the phantom is well above the plastic conical tube cap. Make sure it is embedded in the same thickness of foam as the heads. We estimate that the phantom can appear +/- 20 gray values off if shielded by the cap and +/- 10 grey values off if shielded by parafilm/foam.

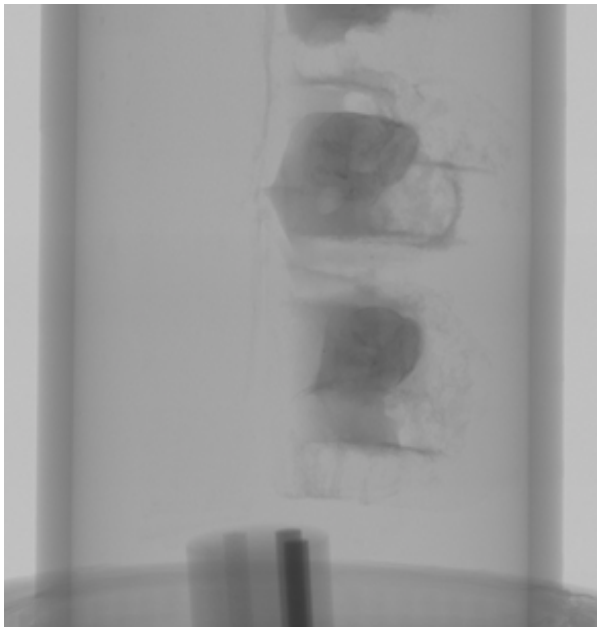

Once you have your reconstructed scan, open the top-most phantom image of the stack in ImageJ. Use the circular selection tool to select the brightest phantom. Do not include the borders of the phantom, but try to include as much as possible.

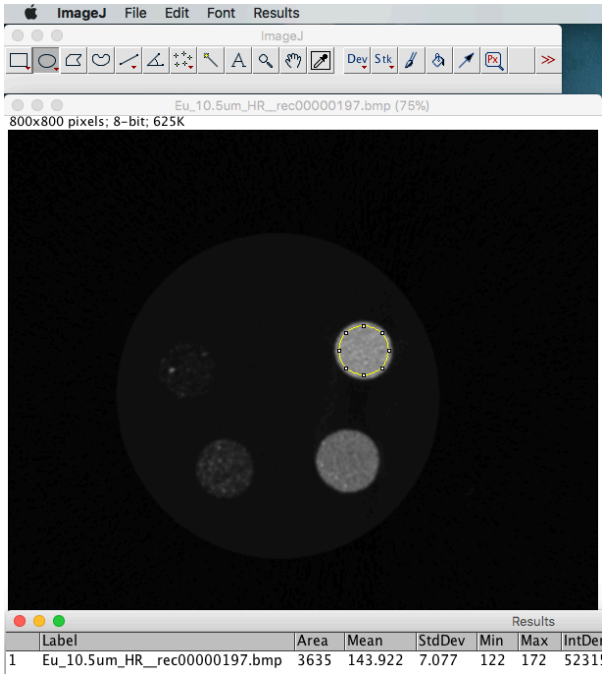

Hit Control+M to measure. A box with **Results** will popup. Record the **mean** measurement (in this case 143.922). Repeat for all 5 phantom rods, including the HA0 which appears invisible.

In Excel, construct the following table. Note that our phantom values are roughly 0, 50, 200, 800, and 1,200 mg HA/cm^3. The brightest/densest phantom is the 1,200 mg HA/cm^3 and the least dense is the 0 mg HA/cm^3.

EU	Calibrated HA (mg/cm3)	Observed Gray values
HA0	0	17.605
HA50	50	22.963
HA200	200	40.343
HA800	800	103.072
HA1200	1200	143.914

Select the 2 columns and generate a Scatterplot.

Right click on one of the points on the line and select **Add Trendline**.

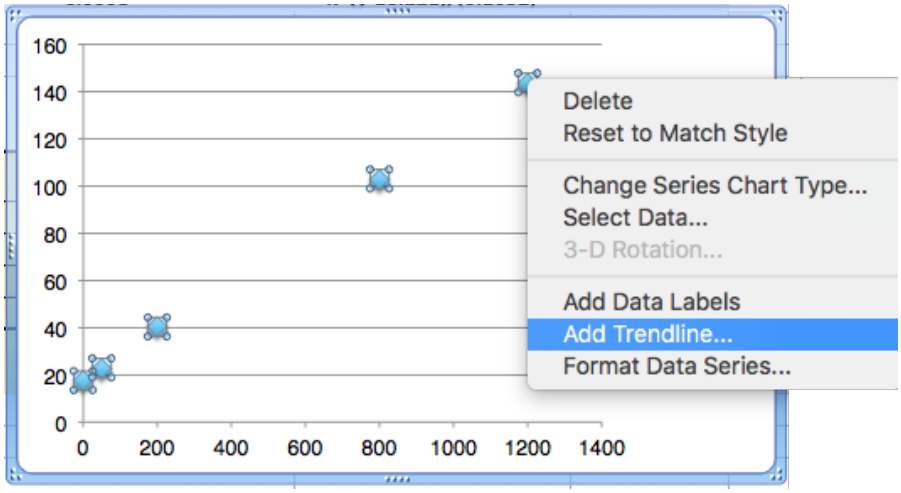

Select Display equation on chart and Display R-squared. Your R-squared value should be very close to 1 to create an accurate calibration curve. In this case the R-squared is 0.9997.

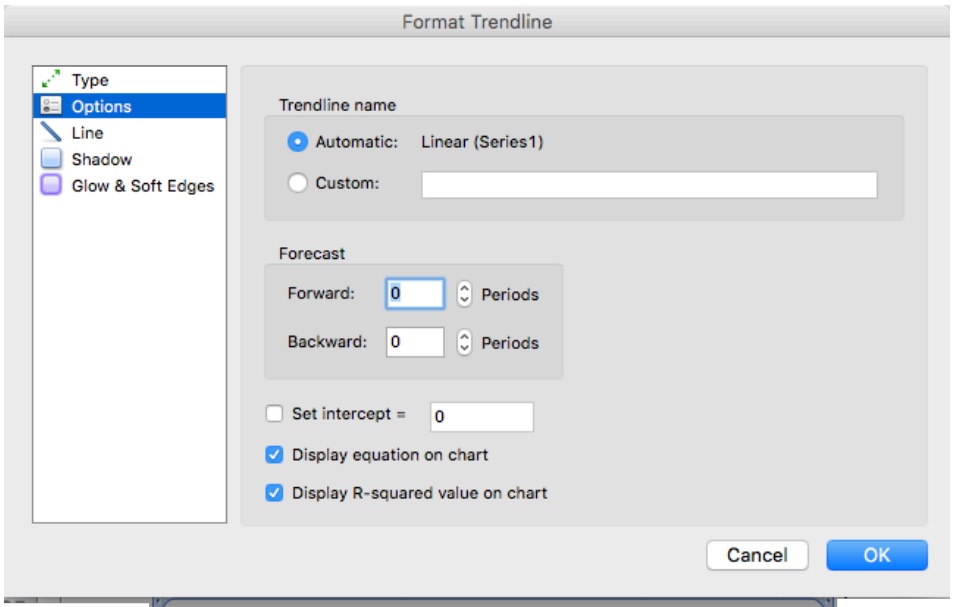

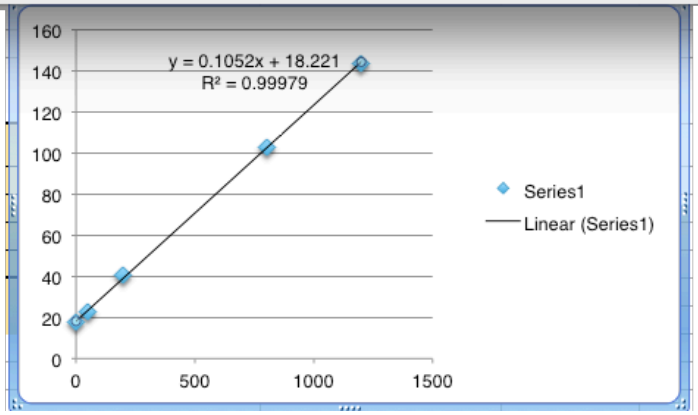

Record the equation in Excel. Create a formula cell in Excel in the form of x=(y-zzz)/(zzz), where y is the density value you got from the Amira quantification file. For instance, the equation from the phantom calibration curve below was **y = 0.1052x + 18.221**. I re-arranged the equation to: **x = (y-18.221)/(0.1052**). I then selected the cell with the density value from the Amira Material Statistics tab (uncalibrated insidedens = 55.84) and plugged it into the equation. This yielded a calibrated value of 357.62 HA/cm^3. I used only calibrated values for my R Studio density quantifications. Save the raw data, as well!

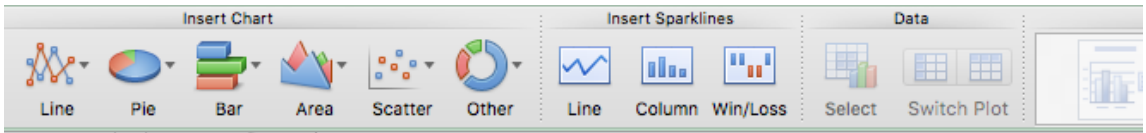

A	B	C	D	E	F
	specimen	group	equation	insidecount	insidedens
raw	eu1	eu	x=(y-18.221)/(0.1052)	1173531.00	55.84
calibrated	eu1	eu		1173531.00	357.62

From the Amira Material Statistics File, you can copy and paste all the relevant cells into a master spreadsheet. Or you can automatically strip the values from the .csv files using a R Studio script.

When conducting density quantifications in R studio, first conduct quality checks on all your data using the Global Linear Model Assumption test, Shapiro-Wilks test and Levene's test. Things to worry about include non-normality, unequal variances, skew and heteroscedasticity. If your bones are not-normally distributed, log transform the data or run Tukey's Ladders of Power test to determine the optimal transformation factor. If all your data meets the basic assumptions of the One-Way ANOVA, you can run your analysis. If not, you will have to use a rank-based non-parametric test, like the Kruskal Wallis One Way Anova by Ranks Test. It is recommended that you run a Power Test or a Sensitivity Analysis beforehand to determine if your sample size is adequate to detect your response variable's effect size.

4.3 R Studio Statistical Scripting

SAMPLE SIZES

```
## [1] "Total N within each treatment group"
##   Eu  TH-  TH+ <NA>
##   37   37   37    0
```

MEASUREMENT MEANS

```
## [1] "Headsize Mean per group"
##       Eu      TH-      TH+
## 4.893784 5.191351 5.114595
## [1] "Bodysize Mean per group"
##       Eu      TH-      TH+
## 21.11108 21.00000 22.00000
## [1] "Age Mean per group"
##       Eu      TH-      TH+
## 11.151622 11.516486  7.135135
```

(2) Data Transformation

Using Tukey's Ladders of Power Analysis, I used recommended lambdas to transform the data

VOLUME CONVERSION

```
#Converting grey value counts (1 um voxels) into volume (10.5 um^3)
df$totaldentvol    <- (10.5)^3 * (df$totaldentcountsum)
df$dentshaftvol    <- (10.5)^3 * (df$dentshaftcount)
df$mslesionvol     <- (10.5)^3 * (df$mslesioncountsum)
df$dermatovol      <- (10.5)^3 * (df$dermatocount)
df$otovol          <- (10.5)^3 * (df$otocount)
df$opervol         <- (10.5)^3 * (df$opercount)
df$kinvol          <-(10.5)^3 * (df$kincount)
df$ceratovol       <- (10.5)^3 * (df$ceratocount)
df$basivol         <- (10.5)^3 * (df$basicount)
df$jointvol        <- (10.5)^3 * (df$jointcount)
df$hyoidvol        <- (10.5)^3 * (df$hyoidcountsum)
df$wholeheadvol <- (10.5)^3 * (df$wholeheadcountsum)
```

LADDERS OF POWER

Tukey's Ladders of Power transformation test to determine optimal lambda

```
library(rcompanion)
par(mfrow = c(2, 2))
T_tuk = transformTukey(df$totaldentdens_calib, start = -5, end = 5, int = 0.001, plotit=TRUE)
##
##     lambda      W Shapiro.p.value
## 5070  0.069 0.9879          0.42
##
## if (lambda >  0){TRANS = x ^ lambda}
## if (lambda == 0){TRANS = log(x)}
## if (lambda <  0){TRANS = -1 * x ^ lambda}
plotNormalHistogram(T_tuk)
```

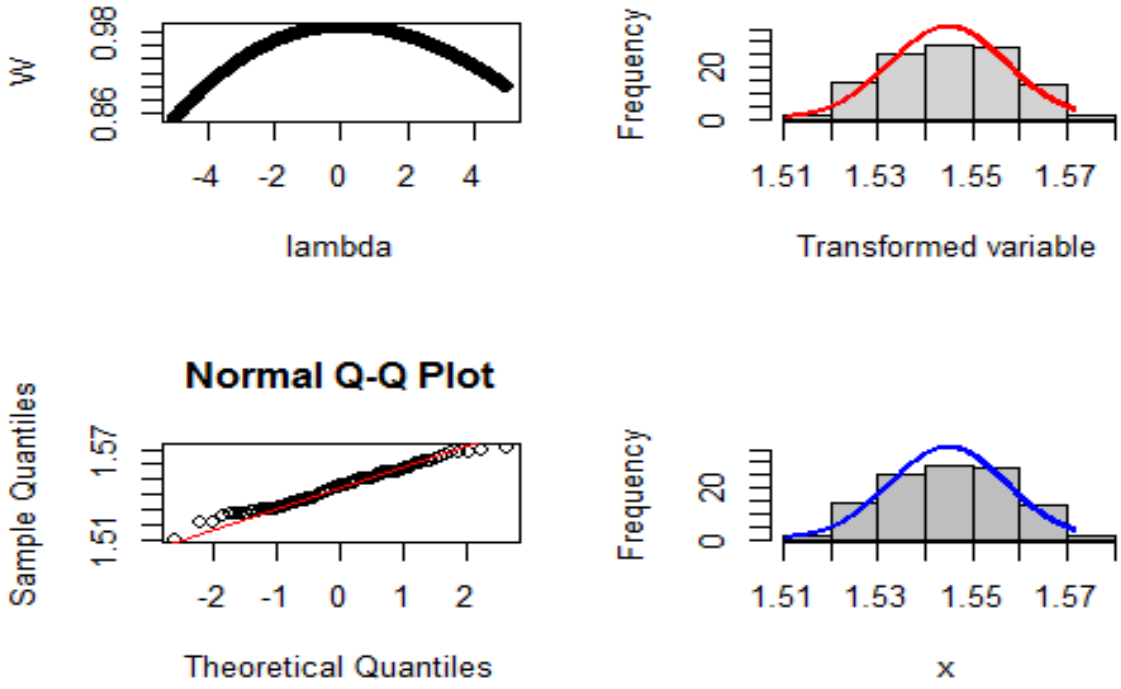


```
#If (lambda >  0) {TRANS = x ^ lambda}
#If (lambda == 0) {TRANS = log(x)}
#If (lambda <  0) {TRANS = -1 * x ^ lambda}
```

DATA TRANSFORMATION FACTORS

I determined the transformation coefficient that optimally provides a normal distribution per bone.

```
df$totaldentdens_tt <-   (df$totaldentdens_calib)^0.069
df$dentshaftdens_tt <-   (df$dentshaftdens)^0.184
df$mslesiondens_tt  <- -1*(df$mslesiondens_calib)^-0.59
df$jointdens_tt     <- -1*(df$jointdens)^-0.842
df$dermatodens_tt   <- -1*(df$dermatodens)^-0.558
df$otodens_tt       <-   (df$otodens)^2.907
df$operdens_tt      <- -1*(df$operdens)^-0.802
df$kindens_tt       <-   (df$kindens)^0.148
df$hyoiddens_tt     <- -1*(df$hyoiddens_calib)^-0.946
df$wholeheaddens_tt <- -1*(df$wholeheaddens_calib)^-0.881
df$totaldentmass_tt <-   (df$totaldentmasssum)^0.151
df$dentshaftmass_tt <-   (df$dentshaftmass)^0.006
df$mslesionmass_tt  <- -1*(df$mslesionmasssum)^-0.38
df$jointmass_tt     <- -1*(df$jointmass)^-0.07
df$dermatomass_tt   <-   (df$dermatomass)^0.135
df$wholeheadmass_tt <- -1*(df$wholeheadmasssum)^-0.184
df$totaldentvol_tt  <-   (df$totaldentvol)^0.186
df$dentshaftvol_tt  <- -1*(df$dentshaftvol)^-0.019
df$mslesionvol_tt   <- -1*(df$mslesionvol)^-0.44
df$jointvol_tt      <- -1*(df$jointvol)^-0.181
df$dermatovol_tt    <-   (df$dermatovol)^0.191
df$wholeheadvol_tt  <- -1*(df$wholeheadvol)^-0.218
df$dentshaftmax_tt  <-   (df$dentshaftmax)^2.107
df$dermatomax_tt    <-   (df$dermatomax)^2.247
df$jointmax_tt      <-   (df$jointmax)^2.134
```

Residuals on transformed data

Using the Linear Model (density ~ group + head size) I generated residuals on the Tukey's transformed data.

```
totaldentdens.lm = lm(df$totaldentdens_tt ~ group + headsize, data=df)
df$totaldentdens.res  = resid(totaldentdens.lm)
dentshaftdens.lm = lm(df$dentshaftdens_tt ~ group + headsize, data=df)
df$dentshaftdens.res  = resid(dentshaftdens.lm)
mslesiondens.lm = lm(df$mslesiondens_tt ~ group + headsize, data=df)
df$mslesiondens.res  = resid(mslesiondens.lm)
jointdens.lm = lm(df$jointdens_tt ~ group + headsize, data=df)
df$jointdens.res  = resid(jointdens.lm)
dermatodens.lm = lm(df$dermatodens_tt ~ group + headsize, data=df)
df$dermatodens.res  = resid(dermatodens.lm)
kindens.lm = lm(df$kindens_tt ~ group + headsize, data=df)
df$kindens.res  = resid(kindens.lm)
hyoiddens.lm = lm(df$hyoiddens_tt ~ group + headsize, data=df)
df$hyoiddens.res  = resid(hyoiddens.lm)
otodens.lm = lm(df$otodens_tt ~ group + headsize, data=df, na.rm=T)
```

```
df$otodens.res  = resid(otodens.lm)
operdens.lm = lm(df$operdens_tt ~ group + headsize, data=df)
df$operdens.res  = resid(operdens.lm)
wholeheaddens.lm = lm(df$wholeheaddens_tt ~ group + headsize, data=df)
df$wholeheaddens.res  = resid(wholeheaddens.lm)
#write.csv(df, file = "density_DATA_EXPORT.csv", row.names = FALSE)
```

RESIDUAL LEVERAGE ANALYSIS

Check residuals for data issues. Residuals vs Fitted plot should show random scatter. Normal Q-Q should be linear with no skew or kurtosis. Scale-Location should have horizontal line with no trend biases. Residuals vs Leverage shows influential outliers, which lie outside of Cook's distance lines.

```
par(mfrow = c(2, 2))
plot(totaldentdens.lm)
```

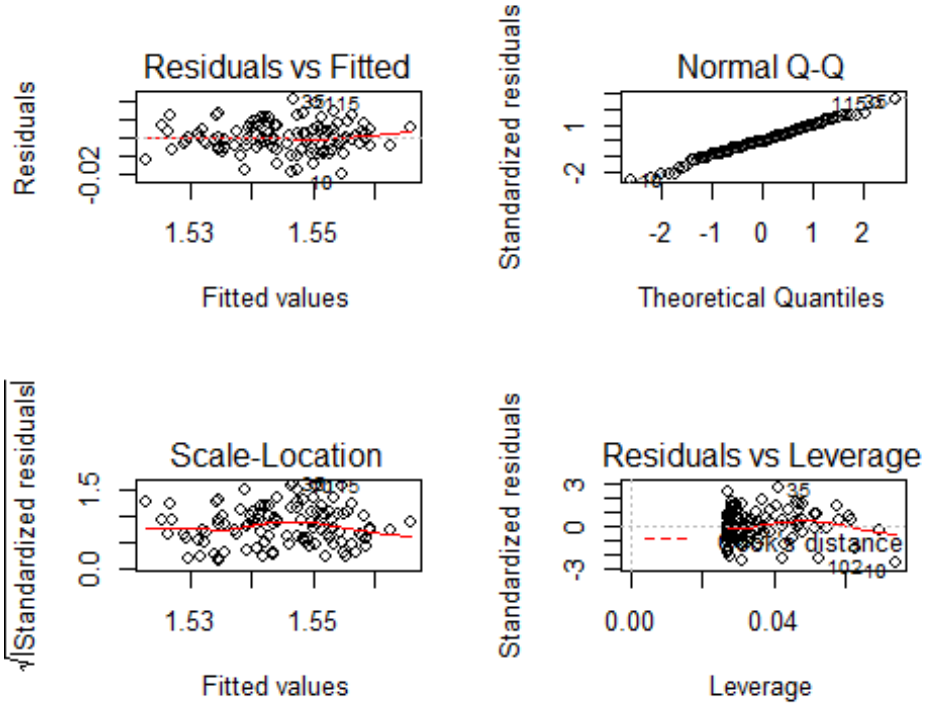

(3) QUALITY CONTROL TESTS

QUALITY CONTROL CHECK FOR OUR DATASET
POWER ANALYSIS

This sensitivity analysis indicates how well powered the study is to detect effect sizes. We can detect effect sizes of 0.299 or larger, which is a medium effect size.

```
f1 <- round(pwr.anova.test(k = 3, n=37, power = 0.8, sig.level = .05)$f, digits=3)
f1
## [1] 0.299
```

```
## [1] "For a power of 0.8 and a sample size of 37, Cohen's F would need to be 0.299** to detect
a p-val of 0.05"
## [1] "Effect Size (  *     **     ***  )"
## [1] "Cohens F -   Small, Medium, Large"
## [1] "Cohens F -   0.10,   0.25,  0.40"
```

GLOBAL TEST MODEL ASSUMPTIONS

Global Linear Model Assumption test on Tukey's Transformed data still shows issues.

```
glob_lm = lm(df$totaldentdens_tt ~ group + headsize, data=df)
glob_lm_model <- gvlma(glob_lm)
summary(glob_lm_model)
##
## Call:
## lm(formula = df$totaldentdens_tt ~ group + headsize, data = df)
##
## Residuals:
##       Min        1Q    Median        3Q       Max
## -0.0194089 -0.0053857 -0.0003403  0.0054650  0.0207298
##
## Coefficients:
##             Estimate Std. Error t value Pr(>|t|)
## (Intercept) 1.465267   0.007630 192.047  < 2e-16 ***
## groupTH-    0.003538   0.001941   1.823   0.0712 .
## groupTH+    0.010465   0.001917   5.459 3.13e-07 ***
## headsize    0.014802   0.001535   9.643 3.29e-16 ***
## ---
## Signif. codes:  0 '***' 0.001 '**' 0.01 '*' 0.05 '.' 0.1 ' ' 1
##
## Residual standard error: 0.008115 on 107 degrees of freedom
## Multiple R-squared:  0.5777, Adjusted R-squared:  0.5659
## F-statistic:  48.8 on 3 and 107 DF,  p-value: < 2.2e-16
##
## ASSESSMENT OF THE LINEAR MODEL ASSUMPTIONS
## USING THE GLOBAL TEST ON 4 DEGREES-OF-FREEDOM:
## Level of Significance =  0.05
##
## Call:
##  gvlma(x = glob_lm)
##
##                    Value p-value             Decision
## Global Stat        0.49875  0.9736 Assumptions acceptable.
## Skewness           0.11672  0.7326 Assumptions acceptable.
## Kurtosis           0.01252  0.9109 Assumptions acceptable.
## Link Function      0.23060  0.6311 Assumptions acceptable.
## Heteroscedasticity 0.13891  0.7094 Assumptions acceptable.
```

Global Model Test Results

Tests performed on Tukey's Transformed factors

```
## [1] "Global Stats Indicated Problems (on transformed variables)"
## [1] "Total Dentary:      All good."
## [1] "Dentary Shaft:      All good."
## [1] "MS/Lesion:          All good."
## [1] "Joint:              All good."
## [1] "Dermatocranium:     All good."
## [1] "Kinethmoid:         All good."
## [1] "Otolith:            Global Stat, Skew, Heteroscedasticity."
## [1] "Opercle:            All good."
## [1] "Hyoid:              All good."
## [1] "Whole Head:         All good."
```

NORMALITY

Do the transformed residuals have normal distributions? Appending '_tt' denotes variables have been transformed according to Tukey's Ladders of Power tests. Histograms of residuals of the transformed data are plotted.

```
par(mfrow = c(3, 3))
hist(df$totaldentdens_tt, breaks = 15, main="totaldentdens_tt")
hist(df$dentshaftdens_tt, breaks = 15, main="dentshaftdens_tt")
hist(df$mslesiondens_tt, breaks = 15, main="mslesion_tt")
hist(df$jointdens, breaks = 15, main="jointdens_tt")
hist(df$dermatodens_tt, breaks = 15, main="dermatodens_tt")
hist(df$kindens_tt, breaks = 15, main="kindens_tt")
hist(df$otodens_tt, breaks = 15, main="otodens_tt")
hist(df$operdens_tt, breaks = 15, main="operdens_tt")
hist(df$hyoiddens_tt, breaks = 15, main="hyoid_tt")
```

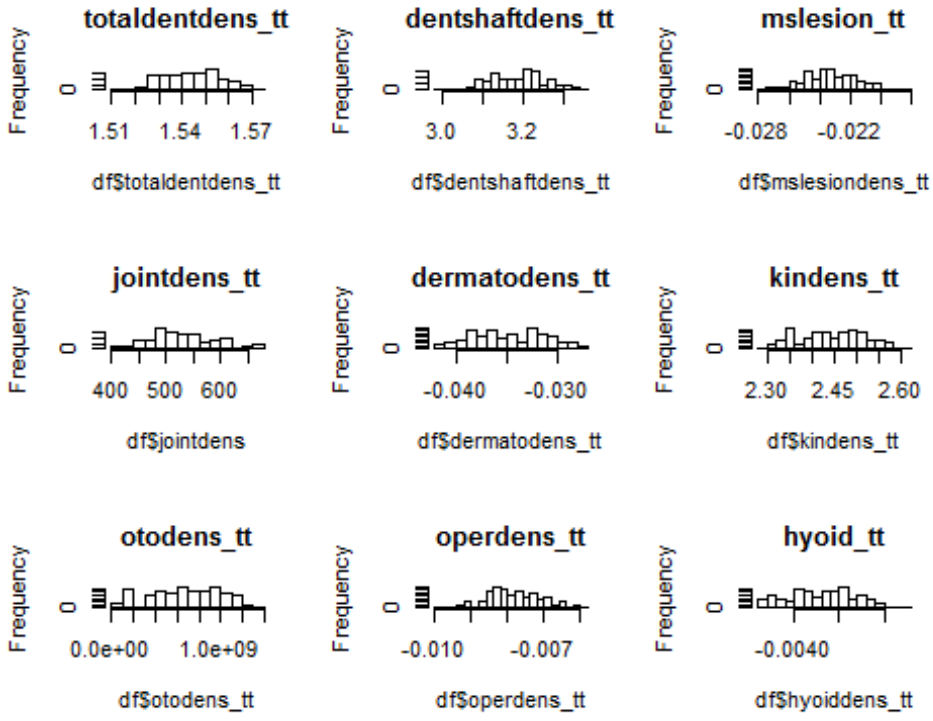

```
#hist(df$wholeheaddens_tt, breaks = 15, main="wholeheaddens_tt")
```

Post-Transformation Shapiro Test

After transforming factors with optimized Tukey's Ladders of transformation, Dermatocranium and otolith bones still do not have a normal distribution. Rather than use One-Way Anovas, Otolith tests must use the Kruskal-Wallis One Way ANOVA by Rank Test.

```
## [1] "Shapiro Test P-values"
## [1] "Total Dentary:          "
## [1] 0.4199603
## [1] "Dentary Shaft:          "
## [1] 0.4493794
## [1] "MS/Lesion:              "
## [1] 0.9355592
## [1] "Joint:                  "
## [1] 0.693254
## [1] "Dermatocranium: NOT normal"
## [1] 0.03677677
## [1] "Kinethmoid:             "
## [1] 0.05801328
## [1] "Otolith:       NOT normal"
## [1] 0.0320423
## [1] "Opercle:                "
## [1] 0.6667047
## [1] "Hyoid:                  "
## [1] 0.08464053
## [1] "Whole Head:             "
## [1] 0.4722639
```

Otolith Skew Directionality

Is the skew between groups in the same direction? Left Hand Tails for all groups

```
par(mfrow = c(2, 2))
all_oto <- df$otodens
eu_oto <- df$otodens[df$group=="Eu"]
mtz_oto <- df$otodens[df$group=="TH-"]
op_oto <-df$otodens[df$group=="TH+"]
hist(eu_oto, breaks = 40)
hist(mtz_oto, breaks = 40)
hist(op_oto, breaks = 40)
hist(all_oto, breaks = 40)
```

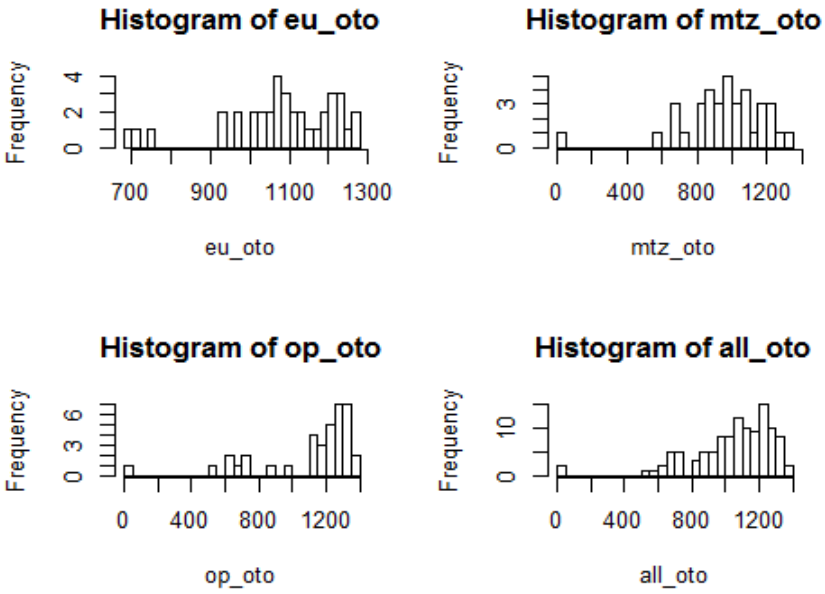

Otolith Q-Q Plots

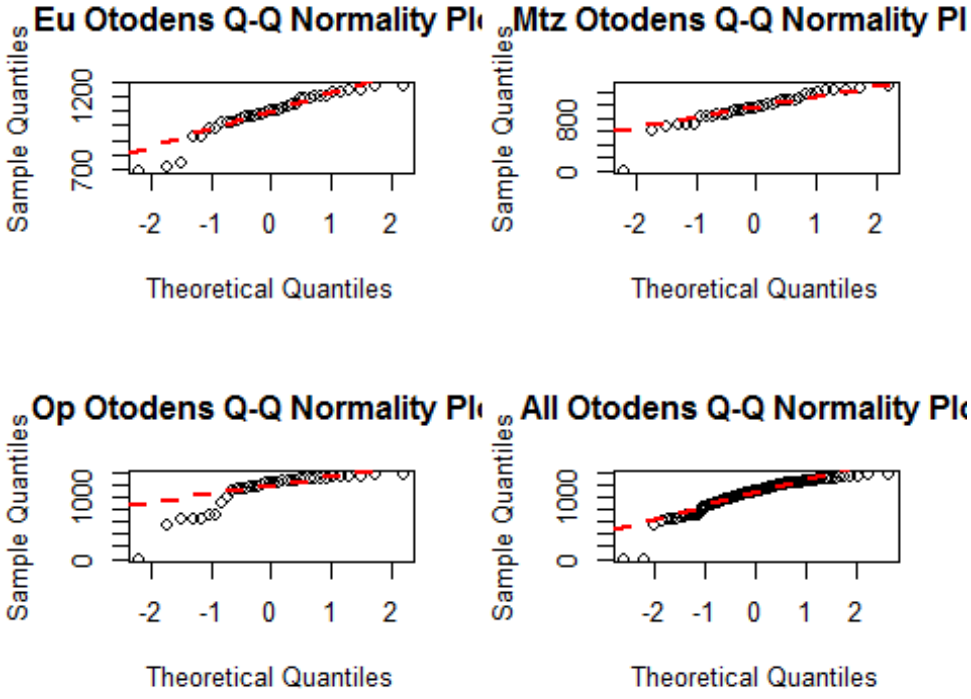

LEVENE'S TEST

Testing the difference in variation of 2 or more groups. Null hypothesis is that all variances are equal, if not equal p>0.05.

```
y <- c(df$otodens_tt[df$group=="Eu"], df$otodens_tt[df$group=="TH-"],
df$otodens_tt[df$group=="TH+"])
```

```
leveneTest(y, df$group, location = c("median", "mean", "trim.mean"),
  trim.alpha = 0.25, bootstrap = FALSE, num.bootstrap = 1000,
  kruskal.test = FALSE, correction.method = c("none",
  "correction.factor", "zero.removal", "zero.correction"))
## Levene's Test for Homogeneity of Variance (center = median: c("median", "mean",
"trim.mean"))
##       Df F value  Pr(>F)
## group   2  3.4339 0.03582 *
##       108
## ---
## Signif. codes:  0 '***' 0.001 '**' 0.01 '*' 0.05 '.' 0.1 ' ' 1
## [1] "Only Otolith has hetereogenous variance, but when transformed is homogenous"
```

VARIANCE

Variance Plots

I used the residuals to check variance between groups for each bone. ANOVAs assume normal equal variances. If variance is greater than 2x, this may violate an underlying assumptions.

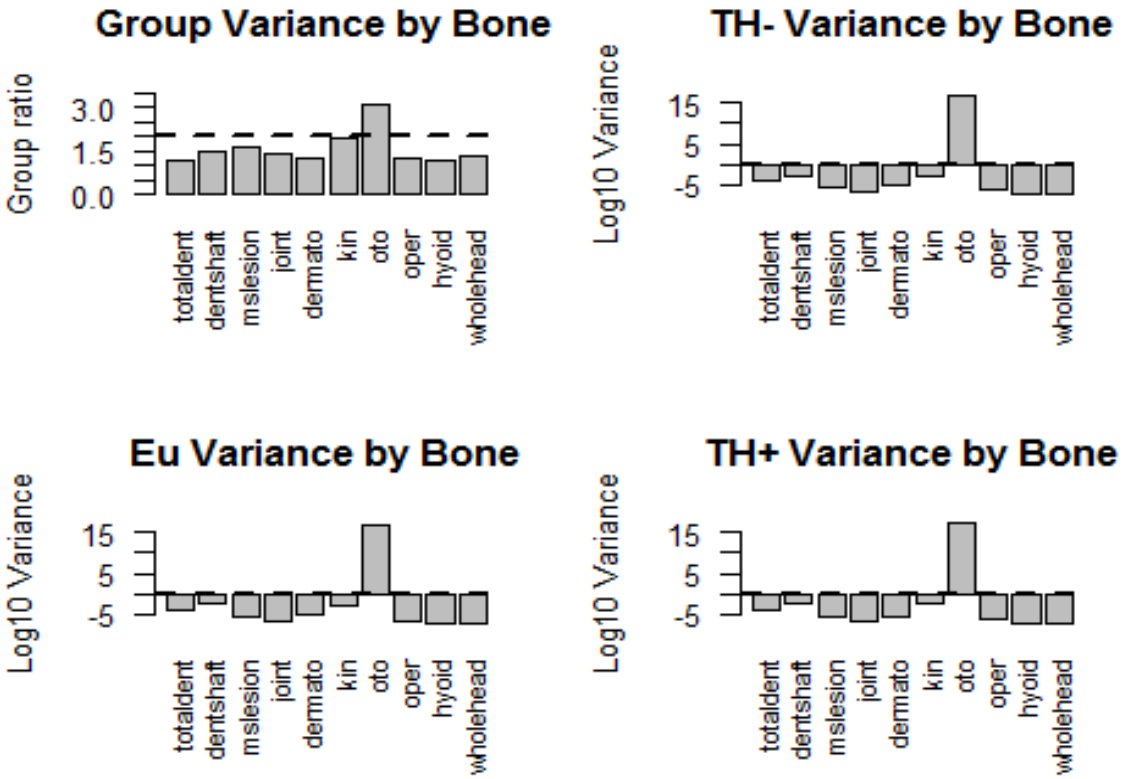

Variance Inflation Factor Test

Using Tukey Transformed data, I ran a Variance Inflation test.

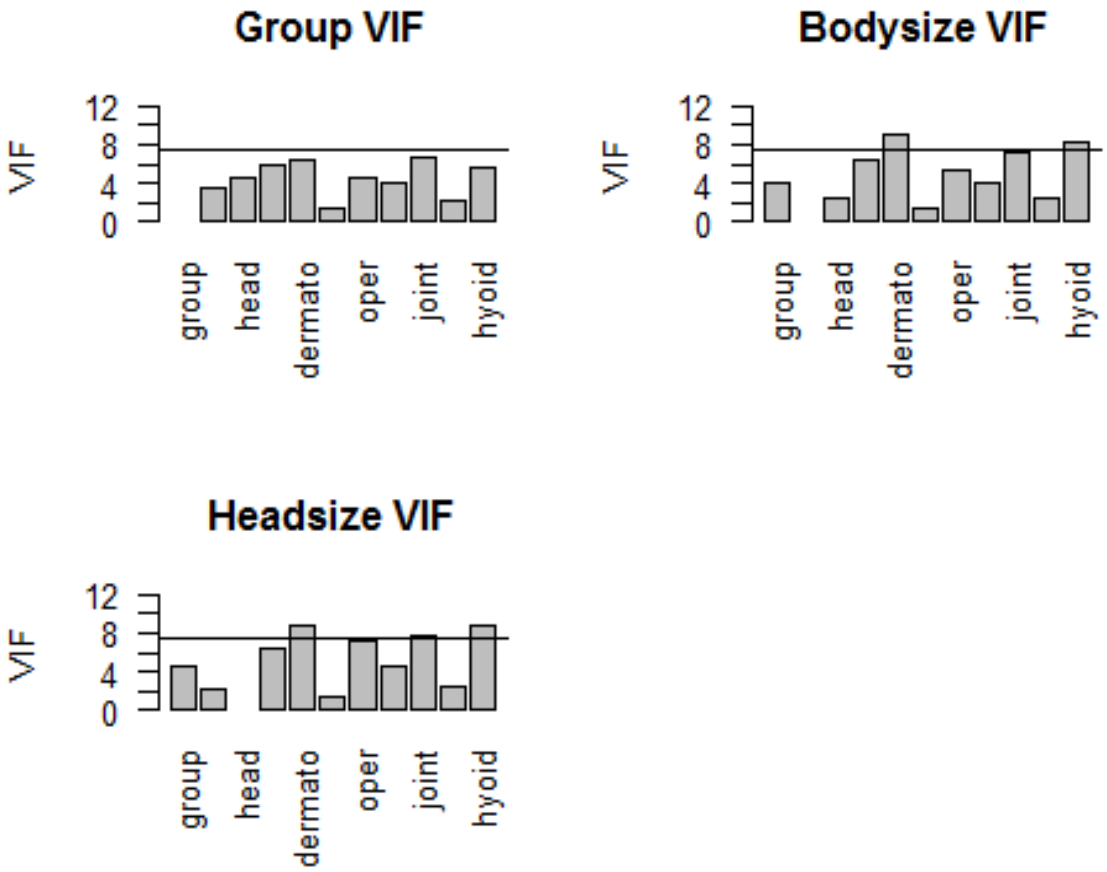

EFFECT SIZES

What is the magnitude of effect of TH on each bone? Yellow lines is small, orange is medium, red is large effect size. Black dotted line is our detection limit for the study based on sensitivity analysis.

```
## [1] "Effect Size ( *      **    ***   )"
## [1] "Cohen's F -  Small,  Medium,  Large"
## [1] "Cohen's F -  0.10,    0.25,    0.40"
## [1] "Cohen's F -  yellow,  orange,  red"
## [1] "Black line = our detection limit"
```

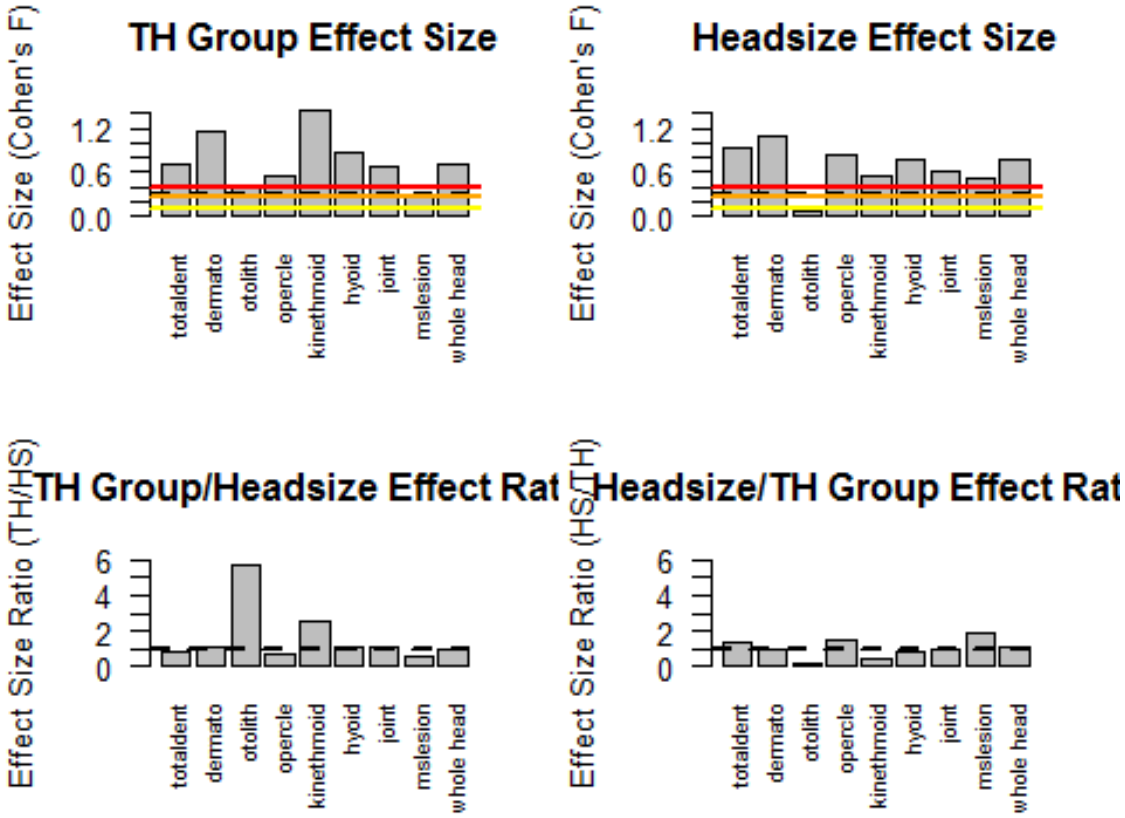

P-VALUE CORRECTIONS - LINEAR MODELS

Bon Ferroni and False Discovery Rate corrections for multiple testing

```
bones <- c("TotalDent", "Dent Shaft",  "MS/Lesion", "Joint",  "Dermato", "Kinethmoid",
"Otolith",  "Opercle",  "Hyoid", "Whole Head")
pvals =  c( 3.9E-10,     8.66E-10   , 1.34E-02,  1.40E-09,  2E-16,    2e-16,    3.3E-04,  6.35E-07,
1.26E-13,  3.05E-10)
FDR <- p.adjust(pvals, method = "fdr", n = length(pvals))
BONF = p.adjust(pvals, "bonferroni")
result = cbind(bones, pvals, "FDR"=round(FDR, 12), "BF"=round(BONF, 12))
result
##      bones       pvals     FDR           BF
##  [1,] "TotalDent"  "3.9e-10"  "7.8e-10"       "3.9e-09"
##  [2,] "Dent Shaft" "8.66e-10" "1.443e-09"     "8.66e-09"
##  [3,] "MS/Lesion"  "0.0134"   "0.0134"        "0.134"
##  [4,] "Joint"      "1.4e-09"  "2e-09"         "1.4e-08"
##  [5,] "Dermato"    "2e-16"    "0"             "0"
##  [6,] "Kinethmoid" "2e-16"    "0"             "0"
##  [7,] "Otolith"    "0.00033"  "0.000366666667" "0.0033"
##  [8,] "Opercle"    "6.35e-07" "7.9375e-07"    "6.35e-06"
##  [9,] "Hyoid"      "1.26e-13" "0"             "1e-12"
## [10,] "Whole Head" "3.05e-10" "7.62e-10"      "3.05e-09"
#write.csv(result, file = "adjusted_p-values.csv", row.names = FALSE)
```

P-VALUE CORRECTIONS - BOXPLOTS

Bon Ferroni and False Discovery Rate corrections for multiple testing

```
bones <- c("TotalDent","DentShaft","DentMax","MSDens","MsMass", "MsVol", "DermDens",
"DermVol", "Otodens", "Operdens", "KinDens", "HyoidDens", "JointDens", "JointMass",
"JointVol", "WholeheadDens")
pvals =  c(2.8E-06,4.7E-06,0.0028,0.323,5.06E-16,2E-16,1.4E-09,7.86E-05,7.86E-05,1.52E-04,2E-
16,9.02E-10,1.71E-07,8.26E-07,5.13E-09,3.39E-07)
FDR <- p.adjust(pvals, method = "fdr", n = length(pvals))
BONF = p.adjust(pvals, "bonferroni")
result = cbind(bones, pvals, "FDR"=round(FDR, 12), "BF"=round(BONF, 12))
result
##      bones         pvals     FDR           BF
##  [1,] "TotalDent"    "2.8e-06"  "4.48e-06"      "4.48e-05"
##  [2,] "DentShaft"    "4.7e-06"  "6.836364e-06"  "7.52e-05"
##  [3,] "DentMax"      "0.0028"   "0.002986666667" "0.0448"
##  [4,] "MSDens"       "0.323"    "0.323"         "1"
##  [5,] "MsMass"       "5.06e-16" "0"             "0"
##  [6,] "MsVol"        "2e-16"    "0"             "0"
##  [7,] "DermDens"     "1.4e-09"  "4.48e-09"      "2.24e-08"
##  [8,] "DermVol"      "7.86e-05" "9.6738462e-05"  "0.0012576"
##  [9,] "Otodens"      "7.86e-05" "9.6738462e-05"  "0.0012576"
## [10,] "Operdens"     "0.000152" "0.000173714286" "0.002432"
## [11,] "KinDens"      "2e-16"    "0"             "0"
## [12,] "HyoidDens"    "9.02e-10" "3.608e-09"     "1.4432e-08"
## [13,] "JointDens"    "1.71e-07" "3.90857e-07"   "2.736e-06"
## [14,] "JointMass"    "8.26e-07" "1.468444e-06"  "1.3216e-05"
## [15,] "JointVol"     "5.13e-09" "1.368e-08"     "8.208e-08"
## [16,] "WholeheadDens" "3.39e-07" "6.78e-07"     "5.424e-06"
#write.csv(result, file = "adjusted_p-values2.csv", row.names = FALSE)
```

(4) MEASUREMENT PLOTS

BODY SIZE

I attempted to collect samples that optimally size matched for both body size and head size between all 3 groups. The distribution of body size is fairly equal among groups, with the mean body size as 21-22 mm SL.

```
xdensity2 <- ggplot(df, aes(headsize, fill=group)) +
geom_density(alpha=.5) +
scale_fill_manual('TH Group', values = c("#87CEFA", "#DC143C", "#F6710B")) +
theme(legend.position = "none") + ggtitle("Head Size Distribution") +
theme(plot.title = element_text(hjust = 0.6, size=12, face="bold")) +
xlab("Head Size") + ylab("Frequency of Fish") +
theme(axis.text=element_text(size=10, face="bold"),
    axis.title=element_text(size=10, face="bold"))
```

```
xdensity2 + theme(legend.position="right")
```

HEAD SIZE

While I tried to collect a balanced dataset for both body size and head size, there are more Mtz fish with bigger heads. This is because Mtz have bigger heads than Eu. The average head size is between 4.8 - 5.1 mm.

AGE

Age is distributed very unevenly in my dataset because Opallus are precocious and Mtz are developmentally delayed. ie. An Opallus may take only 3 months to reach the size of a 6 month old Eu, while Mtz could take 1 year. The average ages for Eu, Mtz and Op are 7-11 months.

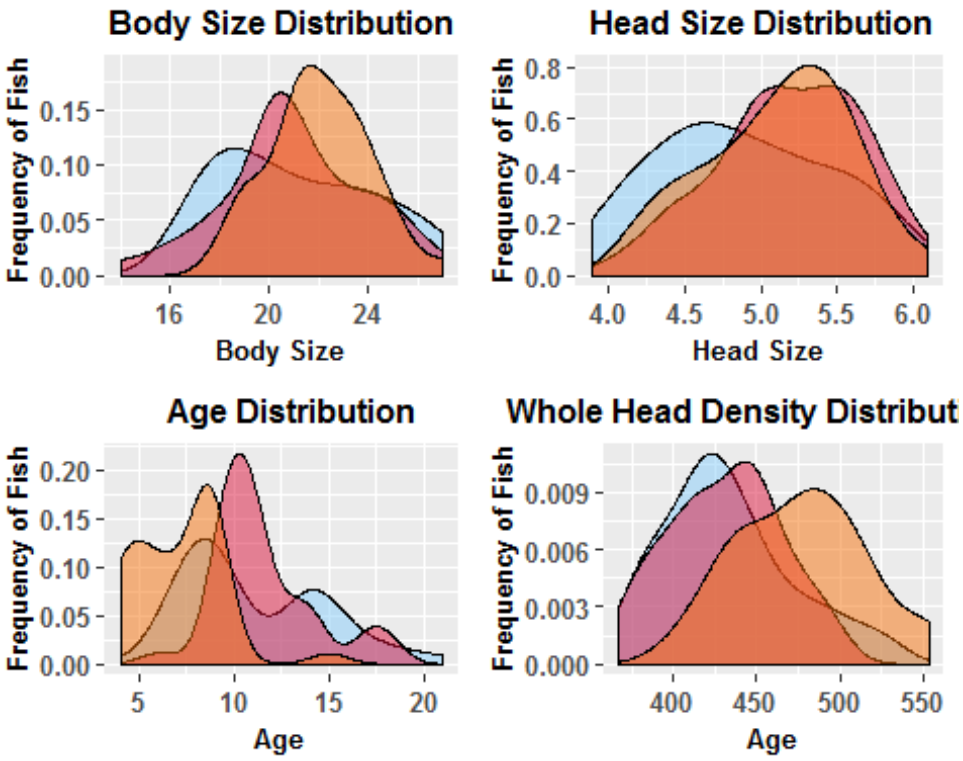

HISTOGRAM OF BONE GREY VALUES

I collected histogram data on individual bone, using 10 per group averaged together.

```
#histo1 <- read.csv("histo_MASTER_15Oct.csv")
par(mfrow = c(2, 2))
group_colors <- c("#87CEFA", "#DC143C", "#F6710B")

histo_all <- ggscatter(histo1, x = "grey", y = "all_avg", color = "group", ylab="Count", xlab="Grey Value", size=1) +
   scale_colour_manual(values= c("#87CEFA", "#DC143C", "#F6710B")) +
   ggtitle("Histogram of Whole Head") + theme(plot.title = element_text(hjust = 0.5))

histo_dent <- ggscatter(histo1, x = "grey", y = "dent_avg", color = "group", ylab="Count",
```

```
xlab="Grey Value", size=1) +
    scale_colour_manual(values= c("#87CEFA", "#DC143C", "#F6710B")) + ggtitle("Histogram of
Dentary") +
    theme(plot.title = element_text(hjust = 0.5))

histo_dermato <- ggscatter(histo1, x = "grey", y = "dermato_avg", color = "group", ylab="Count",
xlab="Grey Value", size=1) +
    scale_colour_manual(values= c("#87CEFA", "#DC143C", "#F6710B")) +
    ggtitle("Histogram of Dermatocranium") + theme(plot.title = element_text(hjust = 0.5))

histo_kin <- ggscatter(histo1, x = "grey", y = "kin_avg", color = "group", ylab="Count",
xlab="Grey Value", size=1) +
    scale_colour_manual(values= c("#87CEFA", "#DC143C", "#F6710B")) +
    ggtitle("Histogram of Kinethmoid") + theme(plot.title = element_text(hjust = 0.5))
ggarrange(histo_all, histo_dermato, histo_dent, histo_kin + rremove("x.text"),
        ncol = 2, nrow = 2)
```

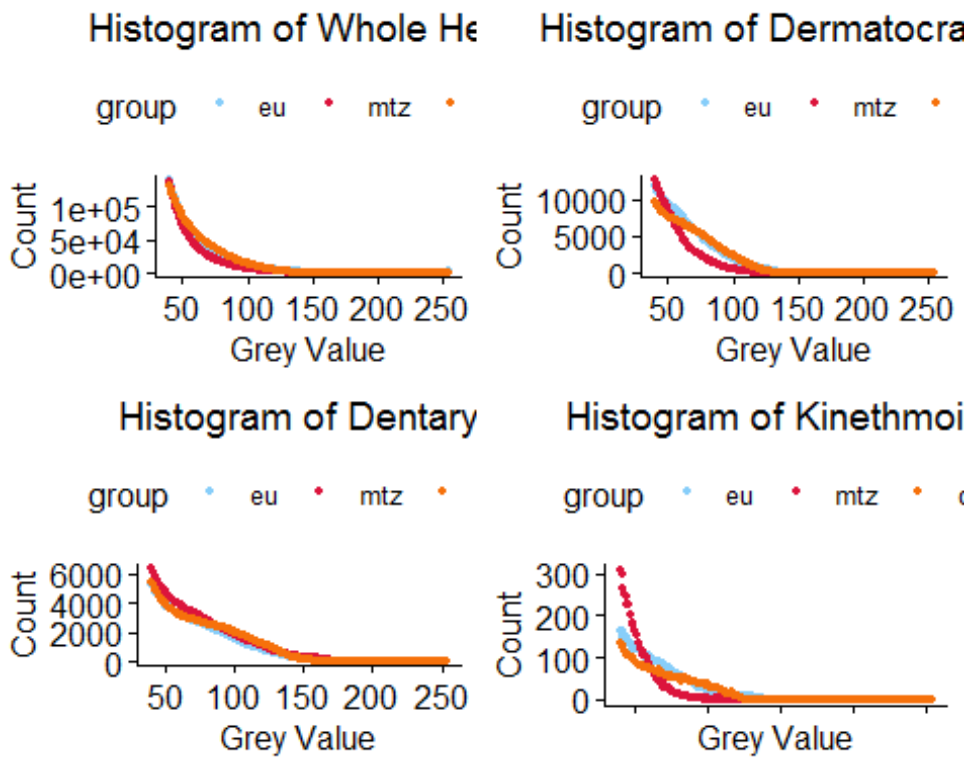

(5) Simple Scatterplots

SIZE COMPARISONS

How well does head size scale with body size between groups?

```
{plot(df$dermatodens,df$age, main="Dermatodens vs. Age", xlim=c(280,620),ylim=c(4,21),
xlab="Density", ylab="Age (mo)",cex=0.50)
 points(df$age[df$group=="Eu"] ~ df$dermatodens[df$group=="Eu"],
      pch=18,col="#87CEFA",cex=1.25)
```

```
points(df$age[df$group=="TH-"] ~ df$dermatodens[df$group=="TH-"],
      pch=15,col="#DC143C",cex=1.25)
points(df$age[df$group=="TH+"] ~ df$dermatodens[df$group=="TH+"],
      pch=17,col="#F6710B",cex=1.25)
legend("topleft",legend = c("TH","TH-","TH+"), col=c("#87CEFA","#DC143C","#F6710B"),
       pch=c(18,15,17),cex=0.8)
# text(pos=3, y=df$age, x=df$dermatodens, labels = df$specimen, col="darkgrey", cex = 0.5)
lmDMSO<-lm(df2$age[df2$group=="Eu"]~df2$dermatodens[df2$group=="Eu"])
abline(col="blue",lmDMSO, lwd=3)
lmMTZ<-lm(df2$age[df2$group=="TH-"]~df2$dermatodens[df2$group=="TH-"])
abline(col="#DC143C",lmMTZ, lwd=3)
lmOP<-lm(df2$age[df2$group=="TH+"]~df2$dermatodens[df2$group=="TH+"])
abline(col="#F6710B",lmOP, lwd=3)}
```

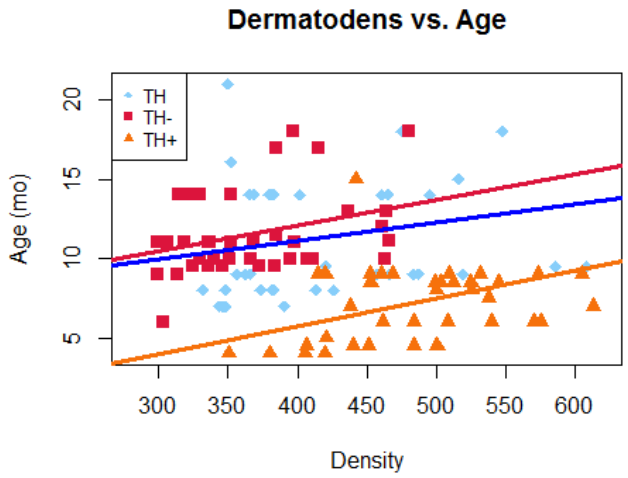

(6) SIMPLE BOXPLOTS

ANOVAs performed on Tukey's Transformed variables. All tests are One Way ANOVAs, with the exception of the dermatocranium and otolith; since they are not normally distributed, the Kruskal Wallis Test One Way Anova by Ranks was used.

DENTARY SHAFT MAX

Dentary Shaft Max differs significantly (p=0.0028)** for Mtz-Eu (p=0.005)*.

```
ggdentmax <- ggplot(df, aes(factor(group), df$dentshaftmax)) +
 geom_boxplot(aes(fill = factor(group)), lwd=1) +
 geom_jitter(width = 0.065) +
 ggtitle("Dentary ShaftMax") +
 xlab("Group") + ylab("Max Density (HA/cm^3)") +
 scale_fill_manual('TH Group', values = c("#87CEFA","#DC143C","#F6710B")) +
 theme(plot.title = element_text(hjust = 0.5, size=20, face="bold")) +
 theme(axis.text=element_text(size=16, face="bold"), axis.title=element_text(size=14)) +
 stat_summary(fun.y = median, fun.ymin = median, fun.ymax = median)
ggdentmax
```

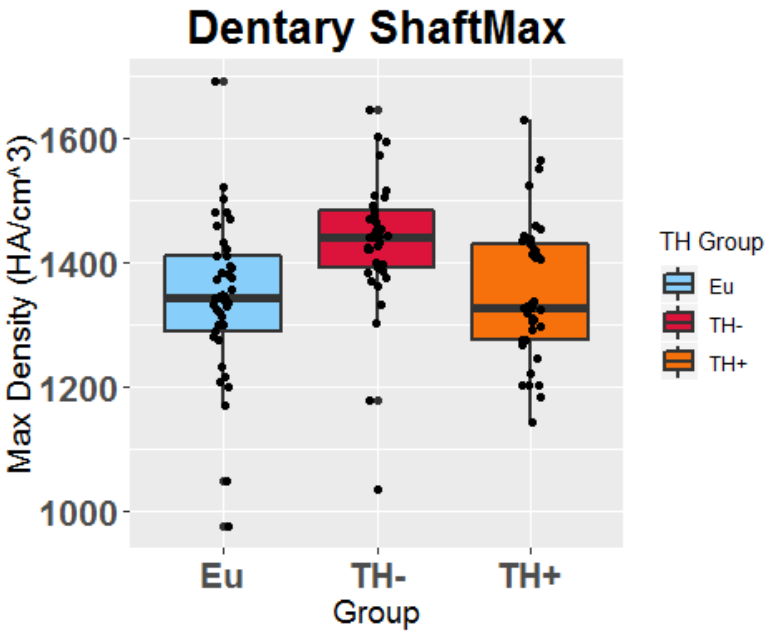


```
print ("One Way ANOVA")
df5b <- rowMeans(data.frame(df$dentshaftmax_tt, na.rm=T))
summary(aov17 <- aov(df5b ~ df$group))
TukeyHSD(aov17)
```

MS/LESION BONE VOLUME

MS/Lesion Bone Volume differs significantly (p=<2e-16)*** between Mtz-Eu (p=<2e-16)***.

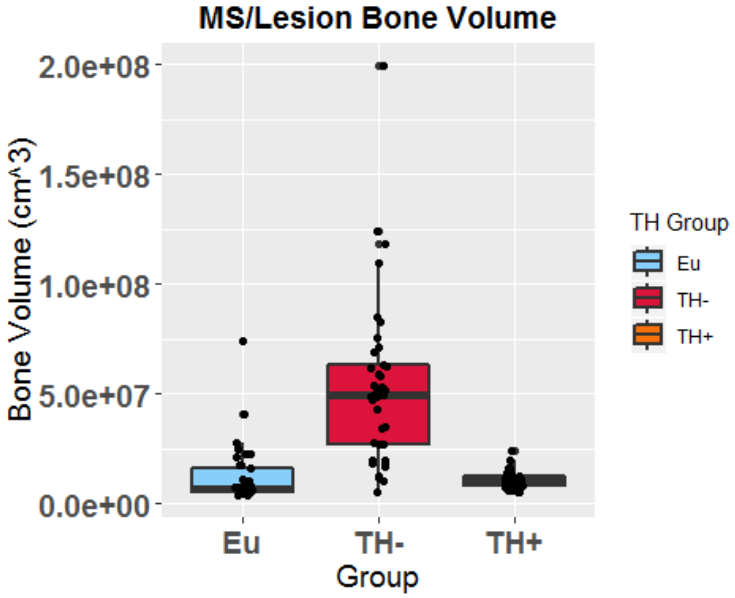

```
## [1] "One Way ANOVA"
##             Df    Sum Sq   Mean Sq F value Pr(>F)
## df$group     2 1.087e-06 5.433e-07   54.37 <2e-16 ***
## Residuals   108 1.079e-06 1.000e-08
## ---
## Signif. codes:  0 '***' 0.001 '**' 0.01 '*' 0.05 '.' 0.1 ' ' 1
##   Tukey multiple comparisons of means
##     95% family-wise confidence level
##
## Fit: aov(formula = df5b ~ df$group)
##
## $`df$group`
##                diff         lwr         upr     p adj
## TH--Eu   2.275423e-04  1.723098e-04  2.827748e-04 0.0000000
## TH+-Eu   4.153404e-05 -1.369843e-05  9.676652e-05 0.1787564
## TH+-TH- -1.860082e-04 -2.412407e-04 -1.307758e-04 0.0000000
```

DERMATOCRANIUM DENSITY

Dermatocranium density differs significantly (p=1.4e-09)*** for Mtz-Eu (p=.00281)* and Op-Eu (p=0.00011)***.

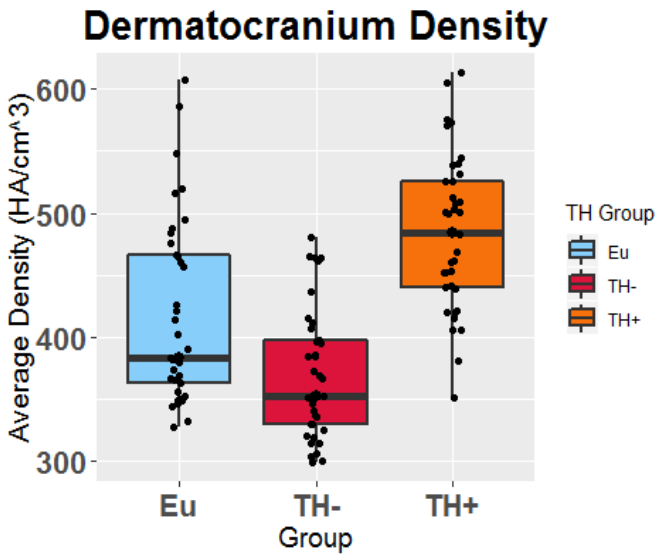


```
## [1] "Kruskal Wallis One Way Anova by Ranks"
x <- df$dermatodens_tt   #numeric, continuous
y <- df$condition        #categorical, with 3 levels
kruskal.test(x~y, data=df)
##
##  Kruskal-Wallis rank sum test
##
## data:  x by y
## Kruskal-Wallis chi-squared = 40.773, df = 2, p-value = 1.4e-09
pairwise.wilcox.test(df$dermatodens_tt, df$group, p.adjust.method = "BH")
```

```
##
##  Pairwise comparisons using Wilcoxon rank sum test
##
## data:  df$dermatodens_tt and df$group
##
##     Eu      TH-
## TH- 0.00281 -
## TH+ 0.00011 4.6e-11
##
## P value adjustment method: BH
#If p-val is less than 0.05, we can conclude that there are significant differences between the
treatment groups.
```

(7) OTOLITH ANALYSIS

We observed extreme differences in otolith morphology, thus I quantified various measures including asymmetry, missing otoliths, ectopic otoliths, misshapened otoliths, and extra otoliths. Each defect was used to calculate an Otolith Severity score, with 0 being no defects.

NUMBER OF OTOLITHS PRESENT

```
#dfo <- read.csv("otolith_quant_1Oct.csv")
x  <- dfo$oto_percent[df$group=="Eu"]
y  <- dfo$oto_percent[df$group=="TH-"]
z  <- dfo$oto_percent[df$group=="TH+"]
z1 <- dfo$oto_percent

xtab  <- table(x)
ytab  <- table(y)
ztab  <- table(z)
z1tab <- table(z1)

par(mfrow = c(2, 2))
barplot(xtab,  ylab="Number of Fish", xlab="Percent Bins", col="red",main="Eu Otolith
Percentage",  ylim=c(0,45))
barplot(ytab,  ylab="Number of Fish", xlab="Percent Bins", col="red",main="TH- Otolith
Percentage", ylim=c(0,45))
barplot(ztab,  ylab="Number of Fish", xlab="Percent Bins", col="red",main="TH+ Otolith
Percentage", ylim=c(0,45))
barplot(z1tab, ylab="Number of Fish", xlab="Percent Bins", col="red",main="All Otolith
Percentage", ylim=c(0,85))
```

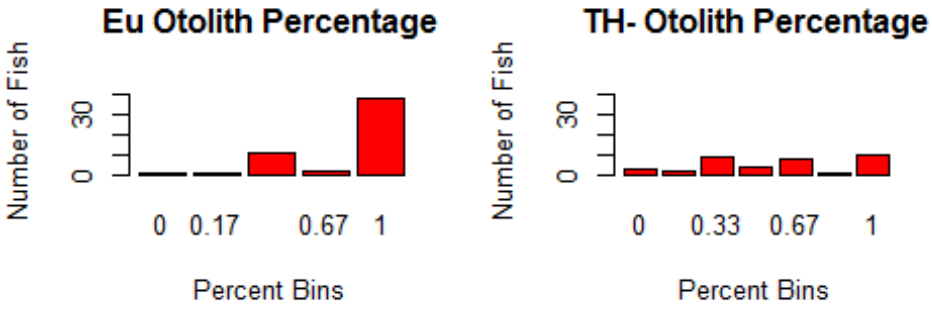

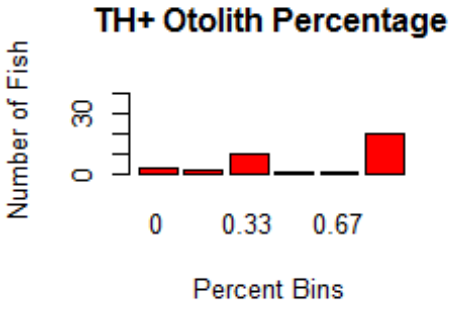

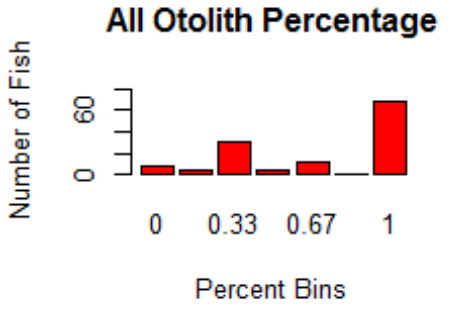

QUANTITY OF OTOLITHS

Lapillus (most anterior), Sagitta (middle), Astericus (most posterior)

```
## [1] "Lapillus Mean per group"
##       Eu      TH-      TH+
## 1.3809524 0.9268293 1.2500000
## [1] "Sagitta Mean per group"
##      Eu     TH-     TH+
## 1.380952 1.000000 1.227273
## [1] "Astericus Mean per group"
##      Eu     TH-     TH+
## 1.952381 2.219512 1.795455
```

CHI-SQUARED CONTINGENCY TESTS

Is there a contingency between TH group and otolith severity?

```
oto   <- read.csv("oto_heatmap.csv")
# Create a Frequency Table
shape1 <- table(oto[,2], oto[,7], dnn = c("Condition", "Shape"))
position1 <- table(oto[,2], oto[,8], dnn = c("Condition", "Position"))
quantity1 <- table(oto[,2], oto[,9], dnn = c("Condition", "Quantity"))

# Transpose table
shape2 <- t(shape1)
position2 <- t(position1)
quantity2 <- t(quantity1)
```

```
# 2. Graph
library("gplots")
balloonplot(t(quantity2), main ="Quantity Score Frequency Table", xlab ="", ylab="Quantity
Score",
        label = FALSE, show.margins = FALSE)
```

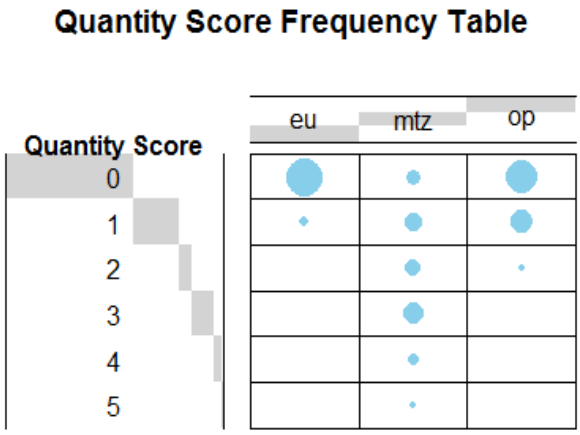


```
quantitychi1 <- chisq.test(quantity2, correct=FALSE)
quantitychi1
##
##  Pearson's Chi-squared test
##
## data:  quantity2
## X-squared = 78.977, df = 10, p-value = 7.965e-13
#Run Chi-Squared
shapechi1 <- chisq.test(shape2, correct=FALSE)
shapechi1$p.value
## [1] 0.001225407
#Critical Values for Chi-Squared and adjusted p-vals
#For 12 degrees of freedom, the critical value is 21.026
```

OTOLITH SEVERITY SCORES

Otolith Severity differs (p=5.64e-10)*** with Mtz-Eu (p=<2e-16)*** and Op-Eu (p=0.02)*.

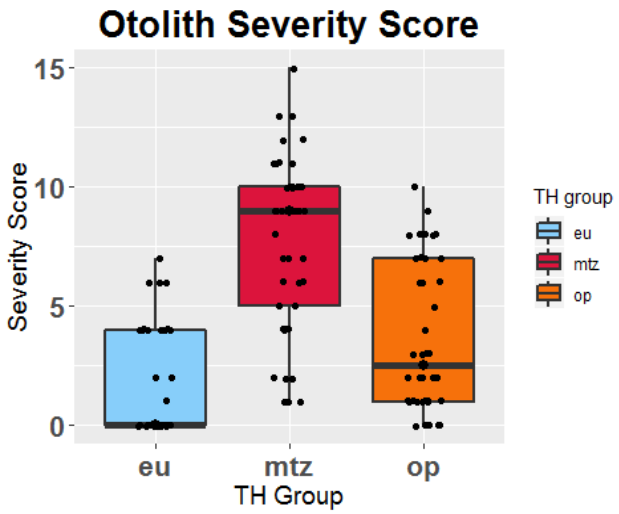


```
## [1] "One Way ANOVA"
##             Df Sum Sq Mean Sq F value   Pr(>F)
## oto$group    2  195.7   97.85   41.34 1.66e-14 ***
## Residuals   125  295.9    2.37
## ---
## Signif. codes:  0 '***' 0.001 '**' 0.01 '*' 0.05 '.' 0.1 ' ' 1
##   Tukey multiple comparisons of means
##     95% family-wise confidence level
##
## Fit: aov(formula = df5b ~ oto$group)
##
## $`oto$group`
##             diff       lwr      upr     p adj
## mtz-eu  3.015315  2.2187472  3.811882 0.0000000
## op-eu   1.061047  0.2785035  1.843590 0.0046815
## op-mtz -1.954268 -2.7464054 -1.162131 0.0000001
```

Testing linear models for best fit, on Tukey's transformed data

(8) LINEAR MODELS

TOTAL DENTARY DENSITY VS. HEAD SIZE

Model used is density ~ group + headsize.

```
sp <-   ggscatter(df, x = "headsize", y = "totaldentdens_calib", color = "group", xlab = "Head Size (mm)", ylab = "Density (HA/cm^3)",
              palette = c("#87CEFA", "#DC143C", "#F6710B"), alpha = 1, ggtheme = theme_bw()) +
 ggtitle("Total Dentary Density vs Head Size") + ylim(390,705) +
 geom_point(aes(color = (group), shape = factor(group)), size = 3)

sp <- sp + geom_smooth(data=subset(df,df$group=="Eu"),  formula = y ~ x, method = "lm", se = T, color="#87CEFA", level=0.95, fill ="#87CEFA", alpha=0.25)
sp <- sp + geom_smooth(data=subset(df,df$group=="TH-"), formula = y ~ x, method = "lm", se =
```

```
T, color="#DC143C", level=0.95, fill ="#DC143C", alpha=0.25)
sp <- sp + geom_smooth(data=subset(df,df$group=="TH+"), formula = y ~ x, method = "lm", se =
T, color="#F6710B", level=0.95, fill ="#F6710B", alpha=0.25)

#Marginal Boxplot
yplot <- ggplot(df, aes(factor(group), df$totaldentdens_calib)) +
 geom_boxplot(aes(fill = factor(group)), lwd=0.5) + ylim(390,705) +
 scale_fill_manual('group', values = c("#87CEFA","#DC143C","#F6710B")) + theme_bw()

# Cleaning the plots
sp <- sp + rremove("legend")
plot_grid(sp, yplot, ncol = 2, align = "hv", rel_widths = c(2, 1), rel_heights = c(1, 2))
```

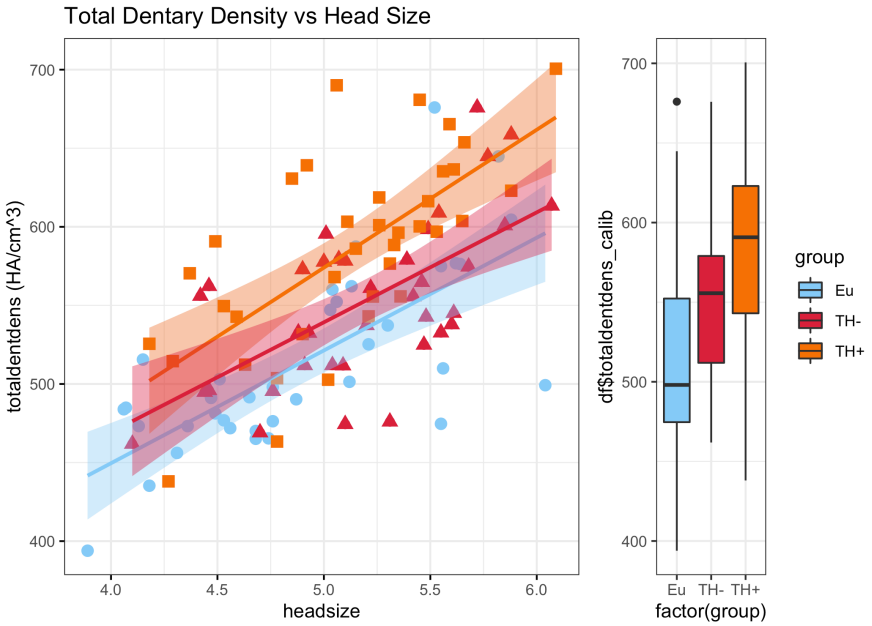


```
lm1_totaldentdens_tt <- lm(df$totaldentdens_tt ~ df$group)
lm2_totaldentdens_tt <- lm(df$totaldentdens_tt ~ df$group + df$headsize)  # controlling for
head size
lm3_totaldentdens_tt <- lm(df$totaldentdens_tt ~ df$group + df$bodysize)  # controlling for
body size

AIC(lm1_totaldentdens_tt,lm2_totaldentdens_tt,lm3_totaldentdens_tt)
ModelSelection <- AIC(lm1_totaldentdens_tt,lm2_totaldentdens_tt,lm3_totaldentdens_tt)
```

AIC Model Performance

Akaike's An Information Criterion determines what model performs best; AIC penalizes for adding predictors. Linear Model 4 is the best fit model

```
#AIC score of 3 or more denotes better fit model
ModelSelection[order(ModelSelection$AIC),]
##                df      AIC
## lm2_totaldentdens_tt  5 -747.7845
```

```
## lm3_totaldentdens_tt  5 -729.0596
## lm1_totaldentdens_tt  4 -680.3667
```

Summary of Best AOV Model

```
#Density ~ controlling for head size
summary(aov(lm2_totaldentdens_tt))
#What are the signficicant groups?
summary(lm2_totaldentdens_tt)
#What are the effect sizes?
cohens_f(lm2_totaldentdens_tt)
## [1] "Best linear model is Total Dentary Density explained by group controlling for headsize (p=3.90e-10)***"
## [1] "Signficant groups is Op-Eu (p=3.13e-07)***"
## [1] "Effect Size/Cohen's F: Density explained by group (0.706) controlling for headsize (0.93)"
## [1] "F-stat critical value for 3 and 107 df is 2.68"
## [1] "Test F-stat is 48.8"
```

Residual Boxplot

What is the spread of the residuals per group?

```
plot(df$group, df$totaldentdens.res, ylab="Residuals", xlab="TH Group", main="Total Dentary Density Transformed Residuals")
abline(0, 0)
beeswarm(df$totaldentdens.res ~ df$group, add =T)
```

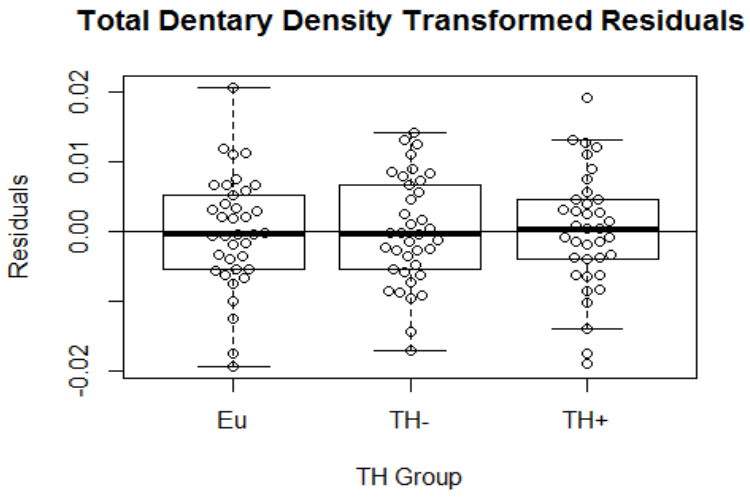

5.0 REFERENCES

[1] Furlow, J. D., & Neff, E. S. (2006). A developmental switch induced by thyroid hormone: Xenopus laevis metamorphosis. *Trends in Endocrinology & Metabolism*, *17*(2), 40-47.
[2] Ishida, H., Bellows, C. G., Aubin, J. E., & Heersche, J. N. M. (1995). Tri-iodothyronine (T3) and dexamethasone interact to modulate osteoprogenitor cell differentiation in fetal rat calvaria cell cultures. *Bone*, *16*(5), 545-549.
[3] Pascual, A., & Aranda, A. (2013). Thyroid hormone receptors, cell growth and differentiation. *Biochimica et Biophysica Acta (BBA)-General Subjects*, 1830(7), 3908-3916.
[4] Sirakov, M., Skah, S., Nadjar, J., & Plateroti, M. (2013). Thyroid hormone's action on progenitor/stem cell biology: new challenge for a classic hormone?. *Biochimica et Biophysica Acta (BBA)-General Subjects*, 1830(7), 3917-3927.
[5] Keer, S., Cohen, K., May, C., Hu, Y., McMenamin, S., & Hernandez, L. P. Anatomical assessment of the adult skeleton of zebrafish reared under different thyroid hormone profiles. *The Anatomical Record*.
[6] Bassett, J. D., & Williams, G. R. (2003). The molecular actions of thyroid hormone in bone. *Trends in Endocrinology & Metabolism*, *14*(8), 356-364.
[7] O'Shea, P. J., Harvey, C. B., Suzuki, H., Kaneshige, M., Kaneshige, K., Cheng, S. Y., & Williams, G. R. (2003). A thyrotoxic skeletal phenotype of advanced bone formation in mice with resistance to thyroid hormone. *Molecular Endocrinology*, *17*(7), 1410-1424.
[8] Weigele, J., & Franz-Odendaal, T. A. (2016). Functional bone histology of zebrafish reveals two types of endochondral ossification, different types of osteoblast clusters and a new bone type. *Journal of anatomy*, 229(1), 92-103.
[9] Carey, E. J. (1920). Studies in the Dynamics of Histogenesis. *The Anatomical Record*: Supplement. (1920), 19, 199.
[10] Wagner, G. P. (2018). Homology, genes, and evolutionary innovation. *Princeton University Press*.
[11] Lema, S. C., & Kitano, J. (2013). Hormones and phenotypic plasticity: implications for the evolution of integrated adaptive phenotypes. *Current zoology*, 59(4), 506-525.
[12] Levine, M., & Davidson, E. H. (2005). Gene regulatory networks for development. Proceedings of the *National Academy of Sciences*, 102(14), 4936-4942.
[13] Denoël, M., Joly, P., & Whiteman, H. H. (2005). Evolutionary ecology of facultative paedomorphosis in newts and salamanders. *Biological Reviews*, 80(4), 663-671.
[14] Rose, C. S. (2005). Integrating ecology and developmental biology to explain the timing of frog metamorphosis. *Trends in Ecology & Evolution*, 20(3), 129-135.
[15] Tata, J. R. (2005). One hundred years of hormones. *EMBO reports*, 6(6), 490-496.
[16] Combs, C. E., Nicholls, J. J., Duncan Bassett, J. H., & Williams, G. R. (2011). Thyroid hormones and bone development. *Minerva Endocrinol*, *36*(1), 71-85.
[17] Gardner, W. U., & Pfeiffer, C. A. (1943). Influence of estrogens and androgens on the skeletal system. *Physiological Reviews*, 23(2), 139-165.
[18] Hall, B. K., Pearson, B. J., & Müller, G. B. (2003). *Environment, development, and evolution.* Towards a Synthesis. Vienna Series.
[19] Robson, H., Siebler, T., Stevens, D. A., Shalet, S. M., & Williams, G. R. (2000). Thyroid hormone acts directly on growth plate chondrocytes to promote hypertrophic differentiation and inhibit clonal expansion and cell proliferation. *Endocrinology*, *141*(10), 3887-3897.
[20] Stevens, D. A., Hasserjian, R. P., Robson, H., Siebler, T., Shalet, S. M., & Williams, G. R. (2000). Thyroid hormones regulate hypertrophic chondrocyte differentiation and expression of parathyroid hormone related peptide and its receptor during endochondral bone formation. *Journal of bone and mineral research*, *15*(12), 2431-2442.

[21] Bohnsack, B. L., & Kahana, A. (2013). Thyroid hormone and retinoic acid interact to regulate zebrafish craniofacial neural crest development. *Developmental biology*, *373*(2), 300-309.
[22] Grimaldi, A., Buisine, N., Miller, T., Shi, Y. B., & Sachs, L. M. (2013). Mechanisms of thyroid hormone receptor action during development: lessons from amphibian studies. *Biochimica et Biophysica Acta (BBA)-General Subjects*, *1830*(7), 3882-3892.
[23] Kapoor, R., Fanibunda, S. E., Desouza, L. A., Guha, S. K., & Vaidya, V. A. (2015). Perspectives on thyroid hormone action in adult neurogenesis. *Journal of neurochemistry*, 133(5), 599-616.
[24] Song, L., & Tuan, R. S. (2004). Transdifferentiation potential of human mesenchymal stem cells derived from bone marrow. *The FASEB Journal*, *18*(9), 980-982.
[25] Havis, E., Sachs, L. M., & Demeneix, B. A. (2003). Metamorphic T3-response genes have specific co-regulator requirements. *EMBO reports*, 4(9), 883-888.
[26] Fisher, S., & Franz-Odendaal, T. (2012). Evolution of the bone gene regulatory network. *Current opinion in genetics & development,* 22(4), 390-397.
[27] Hall, B. K., & Miyake, T. (2000). All for one and one for all: condensations and the initiation of skeletal development. *Bioessays*, 22(2), 138-147.
[28] Giffin, J. L., Gaitor, D., & Franz-Odendaal, T. A. (2019). The Forgotten Skeletogenic Condensations: A Comparison of Early Skeletal Development Amongst Vertebrates. *Journal of developmental biology*, 7(1), 4.
[29] Young, N. M., Hu, D., Lainoff, A. J., Smith, F. J., Diaz, R., Tucker, A. S., ... & Marcucio, R. S. (2014). Embryonic bauplans and the developmental origins of facial diversity and constraint. *Development*, 141(5), 1059-1063.
[30] Merrill, A. E., Eames, B. F., Weston, S. J., Heath, T., & Schneider, R. A. (2008). Mesenchyme-dependent BMP signaling directs the timing of mandibular osteogenesis. *Development*, 135(7), 1223-1234.
[31] Abe, E., Marians, R. C., Yu, W., Wu, X. B., Ando, T., Li, Y., ... & Davies, T. F. (2003). TSH is a negative regulator of skeletal remodeling. *Cell*, 115(2), 151-162.
[32] Dentice, M., Ambrosio, R., Damiano, V., Sibilio, A., Luongo, C., Guardiola, O., ... & Marsili, A. (2014). Intracellular inactivation of thyroid hormone is a survival mechanism for muscle stem cell proliferation and lineage progression. *Cell metabolism*, 20(6), 1038-1048.
[33] Umesono, K., Giguere, V., Glass, C. K., Rosenfeld, M. G., & Evans, R. M. (1988). Retinoic acid and thyroid hormone induce gene expression through a common responsive element. *Nature*, 336(6196), 262.
[34] Wang, X., He, H., Tang, W., Zhang, X. A., Hua, X., & Yan, J. (2012). Two origins of blastemal progenitors define blastemal regeneration of zebrafish lower jaw. *PLoS One*, 7(9), e45380.
[35] Li, N., Felber, K., Elks, P., Croucher, P., & Roehl, H. H. (2009). Tracking gene expression during zebrafish osteoblast differentiation. *Developmental dynamics*, *238*(2), 459-466.
[36] Mork, L., & Crump, G. (2015). Zebrafish craniofacial development: a window into early patterning. In *Current topics in developmental biology* (Vol. 115, pp. 235-269). Academic Press.
[37] Paul, S., Schindler, S., Giovannone, D., de Millo Terrazzani, A., Mariani, F. V., & Crump, J. G. (2016). Ihha induces hybrid cartilage-bone cells during zebrafish jawbone regeneration. *Development*, 143(12), 2066-2076.
[38] Renn, J., Winkler, C., Schartl, M., Fischer, R., & Goerlich, R. (2006). Zebrafish and medaka as models for bone research including implications regarding space-related issues. *Protoplasma*, *229*(2-4), 209-214.
[39] Jomaa, B., Kessels, M. Y., van den Berg, H. H., Aarts, J. M., de Vries, S. C., & Rietjens, I. M. Effect of thyroid hormone on bone development of early stage zebrafish larvae. Carboxypeptidase Z, 85.
[40] Shiao, J. C., & Hwang, P. P. (2004). Thyroid hormones are necessary for teleostean otolith growth. *Marine Ecology Progress Series*, 278, 271-278.
[41] Shkil, F. N., Kapitanova, D. V., Borisov, V. B., Abdissa, B., & Smirnov, S. V. (2012). Thyroid hormone in skeletal development of cyprinids: effects and morphological consequences. *Journal of Applied Ichthyology*, 28(3), 398-405.
[42] Hall, Jane, Andrew H. Jheon, Erin L. Ealba, B. Frank Eames, Kristin D. Butcher, Siu-Shan Mak, Raj Ladher, Tamara Alliston, and Richard A. Schneider. "Evolution of a developmental mechanism: species-specific regulation of the cell cycle and the timing of events during craniofacial osteogenesis." *Developmental biology* 385, no. 2 (2014): 380-395.

[43] Aubin, J. E., Liu, F., Malaval, L., & Gupta, A. K. (1995). Osteoblast and chondroblast differentiation. *Bone*, *17*(2), S77-S83.
[44] Crane, J. F., & Trainor, P. A. (2006). Neural crest stem and progenitor cells. *Annu. Rev. Cell Dev. Biol.*, *22*, 267-286.
[45] Abzhanov, A., Rodda, S. J., McMahon, A. P., & Tabin, C. J. (2007). Regulation of skeletogenic differentiation in cranial dermal bone. *Development*, *134*(17), 3133-3144.
[46] Rutkovskiy, A., Stensløkken, K. O., & Vaage, I. J. (2016). Osteoblast differentiation at a glance. *Medical science monitor basic research*, *22*, 95.
[47] Yuan, Y., & Chai, Y. (2019). Regulatory mechanisms of jaw. *Vertebrate Skeletal Development*, *133*, 91.
[48] Akiyama, H., & Lefebvre, V. (2011). Unraveling the transcriptional regulatory machinery in chondrogenesis. *Journal of bone and mineral metabolism*, 29(4), 390-395.
[49] Bi, W., Deng, J. M., Zhang, Z., Behringer, R. R., & de Crombrugghe, B. (1999). Sox9 is required for cartilage formation. *Nature genetics*, *22*(1), 85.
[50] Yan, Y. L., Miller, C. T., Nissen, R., Singer, A., Liu, D., Kirn, A., ... & Chung, B. C. (2002). A zebrafish sox9 gene required for cartilage morphogenesis. *Development*, *129*(21), 5065-5079.
[51] Wang, L., Shao, Y. Y., & Ballock, R. T. (2007). Thyroid hormone interacts with the Wnt/β-catenin signaling pathway in the terminal differentiation of growth plate chondrocytes. Journal of Bone and Mineral Research, 22(12), 1988-1995.
[52] Yelick, P. C., & Schilling, T. F. (2002). Molecular dissection of craniofacial development using zebrafish. *Critical Reviews in Oral Biology & Medicine*, 13(4), 308-322.
[53] Kimmel, C. B., DeLaurier, A., Ullmann, B., Dowd, J., & McFadden, M. (2010). Modes of developmental outgrowth and shaping of a craniofacial bone in zebrafish. *PloS one*, 5(3), e9475.
[54] Mariotti, M., Carnovali, M., & Banfi, G. (2015). *Danio rerio:* the Janus of the bone from embryo to scale. *Clinical Cases in Mineral and Bone Metabolism*, 12(2), 188.
[55] Chai, Y., Jiang, X., Ito, Y., Bringas, P., Han, J., Rowitch, D. H., ... & Sucov, H. M. (2000). Fate of the mammalian cranial neural crest during tooth and mandibular morphogenesis. *Development*, 127(8), 1671-1679.
[56] Eames, B. F., DeLaurier, A., Ullmann, B., Huycke, T. R., Nichols, J. T., Dowd, J., ... & Kimmel, C. B. (2013). FishFace: interactive atlas of zebrafish craniofacial development at cellular resolution. *BMC developmental biology*, *13*(1), 23.
[57] Rüegsegger, P., Elsasser, U., Anliker, M., Gnehm, H., Kind, H., & Prader, A. (1976). Quantification of bone mineralization using computed tomography. *Radiology*, 121(1), 93-97.
[58] Williams, G. R. (2013). Thyroid hormone actions in cartilage and bone. *European thyroid journal*, 2(1), 3-13.
[59] McMenamin, S. K., Bain, E. J., McCann, A. E., Patterson, L. B., Eom, D. S., Waller, Z. P., ... & Parichy, D. M. (2014). Thyroid hormone–dependent adult pigment cell lineage and pattern in zebrafish. *Science,* 1256251.
[60] Endo, T., & Kobayashi, T. (2011). Thyroid-specific gene expression in chondrocytes. *Biochemical and biophysical research communications*, 416(3-4), 227-231.
[61] Hu, Y., Mauri, A., Donahue, J., Singh, R., Acosta, B., & McMenamin, S. (2019). Thyroid hormone coordinates developmental trajectories but does not underlie developmental truncation in Danionins. *Developmental Dynamics*.
[62] Wilkie, A. O., & Morriss-Kay, G. M. (2001). Genetics of craniofacial development and malformation. *Nature Reviews Genetics*, 2(6), 458.
[63] Friede, H. (1981). Normal development and growth of the human neurocranium and cranial base. *Scandinavian journal of plastic and reconstructive surgery,* 15(3), 163-169.
[64] Britz, R., & Conway, K. W. (2009). Osteology of *Paedocypris*, a miniature and highly developmentally truncated fish (Teleostei: Ostariophysi: Cyprinidae). *Journal of Morphology*, 270(4), 389-412.
[65] Schilling, T. F. (2002). The morphology of larval and adult zebrafish. *Zebrafish*, 261, 59-94.
[66] Hernandez, L.. Patricia, Bird, N. C., & Staab, K. L. (2007). Using zebrafish to investigate cypriniform evolutionary novelties: functional development and evolutionary diversification of the kinethmoid. *Journal of Experimental Zoology Part B: Molecular and Developmental Evolution*, 308(5), 625-641.

[67] McMenamin, S., Carter, C., & Cooper, W. J. (2017). Thyroid hormone stimulates the onset of adult feeding kinematics in zebrafish. *Zebrafish,* 14(6), 517-525.
[68] Coffin, A. B., Raine, J. C., & Hawryshyn, C. W. (2012). Exposure to thyroid hormone in ovo affects otolith crystallization in rainbow trout *Oncorhynchus mykiss*. *Environmental biology of fishes*, 95(3), 347-354.
[69] Cubbage, C. C., & Mabee, P. M. (1996). Development of the cranium and paired fins in the zebrafish *Danio rerio* (Ostariophysi, Cyprinidae). *Journal of Morphology*, 229(2), 121-160.
[70] Schreiber, A. M., Wang, X., Tan, Y., Sievers, Q., Sievers, B., Lee, M., & Burrall, K. (2010). Thyroid hormone mediates otolith growth and development during flatfish metamorphosis. General and comparative endocrinology, 169(2), 130-137.
[71] Zelditch, M. L., Wood, A. R., & Swiderski, D. L. (2009). Building developmental integration into functional systems: function-induced integration of mandibular shape. *Evolutionary Biology*, 36(1), 71-87.
[72] Parsons, K. J., Son, Y. H., Crespel, A., Thambithurai, D., Killen, S., Harris, M. P., & Albertson, R. C. (2018). Conserved but flexible modularity in the zebrafish skull: implications for craniofacial evolvability. Proceedings of the Royal Society B: Biological Sciences, 285(1877), 20172671.
[73] Karl, A., Olbrich, N., Pfeifer, C., Berner, A., Zellner, J., Kujat, R., ... & Mueller, M. B. (2013). Thyroid hormone-induced hypertrophy in mesenchymal stem cell chondrogenesis is mediated by bone morphogenetic protein-4. *Tissue Engineering Part A*, *20*(1-2), 178-188.
[74] Dupin, E., & Sommer, L. (2012). Neural crest progenitors and stem cells: from early development to adulthood. *Developmental biology*, *366*(1), 83-95.
[75] Xing, W., Cheng, S., Wergedal, J., & Mohan, S. (2014). Epiphyseal chondrocyte secondary ossification centers require thyroid hormone activation of Indian hedgehog and osterix signaling. *Journal of bone and mineral research*, *29*(10), 2262-2275.
[76] DeLaurier, A., Eames, B. F., Blanco-Sánchez, B., Peng, G., He, X., Swartz, M. E., ... & Kimmel, C. B. (2010). Zebrafish sp7: EGFP: a transgenic for studying otic vesicle formation, skeletogenesis, and bone regeneration. *Genesis*, 48(8), 505-511.
[77] Collery, R. F., & Link, B. A. (2011). Dynamic smad-mediated BMP signaling revealed through transgenic zebrafish. *Developmental Dynamics*, 240(3), 712-722.
[78] Aghajanian, P., Xing, W., Cheng, S., & Mohan, S. (2017). Epiphyseal bone formation occurs via thyroid hormone regulation of chondrocyte to osteoblast transdifferentiation. *Scientific reports*, *7*(1), 10432.
[79] Reya, T., Morrison, S. J., Clarke, M. F., & Weissman, I. L. (2001). Stem cells, cancer, and cancer stem cells. *nature*, *414*(6859), 105.
[80] Miller, C. T., Yelon, D., Stainier, D. Y., & Kimmel, C. B. (2003). Two endothelin 1 effectors, hand2 and bapx1, pattern ventral pharyngeal cartilage and the jaw joint. *Development*, *130*(7), 1353-1365.
[81] Alibardi, L. (2015). Regeneration of articular cartilage in lizard knee from resident stem/progenitor cells. *International journal of molecular sciences*, 16(9), 20Aa20747.
[82] Nagoshi, N., Shibata, S., Kubota, Y., Nakamura, M., Nagai, Y., Satoh, E., ... & Okada, S. (2008). Ontogeny and multipotency of neural crest-derived stem cells in mouse bone marrow, dorsal root ganglia, and whisker pad. *Cell stem cell*, *2*(4), 392-403.
[83] Ishizuya-Oka, A., Ueda, S., Amano, T., Damjanovski, S., Stolow, M., Shi, Y. B., & Inokuchi, T. (2001). Thyroid hormone-induced expression of sonic hedgehog correlates with adult epithelial development during remodeling of the *Xenopus* stomach and intestine. *Differentiation*, *69*(1), 27-37.
[84] Kan, C., Chen, L., Hu, Y., Ding, N., Li, Y., McGuire, T. L., ... & Kan, L. (2018). Gli1-labeled adult mesenchymal stem/progenitor cells and hedgehog signaling contribute to endochondral heterotopic ossification. *Bone*, *109*, 71-79.
[85] Kinto, N., Iwamoto, M., Enomoto-Iwamoto, M., Noji, S., Ohuchi, H., Yoshioka, H., ... & Yoshiki, S. (1997). Fibroblasts expressing Sonic hedgehog induce osteoblast differentiation and ectopic bone formation. *FEBS letters*, 404(2-3), 319-323.
[86] Leucht, P., Kim, J. B., Amasha, R., James, A. W., Girod, S., & Helms, J. A. (2008). Embryonic origin and Hox status determine progenitor cell fate during adult bone regeneration. *Development*, *135*(17), 2845-2854.
[87] Maruyama, T., Jeong, J., Sheu, T. J., & Hsu, W. (2016). Stem cells of the suture mesenchyme in craniofacial bone development, repair and regeneration. *Nature communications*, 7, ncomms10526.

[88] Mirando, A. J., Maruyama, T., Fu, J., Yu, H. M. I., & Hsu, W. (2010). ß-catenin/cyclin D1 mediated development of suture mesenchyme in calvarial morphogenesis. *BMC developmental biology*, 10(1), 116.
[89] Roelofs, A. J., Zupan, J., Riemen, A. H., Kania, K., Ansboro, S., White, N., ... & De Bari, C. (2017). Joint morphogenetic cells in the adult mammalian synovium. *Nature communications*, 8, 15040.
[90] Smeeton, J., Askary, A., & Crump, J. G. (2017). Building and maintaining joints by exquisite local control of cell fate. *Wiley Interdisciplinary Reviews: Developmental Biology*, *6*(1), e245.
[91] Zhao, H., Feng, J., Ho, T. V., Grimes, W., Urata, M., & Chai, Y. (2015). The suture provides a niche for mesenchymal stem cells of craniofacial bones. *Nature cell biology*, *17*(4), 386.
[92] Billmyre, K. K., & Klingensmith, J. (2015). Sonic hedgehog from pharyngeal arch 1 epithelium is necessary for early mandibular arch cell survival and later cartilage condensation differentiation. *Developmental Dynamics*, *244*(4), 564-576.
[93] Choi, K. Y., Kim, H. J., Lee, M. H., Kwon, T. G., Nah, H. D., Furuichi, T., ... & Ryoo, H. M. (2005). Runx2 regulates FGF2-induced Bmp2 expression during cranial bone development. *Developmental dynamics: an official publication of the American Association of Anatomists*, *233*(1), 115-121.
[94] Niswander, L., Jeffrey, S., Martin, G. R., & Tickle, C. (1994). A positive feedback loop coordinates growth and patterning in the vertebrate limb. *Nature*, 371(6498), 609.
[95] Barna, M., & Niswander, L. (2007). Visualization of cartilage formation: insight into cellular properties of skeletal progenitors and chondrodysplasia syndromes. *Developmental cell*, 12(6), 931-941.
[96] Beachy, P. A., Karhadkar, S. S., & Berman, D. M. (2004). Tissue repair and stem cell renewal in carcinogenesis. *Nature*, *432*(7015), 324.
[97] Altaba, A. R., Sánchez, P., & Dahmane, N. (2002). Gli and hedgehog in cancer: tumours, embryos and stem cells. *Nature Reviews Cancer*, *2*(5), 361.
[98] Yang, W., Liu, X., Choy, E., Mankin, H., Hornicek, F. J., & Duan, Z. (2013). Targeting hedgehog-GLI-2 pathway in osteosarcoma. *Journal of Orthopaedic Research*, *31*(3), 502-509.
[99] Shi, Y., He, G., Lee, W. C., McKenzie, J. A., Silva, M. J., & Long, F. (2017). Gli1 identifies osteogenic progenitors for bone formation and fracture repair. *Nature communications*, *8*(1), 2043.
[100] Hojo, H., Ohba, S., Taniguchi, K., Shirai, M., Yano, F., Saito, T., ... & Suzuki, K. (2013). Hedgehog-Gli activators direct osteo-chondrogenic function of bone morphogenetic protein toward osteogenesis in the perichondrium. *Journal of Biological Chemistry*, *288*(14), 9924-9932.
[101] Askary, A., Smeeton, J., Paul, S., Schindler, S., Braasch, I., Ellis, N. A., ... & Crump, J. G. (2016). Ancient origin of lubricated joints in bony vertebrates. *Elife*, 5, e16415.
[102] Brunt, L. H., Begg, K., Kague, E., Cross, S., & Hammond, C. L. (2017). Wnt signalling controls the response to mechanical loading during zebrafish joint development. *Development*, 144(15), 2798-2809.
[103] Nowlan, N. C., Prendergast, P. J., & Murphy, P. (2008). Identification of mechanosensitive genes during embryonic bone formation. *PLoS computational biology*, 4(12), e1000250.
[104] Parsons, P. A. (1990). Fluctuating asymmetry: an epigenetic measure of stress. *Biological reviews*, 65(2), 131-145.
[105] Widera, D., Zander, C., Heidbreder, M., Kasperek, Y., Noll, T., Seitz, O., ... & Kaltschmidt, B. (2009). Adult palatum as a novel source of neural crest-related stem cells. *Stem cells*, *27*(8), 1899-1910.
[106] Pradeu, T., Callebaut, W., & Schäfer, K. (2004). Environment, development, and evolution: toward a synthesis. Mit Press.
[107] Merchant, A. A., & Matsui, W. (2010). Targeting Hedgehog—a cancer stem cell pathway. *Clinical cancer research*, *16*(12), 3130-3140.
[108] Finch, C. E., & Rose, M. R. (1995). Hormones and the physiological architecture of life history evolution. *The Quarterly Review of Biology,* 70(1), 1-52.
[109] Abouheif, E., Favé, M. J., Ibarrarán-Viniegra, A. S., Lesoway, M. P., Rafiqi, A. M., & Rajakumar, R. (2014). Eco-evo-devo: the time has come. In Ecological genomics (pp. 107-125). *Springer*, Dordrecht.
[110] Gilbert, S. F., Bosch, T. C., & Ledón-Rettig, C. (2015). Eco-Evo-Devo: developmental symbiosis and developmental plasticity as evolutionary agents*. Nature Reviews Genetics*, 16(10), 611-622.
[111] Halsey, L. G., Curran-Everett, D., Vowler, S. L., & Drummond, G. B. (2015). The fickle P value generates irreproducible results. *Nature methods*, 12(3), 179.
[112] Heyland, A., & Moroz, L. L. (2005). Cross-kingdom hormonal signaling: an insight from thyroid hormone functions in marine larvae. *Journal of Experimental Biology*, 208(23), 4355-4361.

[113] Albalat, R., & Canestro, C. (2009). Identification of Aldh1a, Cyp26 and RAR orthologs in protostomes pushes back the retinoic acid genetic machinery in evolutionary time to the bilaterian ancestor. *Chemico-biological interactions*, 178(1-3), 188-196.
[114] Paris, M., Brunet, F., Markov, G. V., Schubert, M., & Laudet, V. (2008). The amphioxus genome enlightens the evolution of the thyroid hormone signaling pathway. *Development genes and evolution*, 218(11-12), 667-680.
[115] Kang, Y. J., Stevenson, A. K., Yau, P. M., & Kollmar, R. (2008). Sparc protein is required for normal growth of zebrafish otoliths. *Journal of the Association for Research in Otolaryngology,* 9(4), 436-451.
[116] Guryev, V., Koudijs, M. J., Berezikov, E., Johnson, S. L., Plasterk, R. H., Van Eeden, F. J., & Cuppen, E. (2006). *Genetic variation in the zebrafish. Genome research,* 16(4), 491-497.
[117] Nasiadka, A., & Clark, M. D. (2012). Zebrafish breeding in the laboratory environment*. ILAR journal,* 53(2), 161-168.
[118] Zurita, E., Chagoyen, M., Cantero, M., Alonso, R., González-Neira, A., López-Jiménez, A., ... & Montoliu, L. (2011). Genetic polymorphisms among C57BL/6 mouse inbred strains. *Transgenic research,* 20(3), 481-489.
[119] Monson, C. A., & Sadler, K. C. (2010). Inbreeding depression and outbreeding depression are evident in wild-type zebrafish lines. *Zebrafish*, 7(2), 189-197.
[120] Kalueff, A. V., Echevarria, D. J., & Stewart, A. M. (2014). Gaining translational momentum: more zebrafish models for neuroscience research.